Point-of-Care-Testing Devices for Sensing and Diagnostics

A thesis submitted

in partial fulfillment of the requirements

for the degree of

Doctor of Philosophy

by

Nilanjan Mandal

Centre for Nanotechnology

Indian Institute of Technology Guwahati

December 2019

C E R T I F I C A T E

It is certified that the works contained in this thesis entitled **"Point-of-Care-Testing Devices for Sensing and Diagnostics"**, by Mr. Nilanjan Mandal, have been carried out under our supervision and have not been submitted as a thesis elsewhere for a Ph.D degree.

Thesis supervisors

Prof. Dipankar Bandyopadhyay
Professor & HOC
Department of Chemical Engineering &
Centre for Nanotechnology
Indian Institute of Technology Guwahati

Prof. Arun Chattopadhyay
Professor
Department of Chemistry &
Centre for Nanotechnology
Indian Institute of Technology Guwahati

December 2019

ACKNOWLEDGEMENT

The journey undertaken for the completion of this thesis has been one of the most amazing experiences of my life, which would have been impossible without these people.

First and foremost, I would like to thank my thesis supervisors **Prof. Dipankar Bandyopadhyay** and **Prof. Arun Chattopadhyay** for giving me the opportunity to work in a very interesting area of research. I am very grateful to them for their continuous guidance, important advices and stimulating discussions. In spite of their busy schedule, they were always happy to dedicate their time to analyze the problems and give necessary suggestions for the betterment of my work. I am certain that the experience of working under their supervision will have far-reaching influences on my life. Their devotion towards their work, their untiring zeal to achieve perfection, and their patience in guiding novice researchers, will always inspire me. I consider it an honor to have been guided by them. I wish to thank my doctoral committee members, **Prof. Harshal B. Nemade**, Department of Electronics and Electrical Engineering, **Prof. Tapas K. Mandal**, and **Dr. Ashok K. Dasmahapatra**, Department of Chemical Engineering, for their valuable suggestions and efforts during my thesis work.

My sincere thanks to **Dr. A. Ananth Praveen Kumar** and **Dr. Kartick Mondal,** alumni from our research group, and **Dr. Nayanmani Das and Dr. Dhrubajyoti Roy,** Institute Post-Doctoral Fellows, for their unhesitating assistance and continuous encouragement throughout my PhD tenure. I wish to express my deepest gratitude to **Prof. Sarmishtha Banerjee,** Department of Design for her insightful suggestions regarding the design and aesthetics of the prototypes developed. I also wish to extend my gratitude to **Dr. Sandip Patil** from E-SPIN Nanotech Pvt. Ltd., Kanpur and **Mr. Sahil Jagnani** from Primary Healthtech Pvt. Ltd., New Delhi for their help in developing commercial prototypes. In addition, I am particularly grateful to **Dr. Amit Kumar Singh, Mrs. Aanchal Gupta, Dr. Seim Timung, Mr. Shirsendu Mitra, Ms. Satarupa Dutta, Dr. Madhumita Das** and **Dr. Mitradip Bhattacharjee,** for their support in experiments and computations.

I am also thankful to all the members of our research group, **Ms. Abhijna Das, Mr. Abhinav Sharma, Dr. Abir Ghosh, Dr. Amit Kumar Singh, Mr. Aniruddha Deb,**

Mrs. Anchal Gupta, Mr. Ankur Pandey, Mr. Anvesh Dixit, Mr. Ankit Chowdhury, Ms. Anuja Tripathi, Dr. Anushree Dutta, Mr. Bhaskarjyoti Sharma, Mrs. Binita Nath, Dr. Bolleddu Ravi, Mr. Chintak K. Parashar, Mr. Debdatta Ghosh, Mr. Debendra Nath Sarkar, Mr. Divesh Ranjan, Mr. Harsha Lankipalli, Mr. Himanshu Raturi, Mr. Jayant Borana, Mr. Joydip Chaudhuri, Mr. Kaniska Murmu, Mr. Manash Pratim Borthakur, Ms. Mitali Basak, Dr. Mitradip Bhattacharjee, Mr. Nayanjyoti Kakati, Mr. Nirmal Roy, Ms. Prasfutita Paul, Mr. Prathu Raja Parmar, Ms. Prerona Gogoi, Mr. Pritam Roy, Md. Rashid Ali Faridi, Mr. Rupam Sinha, Mr. Ravula Rajasekhar, Mr. Sagnik Midda, Mr. Saikat Biswas, Dr. Saptak Rarotra, Ms. Satarupa Dutta, Dr. Seim Timung, Mr. Shaon Sutradhar, Ms. Snigdha Chakraborty, Ms. Shreya Mukherjee, Mr. Shrikant Kashyap, Mr. Shirsendu Mitra, Mr. Siddharth Thakur, Dr. Sunny Kumar, Mr. Sunil Kumar Singh, Mr. Surjendu Maity, Mr. Subhradip Ghosh, Dr. Shrestha Basu, Mrs. Tamanna Bhuyan, Ms. Tanusree Ghoshal, Mr. Vinod Vanarse and last but not the least **Mr. Viswanath Pasumarthi.** I cannot forget to thank my friends and colleagues **Mr. Abhik Bhattacharjee, Mr. Ardhendu Sekhar Chaudhury, Mr. Biplab Ghosh, Dr. Jitendra Kumar, Dr. Manishekhar Kumar, Dr. Shyam Trivedi, Dr. Shamim Rahman, Mr. Saptarshi Gupta, Mr. Siddhanta Roy, Mrs. Soumi Sarkar, Mr. Arunabha Banerjee, Dr. Upashi Goswami, Dr. Madhumita Das, Dr. Sandipan Mukherjee, Mr. Somorjit Singh, Ms. Larionette Mawlong, Dr. Anamika Dey, Dr. Anamika Kalita, Dr. Ashish Singh, Dr. Dipjyoti Das, Ms. Nilanjana Nandi, Ms. Anwesha Chowdhury, Mr. Ritesh Kant Gupta, Mr. Rahul Narasimhan, Mr. Rabindranath Garai, Mrs. Namami Goswami,** and last but not the least **Dr. Rimi Das Mandal** for their role in making my stay at IIT Guwahati memorable.

My special thanks goes to all the faculty and staff members of **Centre for Nanotechnology**, and **Central Instruments Facility**, **IIT Guwahati,** for their co-operation and to **MeitY grant no. 5(9)/2012-NANO** for financial support and to **DST-SERB, grant no. SR/S3/CE/0079/2010** for the facilities provided.

Above all, I wish to thank my **parents, friends,** and **family members** for their love and support throughout everything, as always.

NILANJAN MANDAL

I dedicate this thesis to

My *Family*.

SYNOPSIS

Point-of-Care Testing Devices for Sensing and Diagnostics

1. Introduction

The society in this fast moving contemporary world is prone to diseases and health problems. Therefore, the support of various health monitoring sensors and systems for staying healthy may be necessary. As a result, there is a revolution in the field of innovation in monitoring sensors and devices to make the human life healthier and disease free. In this regard, the researchers and innovators throughout the world are trying to make effective, economical, biodegradable, fast sensors and devices. However, since this task is not a very simple one, there are various existing challenges associated with the portability, sensitivity, selectivity, response time, robustness, miniaturization, reusability, or user-friendliness, among many others. The researchers are thus encouraged to work in multifarious dimensions for finding the solution to each of these important problems. Recently, the focus has also been made upon the use of functionalized nanomaterials, conducting polymers, paper-substrates, open source electronics and their application in the Point-of-Care (POC) testing devices. The advantages of such kind of POC devices are, availability of higher surface to volume ratio, reduction in the amount of the fabricating material as well as in the amount of the sample required for testing, economic and biodegradable sensor substrate, and the emergence of exquisite physical, chemical, optical, electronic, or electrochemical properties at the nanoscale. In a way, expressing the specialties of the nanomaterials inside the microscale devices have paved new directions in the fields of sensor development, healthcare, and environmental monitoring, among others. The present thesis focusses on developing sensors and electronic devices targeting POCT applications in diagnostics and environmental monitoring.

As mentioned earlier the topics selected in the thesis are in context with the increasing health problems due to the rapid industrialization and subsequent changes in the healthcare and environment of the contemporary world. There are many lifestyle related diseases from which humans suffer in this modern era, which go undiagnosed at an early stage, for reasons such as lack of awareness as well as due to the absence of facilities at patients' location. Thus, the doctors in general encounter the diseased patients at the advanced stages. In this current situation, the need of the hour are devices that may detect diseases at the early stage, thus increasing the consciousness about human health on a regular basis. As per World Health Organization (WHO) guidelines, the mandate is to develop devices with ASSURED features – affordable, sensitive, specific, user-friendly, rapid and robust, equipment free, and deliverable. These are envisioned devices which can diagnose the otherwise common diseases in the patient's location such that they can be treated at their early stages. The innovators at well-established commercial organizations are even trying to integrate healthcare devices, which can be integrated to an existing device such as mobile phone or wristwatch, or a glass to obtain the various health parameters, such as blood pressure and temperature, body-mass-index, heartbeat, or pulse, that exclusively help in deciding the current status of health condition of a human being. Moreover, integration of sensors with clothes, spectacles, and directly to different body parts have also been demonstrated by these organizations. Further, flexible and wearable electronics-based sensors are also found extensively in the prior arts.

In view of this background, the present thesis focusses on the use of smart nanomaterials such as the metal nanoparticles, biomaterials or conducting polymers in the paper based microfluidic devices to develop proof-of-concept prototypes targeting biomedical applications and environmental monitoring. The thesis comprises four technical chapters containing scientific and engineering aspects of, (i) point-of-care-testing

of α-amylase activity in human blood serum, (ii) paper-based α-amylase detector for point-of-care diagnostics, (iii) paper-based sensor for point-of-care kidney function monitoring, and (iv) paper-based sensors for point-of-care water quality testing. The technical chapters in the thesis are preceded by an introductory chapter while at the end of the thesis a chapter containing the summary and future scopes have been included. A brief detail of outcomes of this thesis in terms of publications, patents, conferences, and awards has been provided as an APPENDIX.

2. Chapter 1: Point-of-Care-Testing of α-Amylase Activity in Human Blood Serum

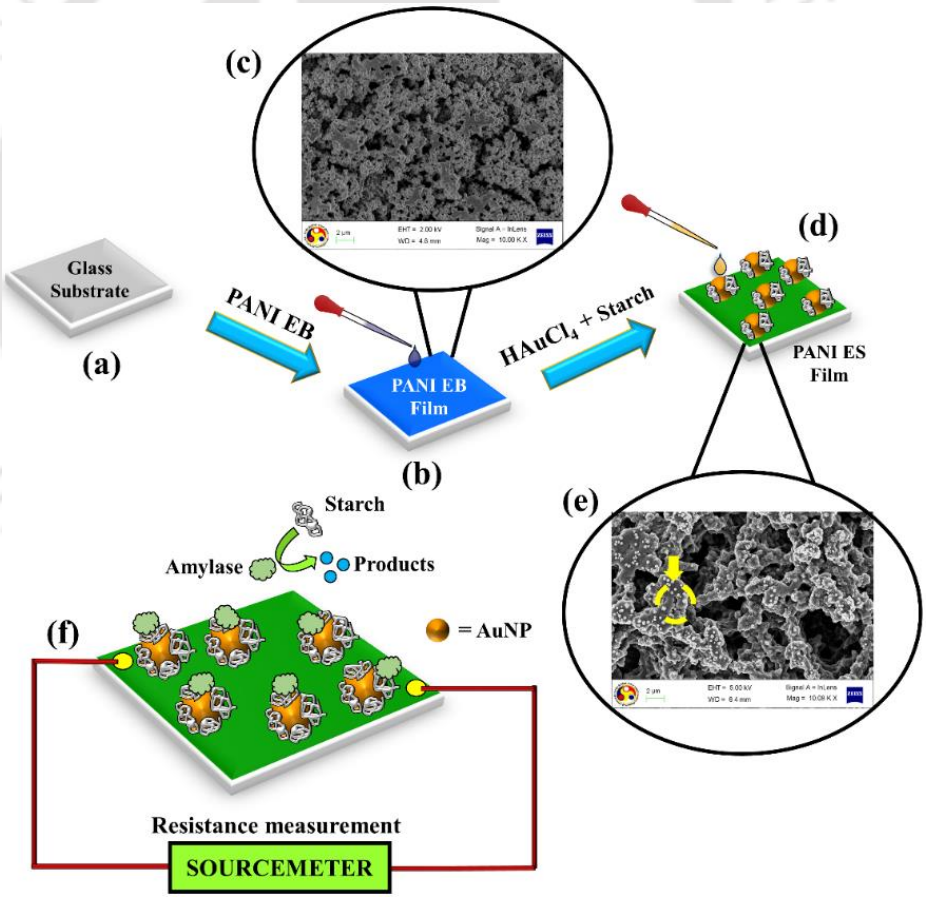

Figure 1: Images (a) and (b) schematically show the coating of a PANI-EB film on a glass substrate. Image (c) shows the FESEM images of surface textures of PANI-EB film. Image (d) shows the formation of SAuNPs on the surface of the film and conversion of PANI-EB to PANI-ES. Image (e) shows the FESEM image of surface textures of the conducting PANI-ES film coated with SAuNPs, marked on the image with arrow. Image (f) illustrates the scheme for measurement of sensor resistance by sourcemeter.

In this chapter, Activity of α-amylase enzyme in human serum indicates the onset of pancreatitis, mumps, cancer, stress, and depression. Herein we design and develop a biosensor for the point-of-care-testing (POCT) of α-amylase concentration in serum. The biosensor is composed of a glass substrate coated with an electrically conducting poly-aniline-emeraldine-salt (PANI-ES) film covered with starch-coated gold nanoparticles (SAuNPs), as shown in the **Figure 1**. Addition of different dosage of α-amylase on the biosensor selectively depletes starch stabilized on the SAuNPs, which changes the electrical resistance of the sensor. The change in electrical resistance show a nearly linear correlation with the concentration of α-amylase in buffer, which helps the detection of unknown α-amylase activity in the blood serum. The biosensor responds in a specific manner owing to the use of selective enzymatic chemical reaction between α-amylase and starch. The pathways to SAuNP formation on PANI-ES, time-dependent starch digestion with α-amylase, and the subsequent variation in electrical response was characterized to uncover the sensing mechanism. The chloride ions and the AuNPs present catalyse the starch-amylase reaction on the PANI surface to enable a sensitive detection of α-amylase in serum (10 – 90 U/l) at a quick response time of ~60 s. Integration of the biosensor with the built-in sourcemeter and a real time display help an immediate presentation of α-amylase level in the serum, comparable to the clinically approved methodologies.

3. Chapter 2: Paper-Based α-Amylase Detector for Point-of-Care Diagnostics

In this chapter, fabrication of a paper-sensor for quantitative detection of α-amylase activity in human blood serum. Pieces of filter papers were coated with starch-iodine solution leading to an intense blue coloration on the surface, as shown in the **Figure 2**. Dispensing α-amylase solution on the starch-iodine coated paper reduced the intensity

of the color because of starch-hydrolysis catalyzed by amylase, as shown in the **Figure 2**. The variation in the intensity of the color with the concentration of amylase was estimated in three stages: (i) initially, the paper-surface was illuminated with a light emitting diode,

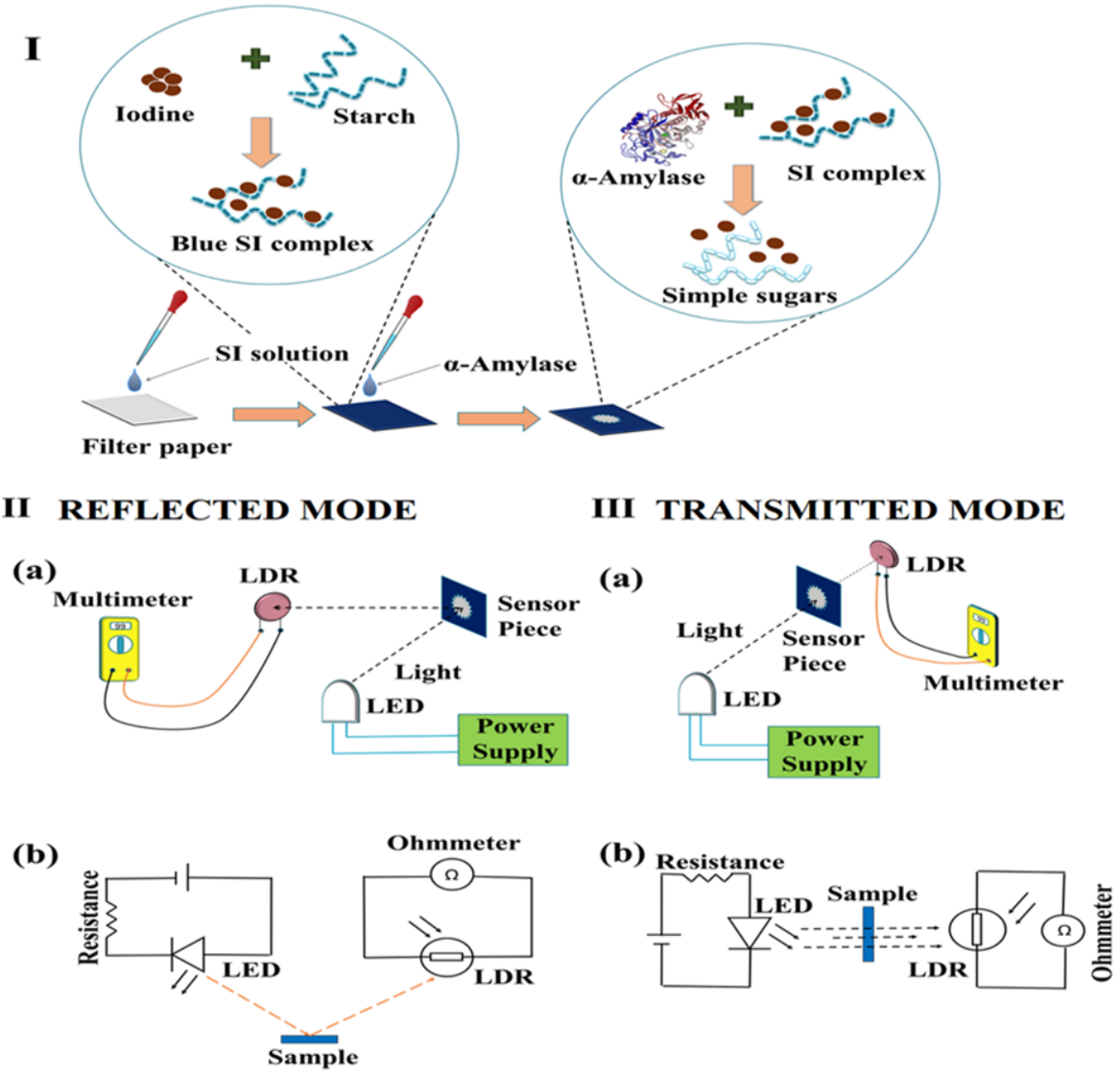

Figure 2: (I) Schematic illustrations of the steps to fabricate paper-sensor. (II) Reflection mode – images (a) and (b) show the experimental setup and corresponding circuit diagram for resistance measurement. (III) Transmitted mode – images (a) and (b) show the experimental setup and the corresponding circuit diagram for resistance measurement. The notation LDR (LED) represents photoresistor or photodetector (light emitting diode).

(ii) then, the transmitted (reflected) rays emitted through (from) the paper was collected on a photoresistor, and (iii) the variations in the electrical resistance of the photoresistor were correlated with the amylase concentration in analyte. The resistance of photoresistor decreased monotonically with an increase in amylase concentration because the intensity of the reflected (transmitted) rays collected from (through) the paper increased with reduction in the color intensity on the paper surface. Since a specific bio-reaction was employed to detect the activity of amylase, the sensor was found to be equally efficient in detecting unknown quantities of amylase in human blood serum. The reported sensor has shown the potential to graduate into a point-of-care detection tool for α-amylase.

4. Chapter 3: Paper-Based Sensor for Point-of-Care Kidney Function Monitoring

In this chapter, development of a paper-based colorimetric sensor for monitoring of kidney function is discussed, as shown in the **Figure 3**. The ratio of albumin to creatinine (ACR) in urine is a measure of human kidney-health. In this study, we report the development of a paper-based point-of-care (POC) kidney function test (KFT) kit, which is composed of paper-based ACR sensors, opto-electrochemical measurement unit, a display, and facility to transfer data to a smartphone. For the albumin sensor, the pieces of filter papers were coated with a mixture of alcoholic bromophenol blue and citric buffer leading to a chrome-yellow coloration while for the creatinine sensor the papers were coated with alkaline picrate solution leading to a lemon-yellow coloration of the surface. Dispensing albumin solution of known concentration on the albumin-sensor led to the conversion of chrome-yellow coloration to bluish-green while dispensing the creatinine solution on the creatinine-sensor led to the conversion of lemon-yellow to orange coloration of the surface.

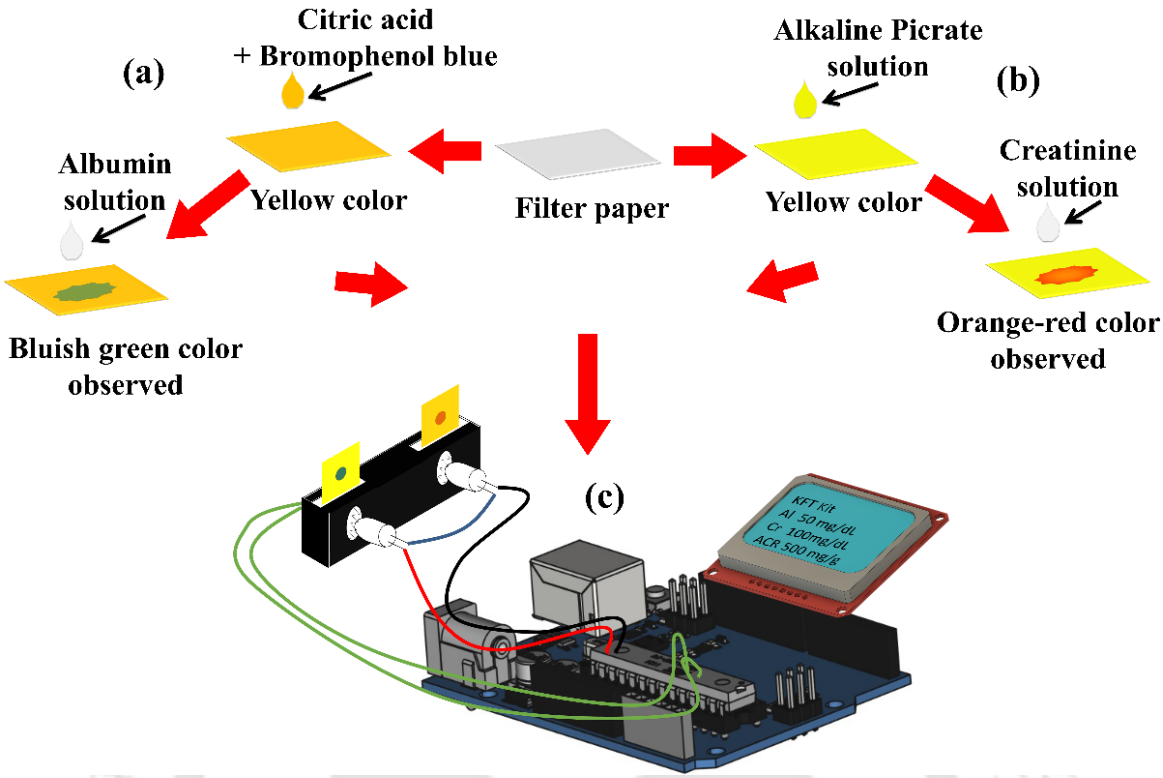

Figure 3: This schematic shows the fabrication process and illustration of working of the sensors. Image (a)-(b) show the different steps of fabricating the albumin and creatinine sensors. Image (c) illustrates the working of the sensors in determining the albumin and creatinine concentration in human blood.

For both the albumin or creatinine sensors, the intensity of the bluish-green or orange coloration varied with the concentration of the analytes in the solutions. The variations in the intensities of colors with albumin and creatinine loadings in the analytes were quantified by integrating a light emitting diode (LED) at one side of each sensor and a light dependent resistor (LDR) on the other side. The intensity of the transmitted rays from the source LED, passing through the sensors, was found to vary the electrical resistance of the LDR monotonically with the loading of the albumin or creatinine in the analyte, which helped in obtaining the calibration plots for the ACR sensors. The portable and fast proof-of-concept POC prototype was employed for the on-spot detection of the unknown ACR in the real human urine samples.

5. Chapter 4: Paper-based Sensors for Point-of-Care Water Quality Testing

In this chapter, multiple paper-based sensors for monitoring of water quality is developed and demonstrated, as shown in the **Figure 4**. Contamination of water bodies due to the disposal of natural and anthropogenic pollutants is one of the major global concerns in the recent times. Regular on-spot monitoring of water quality has become mandatory wherein diverse classes of materials such as organic, inorganic, heavy metals, or biological wastes are detected employing standard protocols. However, most of the existing laboratory techniques are either costly and/or time consuming owing to the process involving the expert driven sophisticated analysis techniques.

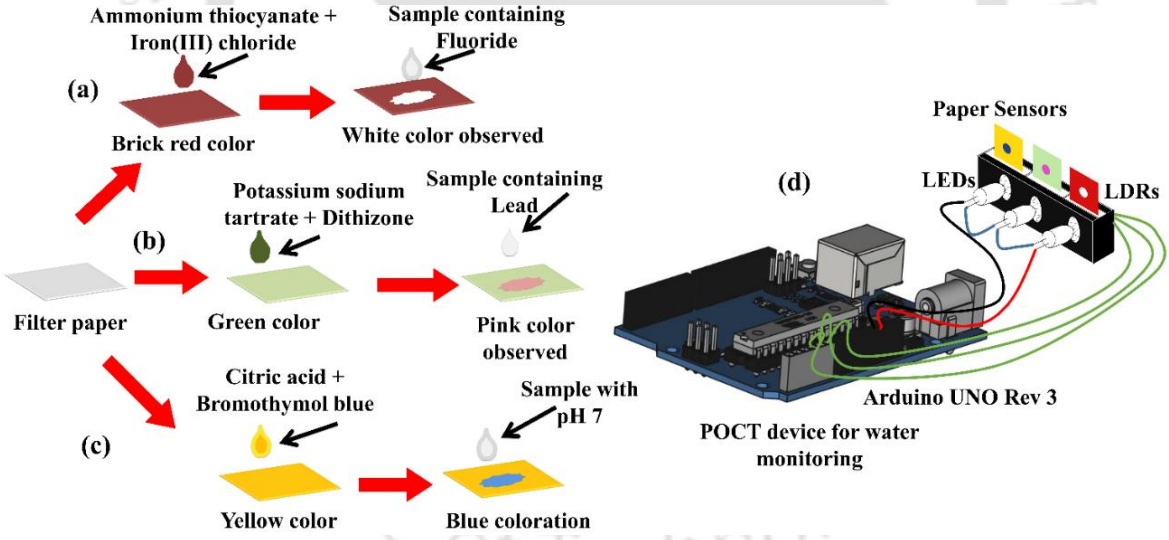

Figure 4: Images (a)-(c) schematically illustrate the steps of colorimetric sensor fabrication for F^-, Pb^{2+} and pH, respectively, and their color change. Image (d) shows the integration of LED and LDR with the sensor and subsequent measurement of the change in resistance using Arduino based POCT device for the display of water quality.

Herein, we report the development of three paper based colorimetric sensors for the on-spot quantitative detection of the levels of fluoride (F^-), lead (Pb^{2+}), and pH in drinking water. The variations in the color-intensities of the paper sensors with the

variation in the concentration of F^{-}, Pb^{2+}, and pH were converted into electronic signals to enable the development of a point-of-care-testing (POCT) device. For this purpose, initially, the sensors were characterized and calibrated with known concentrations of contaminates before successful validations with real samples. Thereafter, the sensors were illuminated with a light emitting diode from one side while the transmitted rays passing through the sensor was captured by a light dependent resistor (LDR) from the other side. The variation in the color intensity of the paper-sensor with the contaminant loading was found linearly varying with the resistance of the LDR. The sensor was then translated into a specific, stable and user friendly POCT device, which enabled inexpensive spot detection of pollutants in drinking water.

List of Figures

List of Tables

Contents

Topic **Page No.**

CHAPTER 1

Introduction

Contents

1.1. Overview

In the modern human life, personal care practices have become indispensable to maintain a minimum quality of health. The point-of-care testing (POCT) devices, are miniaturized, user friendly, rapid, economical, uses low power and help in such round-the-clock health monitoring and diagnostics. In a way, the POCT devices can minimize medical expenses by operating with minute amount of complex biological and chemical samples; such as blood, urine and water, rapidly analysing those samples and allowing prompt treatment before the onset of the infection or disease. Broadly, POCT devices are also used for primary health care in prevention and control of disease as well as monitoring of health conditions in remote areas lacking sophisticated laboratory arrangements and trained medical laboratory technicians.

Recently, there have been significant advancements in the area of design and development of the POCT devices by implementing advanced technologies like, bio-process reaction engineering, nanotechnology, micro or nanoelectronics, microfluidics, smart soft materials, data analytics, and connectivity (Bhattacharjee et al. 2016; Bhattacharya et al. 2007; Gogoi et al. 2011; Gogoi et al. 2012; Kricka 2001; Kricka et al. 1993; Manz et al. 1990; Saliterman 2006; Singh et al. 2014; Vo-Dinh and Cullum 2000; Whitesides 2006; Wu et al. 2012). In particular, micro and nanoscale objects such as the nanoparticles, nanofibers, nanodots, nanopores, and microfluidic devices have shown the potential to improve the efficiency of various highly selective detection techniques by enhancing the accuracy, sensitivity and response time (Ahn et al. 2004; Bashir 2004; Grieshaber et al. 2008; Homola 2008; Nguyen 2007; Vo-Dinh and Cullum 2000) and resulting in immediate detection of diverse ailments.

The guidelines as laid by World Health Organization (WHO) for developing efficient POCT devices are known as ASSURED, in which the abbreviation ASSURED stands for affordable, sensitive, specific, user-friendly, rapid/robust, equipment-free or minimal, and delivered at time of need (Jenkins and Goldberger 2002; Luppa et al. 2016; Peeling and Mabey 2010).

The present thesis aims at the design and development of a host of specialty sensors and portable POCT devices targeting a set of healthcare applications, and environmental monitoring. The background of the aforementioned topics is associated with increasing health hazards that are directly related to the pollutions in the ambient air, water, and soil (Conrad and Hilchey 2011; Spengler and Sexton 1983; Yu et al. 2011). Importantly, due to the lack of awareness and absence of facilities at the patients' site, the early detection of these ailments are not available. Consequently, most of the patients are at advanced stage of disease when they consult the doctors. Considering the current situation, recently, people are trying to develop POCT devices that are capable of an early stage disease detection and increasing the awareness by monitoring their health status regularly.

Globally, the recent research thrust has been directed to obtaining the varied health-related parameters, such as body weight (Fader et al. 2009; Meza and Carrillo 2016; Must et al. 1999), body-mass index (van der Pals et al. 2014), blood sugar or pressure, lipid profiles (Bruen et al. 2017; Flynn et al. 2017), T3-T4-TSH (Christ and Burger 2015; Dayan 2001), hemoglobin (Brown et al. 2003), sodium and potassium (Metheny 1981; Stenvinkel and Alvestrand 2002) body temperature, heartbeat or pulse, which help in deciding the qualitative and quantitative profiling of individual health. Further, flexible and wearable electronics-based sensors, integrated with objects of regular usage such as clothes, or

directly into the patients' affected body part, also have been found in extensive use (Appelboom et al. 2014; McGrath et al. 2014; Schneegass and Amft 2017). Apart from the developing POCT devices for medical purposes, development of POCT devices for environmental monitoring has made a rapid progress in recent times. Development of sensors to detect various toxic chemicals, pH, in the water bodies gained serious interest due to their importance in environmental monitoring and relation with various disease (Clement et al. 1999; Fung and Mykhaylova 2014). In particular, the use of various electronic as well as optoelectronic phenomena have been utilized to develop proof-of-concept prototypes targeting medical as well as environmental applications.

1.2. Classification of POCT devices

In recent past, there have been extensive research and development in the field of POCT devices. Varied applications ranging from healthcare to environmental testing have been developed and demonstrated by integrating different attributes of micro and nano domain to different technological fields such as optoelectronics, electrochemistry, etc. In the following section, an overview of different POCT devices employed in this thesis has been depicted.

1.2.1 Conducting (sensing material) polymer based POCT devices

Conducting polymers based POCT devices have also been developed to monitor the environment and health parameters. Conducting polymers are low cost, fabrication convenient, user-friendly, biodegradable materials, which are used for the sensors design in POCT devices. Conducting polymers have been used on various platforms such as catalytic and affinity biosensors as immobilization matrices, signal transduction systems, and even analyte recognizing components.

Further, Sensor fabrication for POCT devices exploits numerous exciting properties of conducting polymers such as (Yoon and Jang 2009):

- Easily produced using electrochemical or chemical processes.
- Sensitive to an array of analytes at different conditions (i.e. temperature, humidity)
- Response depends on the intrinsic property of the conducting polymer.
- Polymer structure can be readily modified for selective responses toward specific target.
- Sensitivity can also be customized by the fabrication conditions.
- Miniaturization and mass production of sensor array can be easily achieved by using various electrochemical fabrication procedures.

Nanomaterials fabricated from conducting polymer is largely used to detect multifarious analytes for environmental and health monitoring. There are sensors based on conducting polymer nanomaterials, consisting of polypyrrole (PPy), polyaniline (PANI), poly-(3,4-ethylenodioxythiophene) (PEDOT) (Li et al. 2015; Yoon and Jang 2009).

1.2.2 Paper (substrate)-based POCT devices

Paper is the most abundantly available, biodegradable, user-friendly and economic materials used for various purposes ranging from writing to packaging and many more. Recently paper has been used in great deal in POCT devices for its aforementioned qualities (Russo et al. 2011; Yetisen et al. 2013). The varied intrinsic properties of the paper such as thickness, porosity, color, texture etc. can be easily tuned during its manufacturing process. The fiber networks of cellulose in paper helps in fluid flow without any external force making it the most suitable candidate for low cost POCT device in environment as well as in health care applications (Madou et al. 2001; Martinez et al. 2010). Further, paper being

flexible substrate is suitable for use in portable and wearable sensors (Yang and Hsu 2010). In addition, due to their background color paper substrates are widely used in colorimetric based sensor for achieving instantaneous results in POCT based devices. There has been a major gobal development in paper-basd colorimetric sensors in recent times (Segev-Bar and Haick 2013; Sriram et al. 2017; Windmiller and Wang 2013). Lately, numerous paper-based colorimetric sensors for sensing broad range of materials such as, toxic vapor and gases, clinically important analytes (Cheng et al. 2010; Li et al. 2014; Li et al. 2008) have been developed. The paper sensors can be easily fabricated just by soaking them or drop casting the reagent upon their surface which helps in detecting specific target analytes, chemical or biological in nature, quantitatively or qualitatively by variation in colorimetric due to the reaction. However, there is never ending requirements to develop paper-based POCT devices to cater the needs of large section people in its requirement.

1.3 Objectives of the Thesis

The objectives of the thesis are the development of diverse POCT devices for health care and environmental applications. For developing such POCT devices, different principles have been explored such as electrical, electrochemical, optoelectronic, among others. Furthermore, it is also the need of the hour to make people aware about their health and its relation to the environment, which is only possible by giving them easy access to the hassle free testing and diagnosis facility at their location, with the help of POCT devices. With this background survey, the thesis presented demonstrates varied principles and fabrication techniques to develop proof-of-concept prototypes for healthcare and environmental monitoring.

The thesis is broadly divided into six chapters. The first chapter provides the introduction, overview and objectives of this thesis. Following this, four technical chapters are presented such as, (ii) point-of-care-testing of α-amylase activity in human blood serum, (iii) paper-based *α*-amylase detector for point-of-care diagnostics, (iv) paper-based sensors for point-of-care kidney function monitoring, (v) paper-sensors for point-of-care monitoring of drinking water quality. The sixth chapter containing the summary and future scope of this thesis succeeds the technical chapters. A brief detail of contributions from this thesis in terms of patents, publications, conferences, and awards has also been provided in the respective appendices after the conclusion of the thesis.

References

Ahn, C.H., Jin-Woo, C., Beaucage, G., Nevin, J.H., Jeong-Bong, L., Puntambekar, A., Lee, J.Y., 2004. Proc. IEEE 92(1), 154-173.

Appelboom, G., Camacho, E., Abraham, M.E., Bruce, S.S., Dumont, E.L.P., Zacharia, B.E., D'Amico, R., Slomian, J., Reginster, J.Y., Bruyère, O., Connolly, E.S., 2014. Arch. Belg. 72(1), 28.

Bashir, R., 2004. BioMEMS: state-of-the-art in detection, opportunities and prospects. Adv. Drug Delivery Rev. 56(11), 1565-1586.

Bhattacharjee, M., Pasumarthi, V., Chaudhuri, J., Singh, A.K., Nemade, H., Bandyopadhyay, D., 2016. Nanoscale 8(11), 6118-6128.

Bhattacharya, S., Jang, J., Yang, L., Akin, D., Bashir, R., 2007. BioMEMS and Nanotechnology-Based Approaches for Rapid Detection of Biological Entities. J. Rapid Methods Autom. Microbiol. 15(1), 1-32.

Brown, W.W., Peters, R.M., Ohmit, S.E., Keane, W.F., Collins, A., Chen, S.-C., King, K., Klag, M.J., Molony, D.A., Flack, J.M., 2003. Am. J. Kidney Dis. 42(1), 22-35.

Bruen, D., Delaney, C., Florea, L., Diamond, D., 2017. Sensors 17(8), 1866.

Cheng, C.-M., Martinez, A.W., Gong, J., Mace, C.R., Phillips, S.T., Carrilho, E., Mirica, K.A., Whitesides, G.M., 2010. Angew. Chem., Int. Ed. 49(28), 4771-4774.

Christ, E.R., Burger, A.G., 2015. Thyroid Function Tests. In: Huhtaniemi, I., Martini, L. (Eds.), Encyclopedia of Endocrine Diseases (Second Edition), pp. 477-485. Academic Press, Oxford.

Clement, R.E., Yang, P.W., Koester, C.J., 1999. Environmental Analysis. Anal. Chem. 71(12), 257-292.

Conrad, C.C., Hilchey, K.G., 2011. Environ. Monit. Assess. 176(1), 273-291.

Dayan, C.M., 2001. Lancet 357(9256), 619-624.

Fader, A.N., Arriba, L.N., Frasure, H.E., von Gruenigen, V.E., 2009. Gynecol. Oncol. 114(1), 121-127.

Flynn, J.T., Kaelber, D.C., Baker-Smith, C.M., Blowey, D., Carroll, A.E., Daniels, S.R., De Ferranti, S.D., Dionne, J.M., Falkner, B., Flinn, S.K., 2017. Pediatr. 140(3), e20171904.

Fung, A.O., Mykhaylova, N., 2014. J. Lab. Autom. 19(3), 225-247.

Gogoi, S.K., Borah, S.M., Dey, K.K., Paul, A., Chattopadhyay, A., 2011. Langmuir 27(20), 12263-12269.

Gogoi, S.K., Paul, A., Chattopadhyay, A., 2012. RSC Adv. 2(9), 3642-3646.

Grieshaber, D., MacKenzie, R., Vörös, J., Reimhult, E., 2008. Sensors 8(3), 1400-1458.

Homola, J., 2008. Chem. Rev. 108(2), 462-493.

Jenkins, A.J., Goldberger, B.A., 2002. On-Site Drug Testing. Humana Press.

Kricka, L.J., 2001. Clin. Chim. Acta 307(1–2), 219-223.

Kricka, L.J., Nozaki, O., Heyner, S., Garside, W.T., Wilding, P., 1993. Clin. Chem. 39(9), 1944-1947.

Li, B., Fu, L., Zhang, W., Feng, W., Chen, L., 2014. Electrophoresis 35(8), 1152-1159.

Li, C., Thostenson, E.T., Chou, T.-W., 2008. Compos. Sci. Technol. 68(6), 1227-1249.

Li, L., Shi, Y., Pan, L., Shi, Y., Yu, G., 2015. J. Mater. Chem. B 3(15), 2920-2930.

Luppa, P.B., Bietenbeck, A., Beaudoin, C., Giannetti, A., 2016. Biotechnol. Adv. 34(3), 139-160.

Madou, M.J., Lee, L.J., Daunert, S., Lai, S., Shih, C.-H., 2001. Biomed. Microdevices 3(3), 245-254.

Manz, A., Graber, N., Widmer, H.M., 1990. Sens. Actuators, B 1(1–6), 244-248.

Martinez, A.W., Phillips, S.T., Whitesides, G.M., Carrilho, E., 2010. Anal. Chem. 82(1), 3-10.

McGrath, M.J., Scanaill, C.N., Nafus, D., 2014. Sensor Technologies: Healthcare, Wellness and Environmental Applications. Apress.

Metheny, N., 1981. J. Infus. Nurs. 4(1), 38-44.

Meza, M.N., Carrillo, J.A.B., 2016. Biomarkers, Obesity, and Cardiovascular Diseases. In: Wang, Mu., Witzmann, F. (Eds.), Role of Biomarkers in Medicine, Intechopen. pp. 119-147.

Must, A., Spadano, J., Coakley, E.H., Field, A.E., Colditz, G., Dietz, W.H., 1999. J. Am. Med. Assoc. 282(16), 1523-1529.

Nguyen, N.-T., 2007. Fabrication Issues of Biomedical Micro Devices. In: Ferrari, M., Bashir, R., Wereley, S. (Eds.), BioMEMS and Biomedical Nanotechnology, Springer. pp. 93-115.

Peeling, R.W., Mabey, D., 2010. Clin. Microbiol. Infect. 16(8), 1062-1069.

Russo, A., Ahn, B.Y., Adams, J.J., Duoss, E.B., Bernhard, J.T., Lewis, J.A., 2011. Adv. Mater. 23(30), 3426-3430.

Saliterman, S., 2006. Emerging BioMEMS Technology. Fundamentals of BioMEMS and Medical Microdevices, First ed. Wiley. pp. 413-448.

Schneegass, S., Amft, O., 2017. Smart Textiles: Fundamentals, Design, and Interaction. Springer. pp. 161-164.

Segev-Bar, M., Haick, H., 2013. ACS Nano 7(10), 8366-8378.

Singh, A.K., Dey, K.K., Chattopadhyay, A., Mandal, T.K., Bandyopadhyay, D., 2014. Nanoscale 6(3), 1398-1405.

Spengler, J.D., Sexton, K., 1983. Science 221(4605), 9.

Sriram, G., Bhat, M.P., Patil, P., Uthappa, U.T., Jung, H.-Y., Altalhi, T., Kumeria, T., Aminabhavi, T.M., Pai, R.K., Madhuprasad, Kurkuri, M.D., 2017. TrAC, Trends Anal. Chem. 93, 212-227.

Stenvinkel, P., Alvestrand, A., 2002. Semin. Dial. 15(5), 329-337.

van der Pals, M., Myléus, A., Norström, F., Hammarroth, S., Högberg, L., Rosén, A., Ivarsson, A., Carlsson, A., 2014. BMC Pediatr. 14(1), 165.

Vo-Dinh, T., Cullum, B., 2000. Fresenius' J. Anal. Chem. 366(6-7), 540-551.

Whitesides, G.M., 2006. Nature 442(7101), 368-373.

Windmiller, J.R., Wang, J., 2013. Electroanalysis 25(1), 29-46.

Wu, C., Brunelle, F., Harnois, M., Follet, J., Senez, V., 2012. Micro Electro Mechanical Systems (MEMS), 2012 IEEE 25th International Conference on, pp. 777-780.

Yang, C.-C., Hsu, Y.-L., 2010. Sensors 10(8), 7772.

Yetisen, A.K., Akram, M.S., Lowe, C.R., 2013. Lab Chip 13(12), 2210-2251.

Yoon, H., Jang, J., 2009. Adv. Funct. Mater. 19(10), 1567-1576.

Yu, M.H., Tsunoda, H., Tsunoda, M., 2011. Environmental Toxicology: Biological and Health Effects of Pollutants, Third Edition. Taylor & Francis. pp.105-114.

भारतीय प्रौद्योगिकी संस्थान गुवाहाटी
Indian Institute of Technology Guwahati

CHAPTER 2

Point-of-Care-Testing of α-Amylase Activity in Human Blood Serum

Contents

भारतीय प्रौद्योगिकी संस्थान गुवाहाटी
Indian Institute of Technology Guwahati

ABSTRACT

Activity of α-amylase enzyme in human serum indicates the onset of pancreatitis, mumps, cancer, stress, and depression. Herein we design and develop a biosensor for the point-of-care-testing (POCT) of α-amylase concentration in serum. The biosensor is composed of a glass substrate coated with an electrically conducting polyaniline-emeraldine-salt (PANI-ES) film covered with starch-coated gold nanoparticles (SAuNPs). Addition of different dosage of α-amylase on the surface of the biosensor selectively depletes starch stabilized on the SAuNPs, which changes the electrical resistance of the sensor. The change in electrical resistance show a nearly linear correlation with the concentration of α-amylase in buffer, which helps in the detection of unknown α-amylase activity in the blood serum. The biosensor responds in a specific manner owing to the use of selective enzymatic chemical reaction between α-amylase and starch. The pathways to SAuNP formation on PANI-ES, time-dependent starch digestion with α-amylase, and the subsequent variation in electrical response was characterized to uncover the sensing mechanism. The chloride ions and the AuNPs present catalyse the starch-amylase reaction on the PANI surface to enable a sensitive detection of α-amylase in serum (25 – 90 U/L) at a quick response time of ~60 s. Integration of the biosensor with the built-in sourcemeter and a real time display help an immediate presentation of α-amylase level in the serum, comparable to the clinically approved methodologies.

This chapter is published in *Biosensors and Bioelectronics.* **124**-**125**, 75-81 (2019).

2.1. Introduction

Integrating the specialities of bio-processes, reaction engineering, and nanotechology in micro or nanoelectronic devices have opened up new avenues in the design and the development of the next generation micro-electro-mechanical-systems (MEMS) targeting biomedical applications (Bhattacharjee et al. 2016; Bhattacharya et al. 2007; Gogoi et al. 2011; Gogoi et al. 2012; Kricka 2001; Kricka et al. 1993; Manz et al. 1990; Saliterman 2006; Singh et al. 2014; Vo-Dinh and Cullum 2000; Whitesides 2006; Wu et al. 2012). In particular, the highly selective bio-reactions on the surface of nanoscale objects such as nanoparticles have shown the potential to improve the efficiency of various detection techniques by enhancing the sensitivity and response time (Ahn et al. 2004; Bashir 2004; Grieshaber et al. 2008; Homola 2008; Nguyen 2007; Vo-Dinh and Cullum 2000). In near future, the sensors empowered with the special features of the nano- and bio-technology are expected to produce rapid, reliable, portable, and easy to use point-of-care-testing (POCT) tools for the immediate detection of multifarious ailments (Ahn et al. 2004; Bhattacharjee et al. 2017; Chin et al. 2007; Kricka 2001; Sia and Kricka 2008; Vo-Dinh and Cullum 2000; Yager et al. 2008; Yager et al. 2006).

For example, it is well known that the concentration of the α-amylase in different body fluids such as blood, saliva or urine is an important indicator of a number of common ailments (Wilkins 2009). The rise or fall of this enzyme indicates the onset of pancreatitis, pancreatic cancer, mumps, stress or depression, toxaemia in pregnancy, and liver cirrhosis.(Anderson 2002; González et al. 2002; He et al. 2000; Janowitz and Dreiling 1959; Nater et al. 2005; Swaroop et al. 2004; Warshaw and Fuller 1975; Wilkins 2009) However, the presently available methodologies to evaluate the amount of this enzyme from different biological

sources involve time-consuming and expensive multi-step processes.(Cosnier 1999; Foo and Bais 1998; van Staden and Mulaudzi 2000) Furthermore, expert view is also necessary for the detection and analysis. In this direction, the point-of-care diagnostic tools detecting the concentration of α-amylase with immediate electrical or optical response are perhaps the need of the hour.(Robles et al. 2011)

The enzyme α-amylase (endo-1,4-*α*-d-glucan glucanohydrolase, EC 3.2.1.1) is produced in pancreas and salivary glands to hydrolyse starch into simple sugars. The quantification of the enzyme in blood serum facilitates the detection of many important health disorders (Zajoncová et al. 2004). Thus far, the spectrophotometric techniques are the most reliable and accurate pathways to detect the activity of α-amylase in blood serum (Chavez et al. 1990). However, the involvement of costly UV-Vis spectrophotometry for analysis restricts the applicability of this process in the POCT devices (Chavez et al. 1990; Dutta et al. 2016; Shetty et al. 2011). Alternatively, the electrochemical methods (Mahosenaho et al. 2010; Yamaguchi et al. 2005; Zajoncová et al. 2004), fluorometry (Murayama et al. 2006; Zhang et al. 1990), isoelectric focusing (Takeuchi et al. 1975), electrokinetic processes (Watanabe et al. 1998), chromatography (Battershell and Henry 1990), weight based detections (Gibbs et al. 2015; Sasaki et al. 2008), and immunological methods (Svens et al. 1989), have also been employed for α-amylase estimation. A recent study has disclosed the development of a device suitable for the POC detection of α-amylase employing a paper substrate where the differential colorimetric signal generated with the variation in the α-amylase loading has been converted into electrical signal using light dependent resistor (Bandyopadhyay et al. 2016; Dutta et al. 2016). A brief discussion and comparison about the methodologies to estimate α-amylase in the diverse body fluids has been summarized in the Table 2.1.

Table 2.1. Comparison table between the existing methods and the proposed method.

No.	Principle	Analyte	Volume (µL)	Range	Ref.
1	Electrochemical	Salivary	100	0-30 U/ml	(Yamaguchi et al. 2003)
2	Electrochemical	Salivary	35	0.1-3 mM	(Zajoncová et al. 2004)
3	Optical	Salivary	5	0-200 U/ml	(Yamaguchi et al. 2004)
4	Optical	Salivary	30	10-140 U/ml	(Yamaguchi et al. 2006)
5	Optical	Salivary	25	10-230 U/ml	(Shetty et al. 2011)
6	Electrochemical	Salivary	50	0-90 U/ml	(Yamaguchi et al. 2005)
7	Immuno-electrochemical	Salivary	-	0.003-0.0016 ng/ml	(Aluoch et al. 2005)
8	Electrochemical	Salivary	-	60-840 U/ml	(Zou et al. 2008)
9	Electrochemical	Salivary	-	5-250 U/ml	(Mahosenaho et al. 2010)
10	Impedance	Blood	-	< 1 U/ml	(Gibbs et al. 2015)
11	Optical	Blood	5	10-110 U/ml	(Dutta et al. 2016)
12.	Electrical	Blood	5	10-90 U/L	Present Method

The table highlights that indeed there are a very few methods available for the detection of blood serum α-amylase concentration. Among these methodologies, the method described in (Dutta et al. 2016) is a two-step process wherein the first step involves the dispensing of the serum on the starch-iodine coated paper surface and the second one involves the integration of the paper with the device after drying to detect the level of amylase. Further, the blood serum needs to be pre-treated before dispensing it on the sensor in order to reduce the influence of ascorbic acid. In the present method, we need the pre-treatment of the blood serum with potassium iodate to remove the influence of ascorbic acid as described in the study by Dutta et al. 2016. However, after that the present method is one-step process because the sensor is capable of detecting the amylase level in the blood serum electrochemically with the help of the built-in source meter integrated to the device. Thus, the present process is expected to be faster in generating results. Herein we report the development of an electrochemical biosensor and a proof-of-concept prototype for the detection of α-amylase in human blood serum.

The biosensor is composed of an electrically conducting polymer poly-aniline emeraldine salt (PANI-ES) thin film (Malhotra 2001; Singh et al. 2006; Tahir et al. 2005; Trojanowicz and Krawczyński vel Krawczyk 1995; Wang and Mu 1999), which is sparsely populated with starch-coated gold nanoparticles (SAuNPs) on the surface. The PANI-ES film acts as a base material for the electrical signal transport apart from acting as an immobilization matrix for the SAuNPs (Mallick et al. 2006; Pandey and Mishra 1988; Tamer et al. 2011). It is well known that α-amylase selectively catalyses the hydrolysis of starch into simple sugars. Thus, dispensing the solutions of α-amylase of different concentrations on the sensor depletes dissimilar amounts of the starch molecules coated the gold nanoparticles (AuNPs), which leads to the variation in the electrical resistance of the sensor. The change in the electrical resistance vary almost linearly with the concentration of α-amylase in phosphate buffer, which helps in the development of the calibration curve.

The pathway to SAuNP formation on the PANI-ES substrate, the time-dependent starch digestion with α-amylase, and the variation in the subsequent electrical response have also been characterized to uncover the details of the sensing mechanism. Involvement of chloride ions and AuNPs on the PANI-ES film offers a fast response time with a superior stability during the signal processing. A calibrated proof-of-concept prototype has also been developed for the fast (~60 s) detection of α-amylase level in human serum, which promises to be superior to the available clinically approved methodologies. The reported prototype has shown the potential evolve into a portable, easy-to-use, fast, reliable, economic, and biocompatible POCT diagnostic tool for the immediate detection of pancreatitis, cancer, stress, and depression.

2.2. Experimental Section

2.2.1. Materials

Aniline ($C_6H_5NH_2$), hydrochloric acid (HCl), ammonium peroxodisulphate ($(NH_4)_2S_2O_8$), ammonium hydroxide (NH_4OH), starch, 125 mm filter paper (grade 1), were obtained from Merck (India). The gold (III) chloride ($HAuCl_4$) solution, α-amylase enzyme and potassium bromide powder (KBr) were procured from Sigma-Aldrich (India). Phosphate buffer (10X) was procured from SRL (India). Conductive silver paste was obtained from Siltech Corporation (India). The chemicals above were of analytical grade and used without further purification. The Milli-Q grade water was used in all the experiments unless stated otherwise. The Arduino Uno R3 development board, Liquid crystal display (LCD), resistors (1mega ohm and 10 mega ohm) were procured from Rhydo Labz (India).

2.2.2. Synthesis

Poly-aniline emeraldine base (PANI-EB) synthesis: PANI-EB was prepared following a standard protocol.(Li and Kaner 2005) In the beginning, the liquid aniline monomer (0.3 ml) and ammonium peroxodisulphate (0.18 g) were dissolved in two separate vials containing 1.0 M HCL (10 ml). The freshly prepared solutions were mixed inside a 30 ml glass vial in equal proportion and vigorously shaken for ~30 s before settling down for ~2 h. The product obtained was collected and thoroughly washed with water and left as is for ~6 h after the addition of excess 30% aqueous NH_4OH. Thereafter, the product was thoroughly washed with water until there was no trace NH_4OH and dried in vacuum oven at 60°C for ~12 h to obtain a dark blue PANI-EB powder. PANI-EB solution (3%) was prepared by dissolving the blue powder (0.6 g) in n-methyl-2-pyrrolidone (20 mL). The solution was stirred for ~12 h for mixing. Following this, the solution was filtered to remove

any suspended particle and stored in room temperature. The shape and size of PANI molecules was modulated by tuning the process parameters during synthesis to infuse required physical and electrical properties for sensing.

Preparation of gold (III) chloride ($HAuCl_4$)/starch solution: The $HAuCl_4$/starch solution was prepared by mixing 500 µl of 0.001 M $HAuCl_4$ solution with 500 µl of 0.01% starch solution. The solution was stored at 2-8°C.

Fabrication of biosensors: Glass substrates were cut into the size of 1 cm × 1 cm with the help of diamond cutters. The substrates were washed thoroughly and dried by blowing pure argon gas. Following this, 40 µl PANI-EB solution was drop casted on the substrates and dried in vacuum oven for ~24 h at 45°C. Thereafter, 100 µl solution of $HAuCl_4$/starch was poured on the dried PANI-EB films and kept in vacuum oven at 45°C for ~12 h. The sensors were kept in vacuum desiccator at room temperature until further use. The composition (% w/w) of SAuNPs and PANI-ES in the nanocomposite was found to be ~4.75 and ~95.25, respectively. The thickness of the films was of order of ~260 µm while the size of the nanoparticles was ranging from 20 nm to 300 nm. The stability of the nanocomposite deposited on the sensors was confirmed by 10 cycles of cyclic voltammetry (CV) analysis using a two-electrode system in a range of -5 to 5 V. The deviation (hysteresis) of the current density between the first scan and the tenth scan is negligible. A negligible hysteresis helped in inferring that the nanocomposite was stable.

Preparation of the α-amylase solution: A number of solutions of varying concentration from 10 – 90 U/L of α-amylase were prepared by dissolving the required amount of enzyme in 1X phosphate buffer solution of pH 7.0. The solutions were freshly prepared for each measurement.

2.2.3. Methods

The schematic illustration in the Figure 2.1 shows the steps to fabricate the α-amylase biosensor. The non-conducting PANI-EB was synthesized following a standard protocol, as described in the experimental section. Thereafter, the film was coated on a glass substrate by drop-casting the PANI-EB solution, as shown in the Figures 2.1(a) and 2.1(b). Solubility of the non-conducting PANI-EB in the organic solvents helped in the drop-casting of the film. Since the conducting PANI-ES was sparingly soluble in most of the organic and inorganic solvents, we chose to cast the non-conducting PANI-EB film on the glass substrate. The FESEM image in the Figure 2.1(c) shows the surface textures of the non-conducting PANI-EB thin film. After coating the PANI-EB film, a specified amount of the mixture of $HAuCl_4$ and starch was dispensed on the PANI-EB surface, as shown in the Figure 2.1(d). Consequently, reduction of gold (Au) present in $HAuCl_4$/starch solution on PANI-EB film formed AuNPs on the film surface. The FESEM image in the Figure 2.1(e) shows the surface textures of the conducting PANI-ES thin film coated with SAuNPs in which a few of them are marked on the image with an arrow. The starch in the solution mixture acted as the stabilizing agent before bonding on the AuNPs to form SAuNPs. Furthermore, the addition of the acidic solution (pH of 5.2 at 25°C) of $HAuCl_4$/starch mixture on the surface of the non-conducting PANI-EB (low conductivity) infused the conductivity to the film because of the formation of the conducting PANI-ES (high conductivity) (Han et al. 2010;Wang et al. 2001). The change from PANI-EB to the conducting PANI-ES was indicated by the change of dark blue color of the film into dark green.

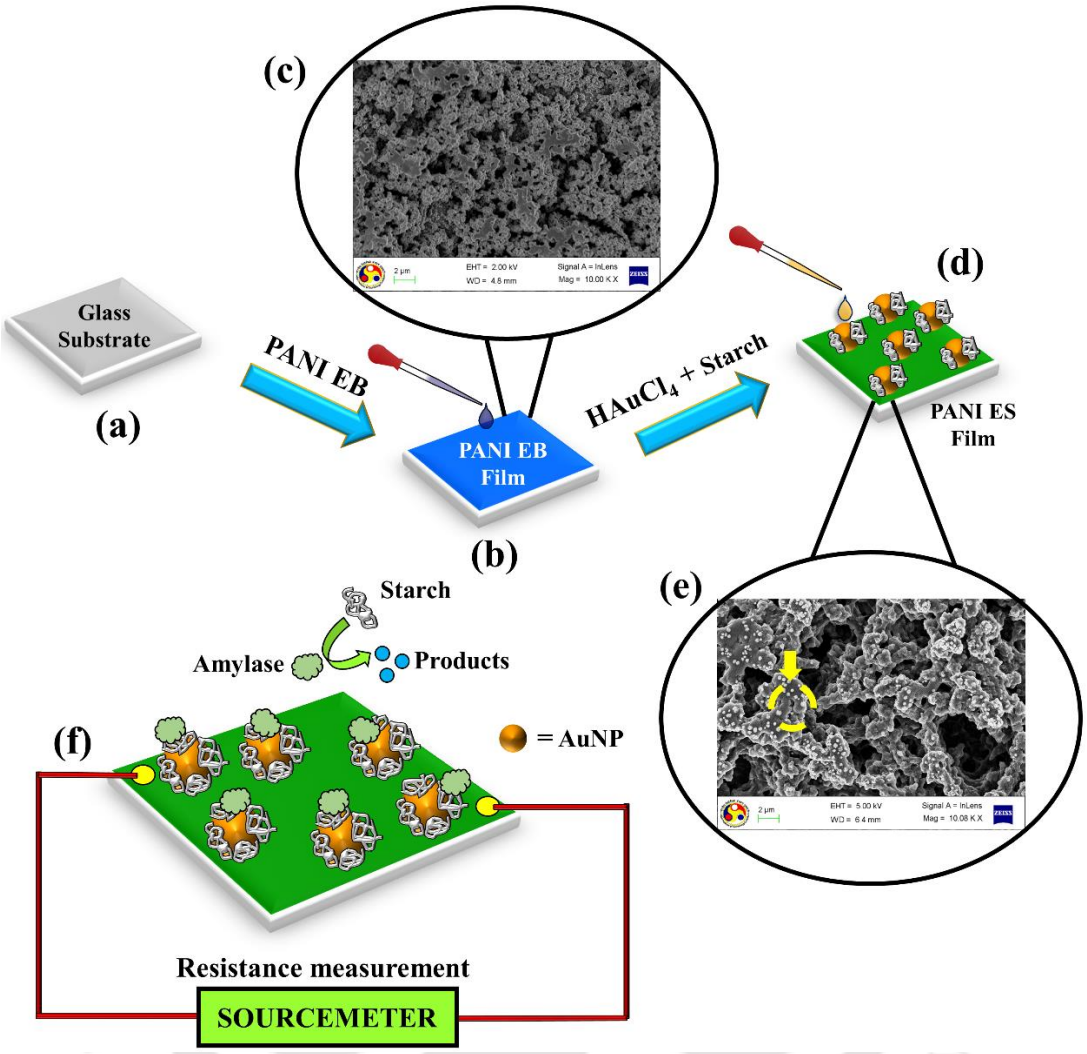

Figure 2.1: Images (a) and (b) schematically show the coating of a PANI-EB film on a glass substrate. Image (c) shows the FESEM images of surface textures of PANI-EB film. Image (d) shows the formation of SAuNPs on the surface of the film and conversion of PANI-EB to PANI-ES. Image (e) shows the FESEM image of surface textures of the conducting PANI-ES film coated with SAuNPs, marked on the image with arrow. Image (f) illustrates the scheme for measurement of sensor resistance by sourcemeter.

Following this, α-amylase solutions of different concentrations were dispensed on the biosensor and the change in the electrical resistance across the sensor was measured by connecting it with a commercially available sourcemeter, using the electrical contacts made with the conducting silver paste on the sensor (Figure 2.1(f)).

The FTIR analysis was performed after lifting of the targeted portions of the film from the glass substrate. The amounts of sample and KBr were kept constant in order to achieve a consistency in the FTIR results reported here.

For the UV-Vis spectroscopy, initially, a 500 µl 0.01% stock solution of starch was taken and nanoparticle synthesis (Deka et al. 2008) was carried out by adding 500 µl of 0.001 M $HAuCl_4$ and 400.0 µl of H_2O_2 to the starch solution. This process was followed by ultrasonication for ~20 min. Following this, aqueous α-amylase solution (90 U/L) was added to the prepared solution having starch coated gold nanoparticles (SAuNPs) and a time-dependent starch digestion study was performed with the help of the UV-Vis spectroscopy. In addition, as a control experiment, the time-dependent studies with the help of the UV-Vis spectroscopy were repeated for digestion of, bare starch-iodine complex (0.01% starch), bare AuNP, only iodine and SAuNPs in absence of Cl^- ions.

While performing the electrical characterization, the sensor was placed on a probe station stage and the initial resistance was measured using a sourcemeter (Model 2400, Keithley U.S.A) without the sample solution. Thereafter, 10 µl of sample solution was put on the sensor and after 60 s, the resistance was measured. The variation in the resistance of the PANI-ES coated with SAuNPs was studied at different concentration values of the α-amylase solution. The measurements were repeated five times for each concentration and the average resistance was reported.

For performing optical and materials characterization field emission scanning electron microscopy (FESEM, Supra 55, Zeiss, Oberkochen, Germany) was used to examine the surface morphology and elemental composition of the sensors. The pH of the solutions was measured with Cyber Scan pH 510 meter (Eutech Instruments). The pictures of the sensor

were taken by Nikon D5100 digital camera (Nikon Corp., Japan). The FTIR analysis was performed using Thermo Scientific Nicolet iS10 FT-IR spectrometer, U.S.A. UV-Vis spectroscopy was carried out using Perkin-Elmer Lambda 25 spectrophotometer, U.S.A. The Raman spectroscopy was done using the Horiba LabRam HR Evolution Raman spectrophotometer, Japan.

For performing the computational simulation, a two-dimensional (2-D) geometry was considered on the *x*-*y* plane, which comprised of a starch film of thickness h loaded with nine AuNPs (dia. 100 nm) resting on a PANI-ES film of thickness 0.5 μm. The width of the biosensor was chosen to be 5 μm along the *x*-coordinate. The 2-D geometry was divided into 11388 triangular elements (meshes) to perform a computational simulation employing COMSOL Multiphysics™. The steady state charge continuity equation, $\nabla.(-\sigma\nabla V + J_e) = 0$, was solved for the entire domain with appropriate boundary conditions. V_a = 10 mV at the zone of terminal metal contact, 0 V at the zone of the grounded portion, and insulation boundary condition in the remaining places. The notations σ, V, and J_e, and Q_j in the equation denote the electrical conductivity, electric field potential, electron current density, and the carrier charge, respectively. The commercial software COMSOL Multiphysics™ employs finite element method to solve the set of governing equations with the boundary conditions. The volume fraction (ϕ) of starch was obtained by evaluating the ratio of the area occupied solely by the starch film to the total area occupied by the starch and AuNPs. The electrical conductivity of PANI-ES and starch are 2.13 S/m and 5.06×10^{-6} S/m, respectively. (Abd El-Kader and Ragab 2013; Zareh et al. 2011) The electrical conductivity for AuNPs is 46.6×10^{6} S/m, as given in the material library of the COMSOL Multiphysics™ software. However, for more comprehensive study many other parameters such as, interfacial

resistance, doping effect etc., needs to be considered which would increase the complexity of the simulation. So, we have kept this for future scope of study

2.3. Results and Discussion

2.3.1 Reaction mechanism

In Figure 2.2, we propose a mechanism of SAuNP formation. It is well known that starch is a poly-hydroxylated macromolecule consisting of glucose units connected by glyosidic bonds to form amylose and amylopectin chains (Figure 2.2(a)).

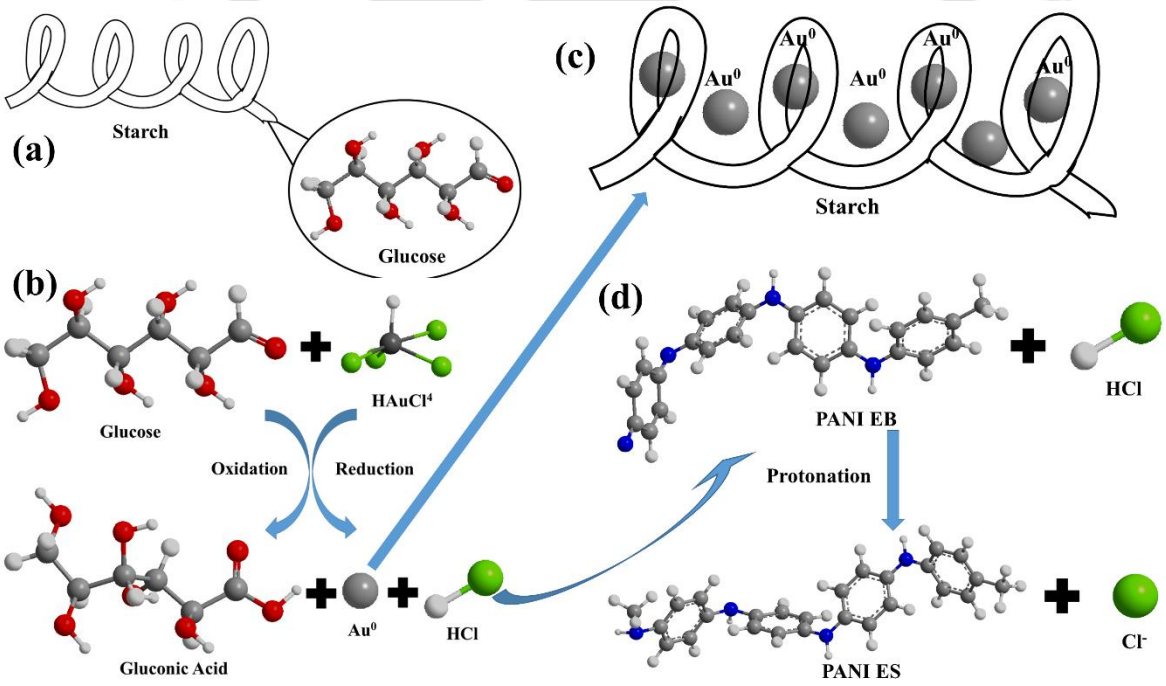

Figure 2.2: Image (a) shows starch consisting of glucose units. Image (b) shows the reduction of the $HAuCl_4$ by glucose to form AuNPs. Image (c) shows formation of SAuNPs and image (d) shows the conversion of PANI-EB to PANI-ES by HCl alongside having Cl^- on the film matrix.

In the present situation, during the reaction, a part of the starch molecules formed glucose owing to the partial hydrolysis of the glycoside bonds. (Wang and Copeland 2015; Wang et

al. 2003) Importantly, the hydroxyl groups of starch facilitated electrostatic bonding with Au^{3+} ions before folding around them to form a helical structure of polysaccharide (Chairam et al. 2009; Imberty et al. 1988; Jenkins and Donald 1995; Raveendran et al. 2003). In such a scenario, the aldehyde terminal of the glucose molecule reduced Au^{3+} ions to AuNPs while glucose was converted to gluconic acid (Figure 2.2(b), (Castillo-López and Pal 2014; Engelbrekt et al. 2009; Pasta et al. 2010). Subsequently, a stable starch-AuNPs composite was formed because of the interaction between the –OH group of the starch with the AuNPs, (Figure 2.2(c), (Engelbrekt et al. 2013; Katti et al. 2009; Tajammul Hussain et al. 2008). Further, while $HAuCl_4$ was reduced to produce SAuNPs particles, a large amount of HCl remained on the film matrix. The HCl in the polymer matrix protonated the non-conducting PANI-EB film and converted it into conducting PANI-ES film (Figure 2.2(d)). The excess Cl^- left in the polymer matrix catalysed the amylase-starch reaction when the samples loaded with α-amylase was dispensed on the sensor.(Engelbrekt et al. 2013) Importantly, presence of the Cl^- ions led to an improved response time of the biosensor (Bernfeld 1955; Levitzki and Steer 1974; Numao et al. 2002; Sky-Peck and Thuvasethakul 1977; Walker and Hope 1963).

2.3.2 Characterization of the sensor material and function

Figure 2.3(a) shows the XRD plots of the PANI-EB film on glass substrate (curve in black) and PANI-ES film with SAuNPs deposited on the surface (curve in red). While the former curve did not show any peak corresponding to the AuNPs, the later shows the presence of peaks at 2θ = 38.35°, 44.31°, and 64.75° to confirm the presence of AuNPs on PANI-ES. (Pillalamarri et al. 2005; Sarma and Chattopadhyay 2004; Zareh et al. 2011) The FTIR spectra in the Figure 2.3(b) shows the peaks for PANI-EB (curve in green) and PANI-ES coated with SAuNPs (curve in blue). The FTIR analysis was performed after lifting of the

targeted portions of the film from the glass substrate. The amount of sample and KBr were kept constant. The characteristic peaks for starch were found at, 1022, 1079, 1156 cm^{-1}, and the region at 1200 – 1500 cm^{-1} (curve in blue). (Snabe and Petersen 2002)

The details of the peaks for PANI-EB (curve in green) and PANI-ES coated with SAuNPs (curve in blue) are provided in the Table 2.2.

Table 2.2: Assignment of the FTIR spectra of PANI-EB and PANI-ES.(Dhivya et al. 2015)

No.	Wavenumber (cm^{-1}) PANI- EB	PANI-ES	Assignments
1	3425	3429	N-H stretch
2	2855	2917	Aromatic C-H stretch/NH_2^+
3	1602	1600	N=Q=N stretch
4	1499	1499	N=B=N stretch
5	1398	1296	C-N stretch
6	1172	1130	Aromatic C-N-C bending
7	824	824	C-H bending
8	758 and 697	702 and 608	C-C ring deformation
9	507	522	C-N-C ring deformation

Figure 2.3(b) confirmed that that the PANI-EB changed to PANI-ES due to protonation by the acidic $HAuCl_4$/starch solution. The starch shows bands at 3424 cm^{-1} corresponding to the stretching frequency of –OH group. Other absorption bands at 1652 cm^{-1} and 1411 cm^{-1} (curve in blue) are due to C–C and C–O stretching vibrations, respectively. The IR analysis also provided further clues of SAuNP formation on PANI-ES. For example, the plots also indicate the formation of the SAuNP composite because of the interaction of the –OH group of starch molecules with the AuNPs on the PANI-ES surface following the mechanism discussed previously in the Figure 2.2 (Engelbrekt et al. 2013; Katti et al. 2009; Tajammul Hussain et al. 2008). Further, the curve in pink in the Figure 2.3(b) shows the FTIR spectra of PANI-ES coated with SAuNPs after the reaction with α-amylase.

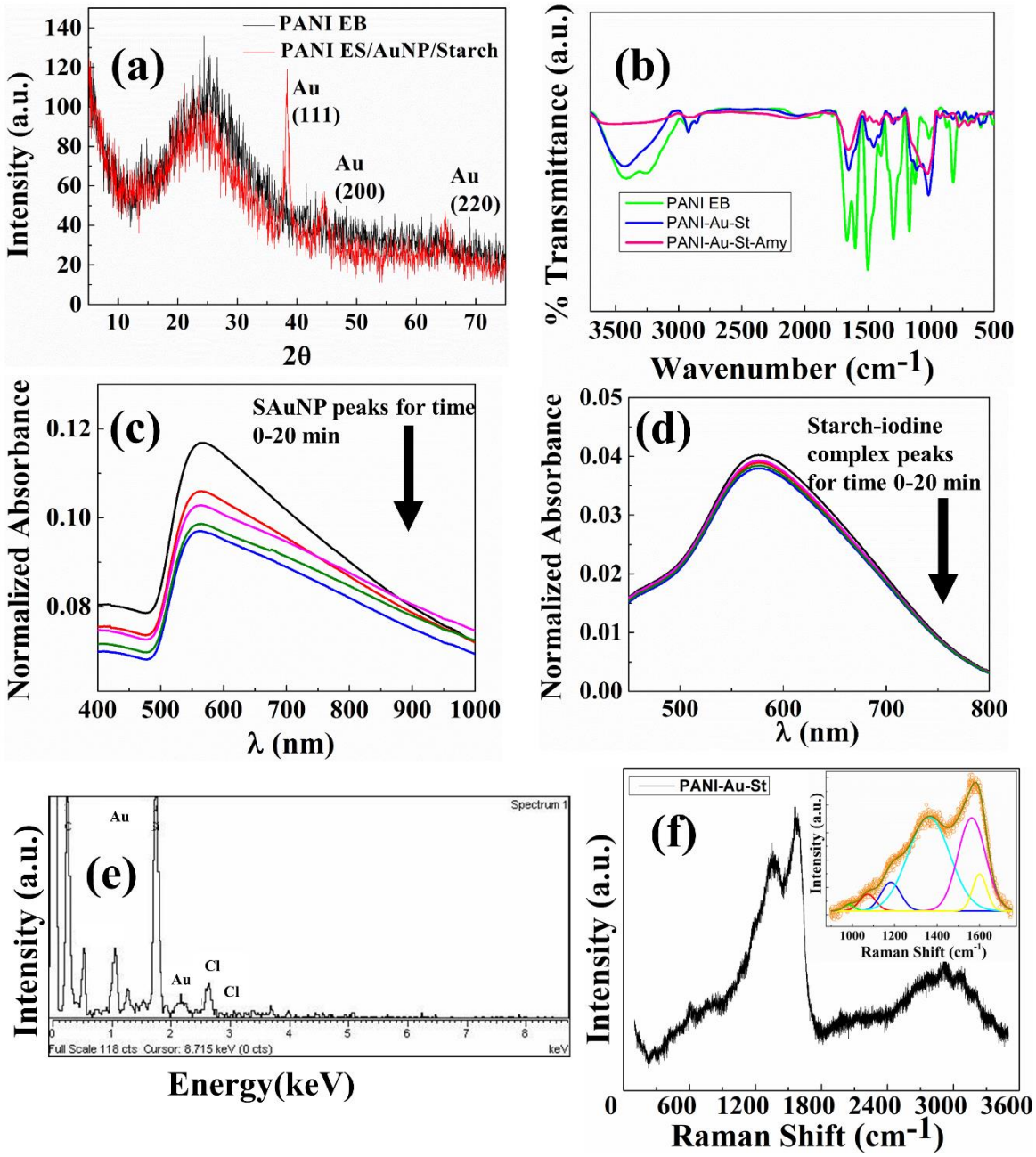

Figure 2.3: The XRD plots in the image (a) correspond to the PANI-EB (darker – black) and PANI-ES coated with SAuNPs (lighter – red). The plot (b) shows the IR spectra of the sensor. The image (c) shows the UV-Vis spectroscopy of α-amylase treated SAuNP composite at different time intervals, 0 min, 5 min, 10 min, 15 min, and 20 min, of starch digestion. The image (d) shows the UV-Vis spectra of starch-iodine complex at the same time intervals of digestion of bare starch. Image (e) shows the EDXS plot of the sensor surface depicting the elemental composition. Image (f) shows the Raman spectra of the sensor surface whereas the inset shows the peak fitting for 900 – 1760 cm^{-1}.

The change in the characteristic peaks suggested the digestion of starch on the surface of the AuNPs, which might have led to the reduction in the electrical resistance of the sensor (Deka et al. 2008). In order to further prove the aforementioned mechanism, we performed a time dependent starch digestion study employing UV-Vis spectroscopy. The plots in the Figure 2.3(c) show that the area under the curve for the SAuNP peak rapidly reduced with time due to the faster digestion of starch in presence of the AuNPs and Cl^- ions upon α-amylase addition. In comparison, the degradation of starch-iodine complex in absence AuNPs and Cl^- ions were found to be much slower, which was reflected in smaller reduction in the area under the curve with time corresponding to the starch-iodine peak, as shown in the Figure 2.3(d). Figure 2.3(e) shows the energy-dispersive x-ray spectroscopy (EDXS) of the sensor, which confirmed the presence of Cl^- on surface. The plot in Figure 2.3(f) shows the Raman spectroscopy of the sensor surface. The peak for gluconic acid at 1072 cm^{-1} (Al-Ogaidi et al. 2014; Kaminský et al. 2009) supports the conversion of glucose into gluconic acid during the reduction of Au^{3+} ions in $HAuCl_4$ into SAuNPs.

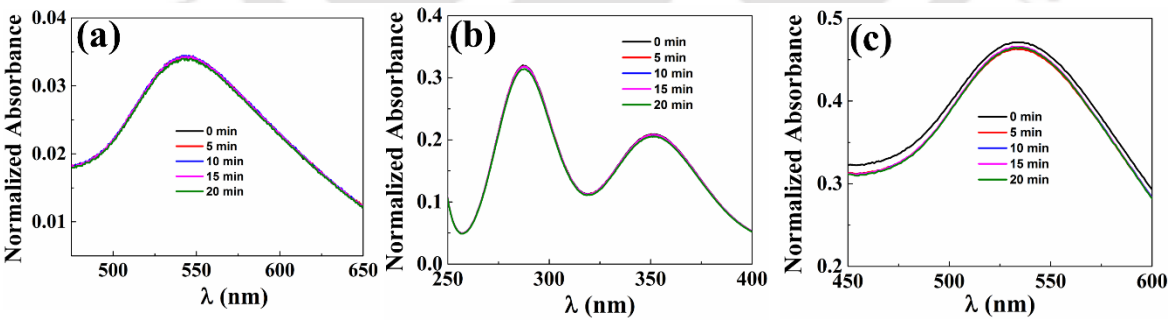

Figure 2.4: (a) shows the UV-Vis spectroscopy of interaction of α-amylase with AuNPs at different time intervals, 0 min, 5 min, 10 min, 15 min, and 20 min. The image (b) shows the UV-Vis spectroscopy of interaction of α-amylase with only iodine at the same time intervals. The image (c) shows the UV-Vis spectroscopy of α-amylase treated SAuNPs composite in absence of Cl^- ions.

Interaction of α-amylase with only AuNPs (Figure 2.4(a)), interaction of α-amylase with only iodine (Figure 2.4(b)) and α-amylase treated SAuNPs composite in absence of the Cl^-

ions (Figure 2.4(c)) were carried out as a part of control experiments. In these plots, the data were obtained after, t_0 = 0 min, t_1 = 5 min, t_2 = 10 min, t_3 = 15 min, and t_4 = 20 min, as indicated on the figure. The Figures 2.4(a) and 2.4(b) suggest that α-amylase did not interact with the bare AuNPs or the Iodine molecules. Further, the Figure 2.4(c) suggest that in the absence of Cl^- ions the starch digestion was much slower as compared to the kinetics shown in the Figure 2.3(c) where α-amylase decomposed SAuNPs in presence of the Cl^- ions. It may be noted here that the increase in the activity of α-amylase due to presence of Cl^- ions is a well-established fact (Levitzki and Steer 1974; Numao et al. 2002). The small sized Cl^- ions can easily fit into the cleft present in the enzyme, which brings in structural change resulting in the increased activity of the enzyme. Along these similar lines, the Figures 2.3(c) and 2.4(c) corroborate that Cl^- ions helped in the faster starch digestion from SAuNP. The starch digestion kinetics study obtained by the IR and UV-Vis spectroscopy together with EDXS suggested the presence of AuNPs and Cl^- ions were the major reasons behind, (i) the reduction in the electrical resistance with α-amylase loading and (ii) a smaller response time of sensor. Previous studies suggested that during the formation of the SAuNPs, the intrinsic electrical properties may change with time. (Zareh et al. 2011) In this direction, we characterized the electrical properties of the sensing materiel composed of polyaniline, AuNP, and starch. The experimental data provided in Table 2.3 uncover that while PANI-ES-AuNP showed an electrical resistance of about 200 kΩ the PANI-ES-SAuNP showed about 440 MΩ. Furthermore, in this regard the optimized concentrations, for the $HAuCl_4$ and starch, were acquired by employing a trial and error method. For example, initially, the $HAuCl_4$ concentration was fixed to 0.001M and the starch concentration was varied between 0.005% – 0.5% (w/v). In such a situation. It was noted, from the data provided in Table 2.4 that the resistance varied from very low to nearly open circuit resistance.

Table 2.3: Current output of PANI ES AuNP and PANI ES SAuNP

	Current (A)					
	Voltage (V)	Sensor 1	Sensor 2	Sensor 3	Sensor 4	Sensor 5
PANI ES AuNP	5	32.394×10^{-6}	27.262×10^{-6}	21.173×10^{-6}	12.766×10^{-6}	21.238×10^{-6}
PANI ES SAuNP	5	6.5615×10^{-9}	2.0584×10^{-9}	11.478×10^{-9}	28.6786×10^{-9}	7.887×10^{-9}

The primary set of experiments showed that at 0.01% starch loading the resulting resistance could reliably convert the entire range of the α-amylase concentration into the detectable resistances, which was in the quantifiable range of the signal-processing unit. The starch concentrations beyond 0.01% (w/v) was undetectable because the electrical resistances were rather large and out of measuring range of the signal-processing unit. The other set of trial experiments were done fixing the starch concentration to 0.01% (w/v) and then varying the $HAuCl_4$ concentration between 0.0005M – 0.005M. The experiments revealed that at 0.001M of $HAuCl_4$ loading, the resistances were detected and quantified by the signal processing unit whereas the $HAuCl_4$ loading beyond this level gave a very

Table 2.4: Current output using different conc. of starch in PANI ES SAuNP

	Current (A)					
Starch Conc.	Voltage (V)	Sensor 1	Sensor 2	Sensor 3	Sensor 4	Sensor 5
0.5	5	36.296×10^{-15}	30.108×10^{-15}	54.945×10^{-15}	39.986×10^{-15}	47.805×10^{-15}
0.1	5	6.5615×10^{-9}	2.0584×10^{-9}	11.4786×10^{-9}	28.6786×10^{-9}	7.8874×10^{-9}
0.005	5	9.104×10^{-6}	8.365×10^{-6}	10.333×10^{-6}	9.3119×10^{-6}	9.2053×10^{-6}

low resistance, near to the short-circuit resistance. The aforementioned experiments helped us in deciding the starch and $HAuCl_4$ loading to 0.01% (w/v) and 0.001M because these values ensured that the capacity of the signal-processing unit was utilized to the fullest for the detection of the α-amylase. Mixing the equal volumes of optimum 0.01% (w/v) starch and 0.001M $HAuCl_4$ solutions led to the optimized solution, which was dispensed on the

surface coated with PANI-EB to fabricate the sensors. The variation in initial resistance of the sensor was ~1% over six months', as illustrated in the Figure 2.5.

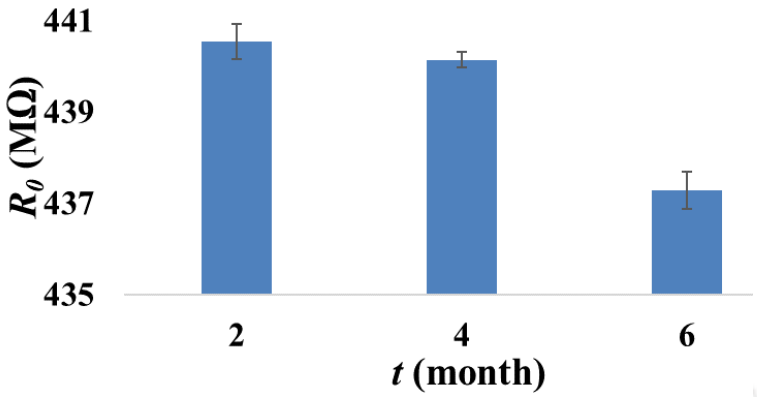

Figure 2.5: The image shows the variation in the electrical resistance (R_0) of a sensor with time (t).

2.3.3 Electrical Response of the sensor

The experimental setup shown in the Figure 2.6 was employed for measuring the change in resistance of the biosensor with the concentration of the aqueous α-amylase solution. Figure 2.6(a) shows the image of the sourcemeter, which measured the change in resistance. Figures 2.6(b) and 2.6(c) show that the electrical contacts were made with a conductive silver paste. Figure 2.6(d) depicts the change in normalized resistance (R/R_0) of the sensor with the variation in the α-amylase concentration (C). In the beginning of the experiments, the resistance of the PANI-ES film loaded with SAuNPs was evaluated as the base resistance R_0. The resistance (R) obtained after the addition of the aqueous α-amylase solution on the sensor was normalized with R_0 while plotting in Figure 2.6(d). It may be noted here that each experiment was repeated for five times and the deviation in the data was represented as the error bars in the Figure 2.6(d). The normal level of α-amylase in blood serum is between 24 – 85 U/L, which was the basis for the chosen concentration range in Figure 4(d). (Nater et al. 2005; Wilkins 2009) The figure shows that R/R_0 reduced when C increased in

the droplet dispensed on the sensor. A larger α-amylase loading depleted larger amount of starch present on the SAuNPs, which led to the reduction in resistance of the sensor. The variation of R/R_0 with C was employed as the calibration plot to detect unknown quantities of α-amylase in human serum. The triangular symbols of Figure 2.6(d) shows the results of the human serum samples alongside the calibration curve obtained. In this case, initially, we employed clinically approved samples and methodology involving the equipment Dimension RxL Max Integrated Chemistry System (SIEMENS), to obtain the activity of α-amylase in a sample of human serum (Chen et al. 2014; Fei et al. 2015). Thereafter, we dispensed the same sample to obtain the amount of α-amylase to form the proposed sensor using the calibration plot. In this regard, we dispensed the serum directly on the sensor without any further treatment. Figure 2.6(d) suggests that the α-amylase levels in the serum samples could be predicted accurately using the proposed sensor. Figure 2.6(e) shows the working prototype of the proposed α-amylase sensor. The prototype was composed of a biosensor, a sample stage, a SPU with a built-in sourcemeter, and a LC-RTD. Figure 2.6(f) illustrates the circuit diagram for the proposed POCT device in which the domain (i) corresponds to the open source microcontroller board, (ii) is the LC-RTD, and (iii) is the modified voltage divider circuit with the built-in sourcemeter to integrate the biosensor and microcontroller.

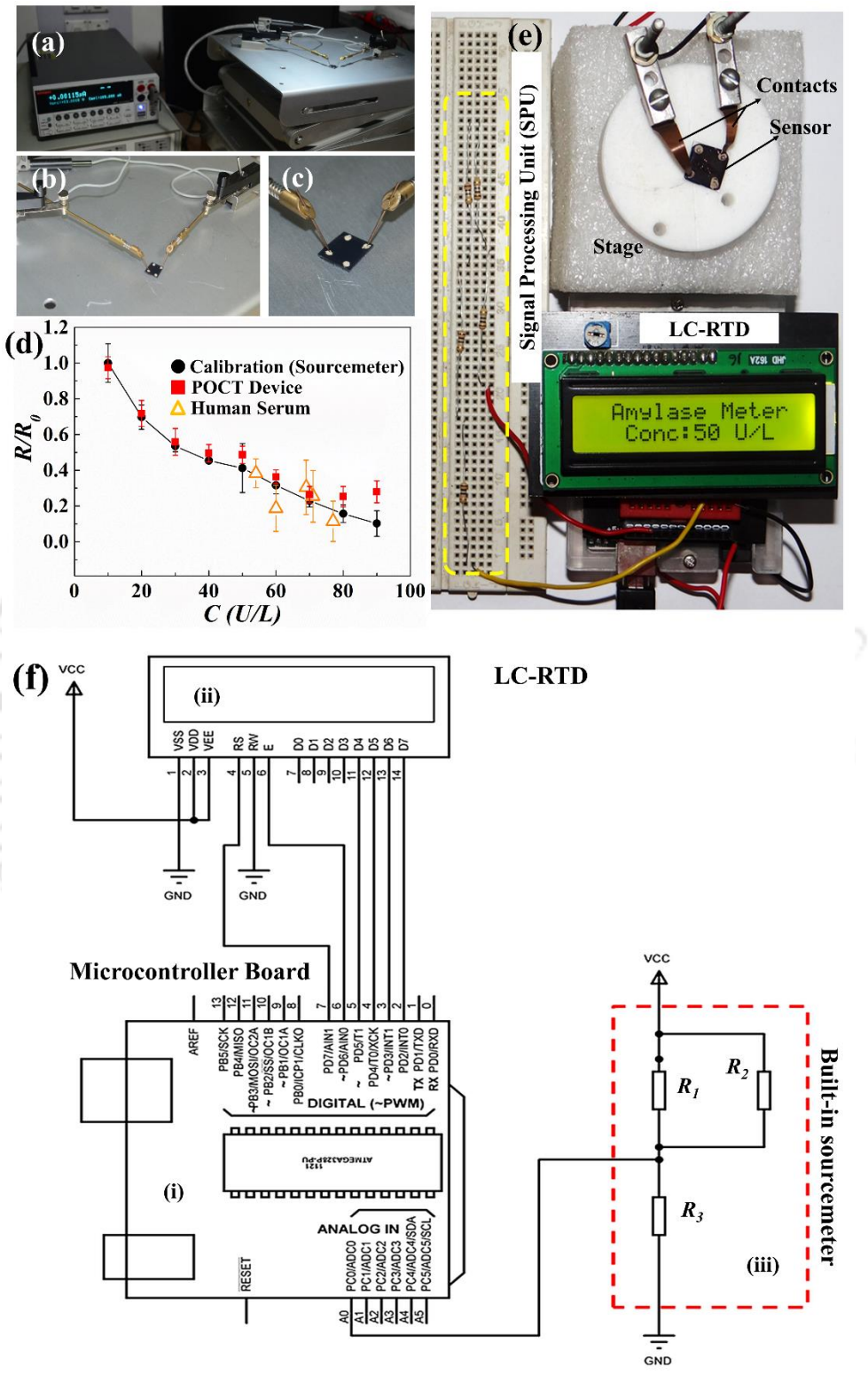

Figure 2.6: The image (a) shows the commercial sourcemeter for resistance measurement and the image (b) shows the silver paste electrical contacts on the sensor, which is magnified in image (c). The image (d) shows the variation in the normalized resistance (R/R_0) with α-amylase concentration in the analyte (C). The image shows the calibration

plot using the commercially available sourcemeter (circular symbols) using α-amylase solution prepared in the laboratory, the same data reproduced by the POCT device (square symbols), and the test data measured by the POCT device using human serum of unknown level of α-amylase (triangular symbols). Image (e) shows the photograph of the POCT device composed of a sensor, a sample stage, a signal-processing unit (SPU) with a built-in sourcemeter, and a liquid-crystal-real-time-display (LC-RTD). The image (f) illustrates the circuit diagram of the POCT device where, (i) corresponds to microcontroller board, (ii) LC-RTD, and (iii) voltage divider circuit with the built-in sourcemeter.

The microcontroller unit of the POCT device was loaded with the calibration data to perform the tests with human serum while the built-in sourcemeter transferred the electrical resistance directly to the controller. The circular and square symbols in the Figure 2.6(d) show that the POCT device was able to reproduce the electrical resistance of the biosensor obtained from the commercially available sourcemeter. Integration of this step helped in excluding the use of the commercial sourcemeter for resistance measurement, which in turn facilitated the lowering of the device cost and operation time as a POCT device. The Table 2.5 shows the typical comparison of the unknown level of α-amylase in human serum measured by the proposed methodology with the clinically approved protocol.

Table 2.5. Amylase in Serum using POCT and Commercial Devices.

No.	Amylase level in blood serum from clinically approved method (U/L)	Calibration curve (R/R_0)	POCT device (R/R_0)	POCT device (U/L)
1	54	0.37210	0.38337 ± 0.08061	52
2	60	0.31511	0.18647 ± 0.11237	75
3	69	0.26395	0.30468 ± 0.12866	61
4	71	0.22218	0.25431 ± 0.15227	66
5	77	0.18138	0.11454 ± 0.14471	87

The table suggests that the predictions by the POCT device was rather close with some deviations as compared to the clinically approved methodology. The deviations obtained in the proposed POCT methodology as compared to those obtained in the costly clinically approved methods could be rectified by to the optimization and improvement of the

proposed biosensor. Importantly, the tests involving human serum were carried out under the supervision of medical experts in a nearby diagnostic centre.

2.3.4 Computational Simulations to Estimate the Change in Resistance

The simulations suggested that the resistance of the sensor decreased with the decrease in the volume fraction (ϕ) of starch, obtained by evaluating the ratio of the area occupied solely by starch film to the total area occupied by the starch and AuNPs inside the starch layer, as shown in Figure 2.7. It is well known that starch is a material with small electrical conductivity. Thus, the presence of a thick layer of starch is bound to increase the effective total resistance of the sensor. However, with the addition of higher dosage of α-amylase, the depletion of higher amount of starch on the sensor caused the reduction in the effective resistance of the sensor, which was observed both experimentally and computationally as shown in the Figures 2.6(d) and 2.7.

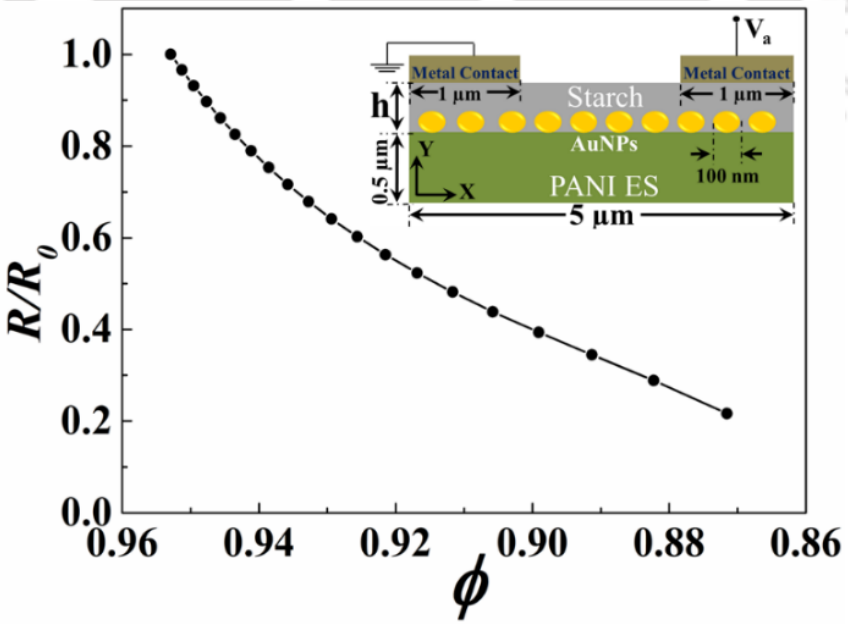

Figure 2.7. The variation in normalized resistance (R/R_0) with volume fraction (ϕ) of the starch layer. The value of ϕ was obtained by evaluating the ratio of the area occupied solely by starch film to the total area occupied by the starch and AuNPs. The inset shows the

schematic diagram with the dimensions of the sensor employed for the simulation in which V_a = 10 mV was the input voltage.

Although the comparison between the experimental and computational results was rather qualitative, the reduction in the resistance with the increase (reduction) in the dosage (amount) of α-amylase (starch) was found to be monotonic and linear. A detailed computational investigation on the exact characteristics of the sensing mechanism is kept as a future scope of research.

2.4. Conclusions

We report the fabrication of a simple, rapid, reliable, and economic POCT device for the detection of α-amylase enzyme in human serum. The device is composed of an electrical biosensor, a sample stage, a signal processing unit with a built in sourcemeter, and a real time display. The biosensor is composed of an electrically conducting PANI-ES thin film covered with starch-coated gold nanoparticles (SAuNPs). Experiments uncovered the pathways to SAuNP formation on PANI-ES, time-dependent starch digestion of the same with α-amylase loading, and the subsequent variation in electrical response. Presence of AuNPs and Cl^- ions on the biosensor surface helped in a rapid starch hydrolysis with α-amylase while the use of the conducting polymer film as substrate provided stability in obtaining the electronic signals.

The reduction in the resistance with the increase (reduction) in the dosage (amount) of α-amylase (starch) was monotonic and linear, which helped in calibrating the microcontroller unit. Since we employed a very selective and specific bio-reaction – starch hydrolysis by α-amylase, the POCT device was equally efficient in detecting the unknown level of α-amylase in human serum. The accuracy of the POCT device compared and contrasted with

a clinically approved method. Integration of the built-in sourcemeter facilitated *in-situ* measurement of electrical resistance, excluding the necessity of a commercial sourcemeter.

The proposed POCT device can be employed for the immediate detection of α-amylase in human serum, which helps in the diagnosis of pancreatitis, cancer, mumps, stress, and depression. With some simple modifications, the device can also be employed to detect α-amylase in serum, saliva, or sebum, which is kept as a future scope of research work.

References

Abd El-Kader, M.F.H., Ragab, H.S., 2013. Ionics 19(2), 361-369.

Ahn, C.H., Jin-Woo, C., Beaucage, G., Nevin, J.H., Jeong-Bong, L., Puntambekar, A., Lee, J.Y., 2004. Proc. IEEE 92(1), 154-173.

Al-Ogaidi, I., Gou, H., Al-kazaz, A.K.A., Aguilar, Z.P., Melconian, A.K., Zheng, P., Wu, N., 2014. Anal. Chim. Acta 811, 76-80.

Aluoch, A.O., Sadik, O.A., Bedi, G., 2005. Anal. Biochem. 340(1), 136-144.

Anderson, K.L., 2002. Anaerobe 8(5), 269-276.

Bandyopadhyay, D., Mandal, N., Dutta, S., 2016. A transmittance based system/kit for point-of-care quantification of biomerkers sample and use thereof.

Bashir, R., 2004. Adv. Drug Delivery Rev. 56(11), 1565-1586.

Battershell, V.G., Henry, R.J., 1990. J. Cereal Sci. 12(1), 73-81.

Bernfeld, P., 1955. Amylases, α and β. In: Colowick, S.P., Kaplan, N.O. (Eds.), Methods in Enzymology, Academic Press. pp. 149-158.

Bhattacharjee, M., Nemade, H.B., Bandyopadhyay, D., 2017. Biosens. Bioelectron. 94, 544-551.

Bhattacharjee, M., Pasumarthi, V., Chaudhuri, J., Singh, A.K., Nemade, H., Bandyopadhyay, D., 2016. Nanoscale 8(11), 6118-6128.

Bhattacharya, S., Jang, J., Yang, L., Akin, D., Bashir, R., 2007. J. Rapid Methods Autom. Microbiol. 15(1), 1-32.

Castillo-López, D.N., Pal, U., 2014. J. Nanopart. Res. 16(8), 2571.

Chairam, S., Poolperm, C., Somsook, E., 2009. Carbohydr. Polym. 75(4), 694-704.

Chavez, R.G., David, H., Metzner, E.K., Sigler, G.F., Winn-Deen, E.S., 1990. US Patent No. 4963479A.

Chen, Y.C., Chiou, C., Lin, M.-N., Lin, C.L., 2014. PLoS One 9(12), e115145.

Chin, C.D., Linder, V., Sia, S.K., 2007. Lab Chip 7(1), 41-57.

Cosnier, S., 1999. Biosens. Bioelectron. 14(5), 443-456.

Deka, J., Paul, A., Ramesh, A., Chattopadhyay, A., 2008. Langmuir 24(18), 9945-9951.

Dhivya, C., Vandarkuzhali, S.A.A., Radha, N., 2015. Arabian J. Chem.

Dutta, S., Mandal, N., Bandyopadhyay, D., 2016. Biosens. Bioelectron. 78, 447-453.

Engelbrekt, C., Jensen, P.S., Sørensen, K.H., Ulstrup, J., Zhang, J., 2013. J. Phys. Chem. C 117(22), 11818-11828.

Engelbrekt, C., Sorensen, K.H., Zhang, J., Welinder, A.C., Jensen, P.S., Ulstrup, J., 2009. J. Mater. Chem. 19(42), 7839-7847.

Fei, K., Xiangshu, H., Kun, X., 2015. Nanotechnology 26(40), 405707-405715.

Foo, A.Y., Bais, R., 1998. Clin. Chim. Acta 272(2), 137-147.

Gibbs, M.J., Biela, A., Krause, S., 2015. Biosens. Bioelectron. 67, 540-545.

Gogoi, S.K., Borah, S.M., Dey, K.K., Paul, A., Chattopadhyay, A., 2011. Langmuir 27(20), 12263-12269.

Gogoi, S.K., Paul, A., Chattopadhyay, A., 2012. RSC Adv. 2(9), 3642-3646.

González, C.F., Fariña, J.I., Figueroa, L.I.C., 2002. Enzyme Microb. Technol. 30(2), 169-175.

Grieshaber, D., MacKenzie, R., Vörös, J., Reimhult, E., 2008. Sensors 8(3), 1400-1458.

Han, J., Li, L., Guo, R., 2010. Macromolecules 43(24), 10636-10644.

He, D., Cai, Y., Wei, W., Nie, L., Yao, S., 2000. Biochem. Eng. J. 6(1), 7-11.

Homola, J., 2008. Chem. Rev. 108(2), 462-493.

Imberty, A., Chanzy, H., Pérez, S., Bulèon, A., Tran, V., 1988. J. Mol. Biol. 201(2), 365-378.

Janowitz, H.D., Dreiling, D.A., 1959. Am. J. Med. 27(6), 924-935.

Jenkins, P.J., Donald, A.M., 1995. Int. J. Biol. Macromol. 17(6), 315-321.

Kaminský, J., Kapitán, J., Baumruk, V., Bednárová, L., Bouř, P., 2009. J. Phys. Chem. A 113(15), 3594-3601.

Katti, K.K., Kattumuri, V., Bhaskaran, S., Katti, K.V., Kannan, R., 2009. Int. J. Green Nanotechnol. 1(1), B53-B59.

Kricka, L.J., 2001. Clin. Chim. Acta 307(1–2), 219-223.

Kricka, L.J., Nozaki, O., Heyner, S., Garside, W.T., Wilding, P., 1993. Clin. Chem. 39(9), 1944-1947.

Levitzki, A., Steer, M.L., 1974. Eur. J. Biochem. 41(1), 171-180.

Li, D., Kaner, R.B., 2005. J. Am. Chem. Soc. 128(3), 968-975.

Mahosenaho, M., Caprio, F., Micheli, L., Sesay, A., Palleschi, G., Virtanen, V., 2010. Microchim. Acta 170(3-4), 243-249.

Malhotra, B.D., 2001. Conducting Polymers in Molecular Electronics. Handbook of Polymers in Electronics, pp. 393-423. Rapra Technology Limited. pp.393-423.

Mallick, K., Witcomb, M., Scurrell, M., 2006. Gold Bull. 39(4), 166-174.

Manz, A., Graber, N., Widmer, H.M., 1990. Sens. Actuators, B 1(1–6), 244-248.

Murayama, T., Tanabe, T., Ikeda, H., Ueno, A., Bioorg. Med. Chem. 14(11), 3691-3696.

Nater, U.M., Rohleder, N., Gaab, J., Berger, S., Jud, A., Kirschbaum, C., Ehlert, U., 2005. Int J Psychophysiol 55(3), 333-342.

Nguyen, N.-T., 2007. Fabrication Issues of Biomedical Micro Devices. In: Ferrari, M., Bashir, R., Wereley, S. (Eds.), BioMEMS and Biomedical Nanotechnology, Springer. pp. 93-115.

Numao, S., Maurus, R., Sidhu, G., Wang, Y., Overall, C.M., Brayer, G.D., Withers, S.G., 2002. Biochemistry 41(1), 215-225.

Pandey, P.C., Mishra, A.P., 1988. Analyst 113(2), 329-331.

Pasta, M., La Mantia, F., Cui, Y., 2010. Electrochim. Acta 55(20), 5561-5568.

Pillalamarri, S.K., Blum, F.D., Tokuhiro, A.T., Bertino, M.F., 2005. Chem. Mater. 17(24), 5941-5944.

Raveendran, P., Fu, J., Wallen, S.L., 2003. J. Am. Chem. Soc. 125(46), 13940-13941.

Robles, T.F., Shetty, V., Zigler, C.M., Glover, D.A., Elashoff, D., Murphy, D., Yamaguchi, M., 2011. Biol. Psychol. 86(1), 50-56.

Saliterman, S., 2006. Emerging BioMEMS Technology. Fundamentals of BioMEMS and Medical Microdevices, First ed. Wiley. pp. 413-448.

Sarma, T.K., Chattopadhyay, A., 2004. Langmuir 20(11), 4733-4737.

Sasaki, T., Noel, T.R., Ring, S.G., 2008. J. Agric. Food Chem. 56(3), 1091-1096.

Shetty, V., Zigler, C., Robles, T.F., Elashoff, D., Yamaguchi, M., 2011. Psychoneuroendocrinology 36(2), 193-199.

Sia, S.K., Kricka, L.J., 2008. Lab Chip 8(12), 1982-1983.

Singh, A.K., Dey, K.K., Chattopadhyay, A., Mandal, T.K., Bandyopadhyay, D., 2014. Nanoscale 6(3), 1398-1405.

Singh, S., Solanki, P.R., Pandey, M.K., Malhotra, B.D., 2006. Sens. Actuators, B 115(1), 534-541.

Sky-Peck, H., Thuvasethakul, P., 1977. Ann. Clin. Lab. Sci. 7(4), 310-317.

Snabe, T., Petersen, S.B., 2002. J Biotechnol. 95(2), 145-155.

Svens, E., Käpyaho, K., Tanner, P., Weber, T.H., 1989. Clin. Chem. 35(4), 662-664.

Swaroop, V., Chari, S.T., Clain, J.E., 2004. J. Am. Med. Assoc. 291(23), 2865-2868.

Tahir, Z.M., Alocilja, E.C., Grooms, D.L., 2005. Biosens. Bioelectron. 20(8), 1690-1695.

Tajammul Hussain, S., Iqbal, M., Mazhar, M., 2008. J. Nanopart. Res. 11(6), 1383.

Takeuchi, T., Matsushima, T., Sugimura, T., 1975. Clin. Chim. Acta 60(2), 207-213.

Tamer, U., Seçkin, A.İ., Temur, E., Torul, H., 2011. Int. J. Electrochem. 2011, 1-7.

Trojanowicz, M., Krawczyński vel Krawczyk, T., 1995. Microchim. Acta 121(1-4), 167-181.

van Staden, J.F., Mulaudzi, L.V., 2000. Anal. Chim. Acta 421(1), 19-25.

Vo-Dinh, T., Cullum, B., 2000. Fresenius' J Anal Chem 366(6-7), 540-551.

Walker, G.J., Hope, P.M., 1963. Biochem. J. 86(3), 452-462.

Wang, H., Mu, S., 1999. Sens. Actuators, B 56(1–2), 22-30.

Wang, J., Neoh, K.G., Kang, E.T., 2001. J. Colloid Interface Sci. 239(1), 78-86.

Wang, S., Copeland, L., 2015. Crit. Rev. Food Sci. Nutr. 55(8), 1081-1097.

Wang, Y.J., Truong, V.-D., Wang, L., 2003. Carbohydr. Polym. 52(3), 327-333.

Warshaw, A.L., Fuller, A.F., 1975. N. Engl. J. Med. 292(7), 325-328.

Watanabe, T., Yamamoto, A., Nagai, S., Terabe, S., 1998. Electrophoresis 19(13), 2331-2337.

Whitesides, G.M., 2006. The origins and the future of microfluidics. Nature 442(7101), 368-373.

Wilkins, L.W., 2009. Blood Chemistry tests. Diagnostic Tests Made Incredibly Easy!, Lippincott Williams & Wilkins. pp. 29-252.

Wu, C., Brunelle, F., Harnois, M., Follet, J., Senez, V., 2012. Micro Electro Mechanical Systems (MEMS), IEEE 25th International Conference on, pp. 777-780.

Yager, P., Domingo, G.J., Gerdes, J., 2008. Annu. Rev. Biomed. Eng. 10(1), 107-144.

Yager, P., Edwards, T., Fu, E., Helton, K., Nelson, K., Tam, M.R., Weigl, B.H., 2006. Nature 442(7101), 412-418.

Yamaguchi, M., Deguchi, M., Wakasugi, J., 2005. Biomed Microdevices 7(4), 295-300.

Yamaguchi, M., Deguchi, M., Wakasugi, J., Ono, S., Takai, N., Higashi, T., Mizuno, Y., 2006. Biosens. Bioelectron. 21(7), 1007-1014.

Yamaguchi, M., Kanemaru, M., Kanemori, T., Mizuno, Y., 2003. Biosens. Bioelectron. 18(5), 835-840.

Yamaguchi, M., Kanemori, T., Kanemaru, M., Takai, N., Mizuno, Y., Yoshida, H., 2004. Biosens. Bioelectron. 20(3), 491-497.

Zajoncová, L., Jílek, M., Beranová, V., Peč, P., 2004. Biosens. Bioelectron. 20(2), 240-245.

Zareh, E.N., Moghadam, P.N., Azariyan, E., Sharifian, I., 2011. Iran. Polym. J. 20(4), 319-328.

Zhang, Z., Seitz, W.R., O'Connell, K., 1990. Anal. Chim. Acta 236, 251-256.

Zou, C.-S., Zhou, M., Xie, G.M., Luo, P., Xiong, X.-L., Xu, H.J., Zheng, J., 2008. Chinese J. Anal. Chem. 36(9), 1217-1220.

CHAPTER 3

Paper-Based *α*-Amylase Detector for Point-of-Care Diagnostics

Contents

भारतीय प्रौद्योगिकी संस्थान गुवाहाटी
Indian Institute of Technology Guwahati

ABSTRACT

We report the fabrication of a paper-sensor for quantitative detection of α-amylase activity in human blood serum. Pieces of filter papers were coated with starch-iodine solution leading to an intense blue coloration on the surface. Dispensing α-amylase solution on the starch-iodine coated paper reduced the intensity of the color because of starch-hydrolysis catalyzed by amylase. The variation in the intensity of the color with the concentration of amylase was estimated in three stages: (i) initially, the paper-surface was illuminated with a light emitting diode, (ii) then, the transmitted (reflected) rays emitted through (from) the paper were collected on a photoresistor, and (iii) the variations in the electrical resistance of the photoresistor were correlated with the amylase concentration in the analyte. The resistance of photoresistor decreased monotonically with increase in the amylase concentration because the intensity of the reflected (transmitted) rays collected from (through) the paper increased with reduction in the color intensity on paper surface. Since a very selective and specific bio-reaction was employed to detect the activity of amylase, the sensor was found to be equally efficient in detecting unknown quantities of amylase in human blood serum. The reported sensor has shown the potential to graduate into a point-of-care detection tool for α-amylase.

This chapter is published in *Biosensors and Bioelectronics.* **78**, 447-453 (2016). This work is done with collaboration of Ms. Satarupa Dutta, M. Tech, Department of Chemical Engineering, Indian Institute of Technology Guwahati.

3.1. Introduction

Quantitative estimation of biomarkers for close monitoring of the health conditions has become an essential part of contemporary human life (Chen et al. 2015; Chin et al. 2007; Mao and Huang 2012; Martinez et al. 2010b)The glucometer, blood pressure meters, and pregnancy kits are already commercially available to fulfil some of the necessities. However, there are other important biomarkers for which either there is no such technique available for quantitative estimation (Peeling 2006) or the presently available measuring techniques are rather costly and time consuming (Haschek et al. 2013). Further, the facilities associated with the tests are available only through the centralized pathological agencies, which fail to fulfil the immediate necessities of a significantly large number of populations across the globe (Haschek et al. 2013; Peeling 2006). In this situation, the next 'tipping point' is anticipated to be the cost-effective point-of-care diagnostic tools aided by the efficacies of micro or nanotechnology (Chin et al. 2011; Ellerbee et al. 2009; Li et al. 2014a; Li et al. 2014c; Martinez et al. 2008a; Yetisen et al. 2013). As per World Health Organization (WHO) guidelines, ASSURED – affordable, sensitive, specific, user-friendly, rapid and robust, equipment free, and deliverable, healthcare is the need of the hour (Chin et al. 2012; Costa et al. 2014).

Among other important biomarkers, activity of α-amylase (endo-1,4-α-d-glucan glucanohydrolase, EC 3.2.1.1) in different body fluids requires regular monitoring because abnormal values of this enzyme in saliva, urine, sebum or blood serum indicate diseased state of health. Amylase is produced in human pancreas and salivary glands to hydrolyze starch into simple sugars such as glucose, maltose, and limit dextrin (Metzler 2012). A trace amount of this enzyme is always found in most of the body fluids and a healthy

human body contains α-amylase in the range 25–85 U/L (units/litre) in the blood serum (Donofrio and Labus 2009). While the increased level of amylase indicates the onset of acute pancreatitis, pancreatic cancer, salivary gland infection, bile duct blockage, or gastroenteritis, the reduced level indicates pancreatic or kidney malfunctioning, and toxemia in pregnancy (Donofrio and Labus 2009). There are number of methods available to estimate amylase activity in body fluids, which encompass spectrophotometry (Attia et al. 2014; Gella et al. 1997; van Staden and Mulaudzi 2000), colorimetry (Foo and Bais 1998), fluorometry (Murayama et al. 2006; Zhang et al. 1990), isoelectric focusing (Takeuchi et al. 1975), electrokinetic processes (Watanabe et al. 1998), chromatography (Battershell and Henry 1990), weight based detections (Sasaki et al. 2008), electrochemical methods (Mahosenaho et al. 2010; Sakač and Sak-Bosnar 2012; Sakač et al. 2011; Yamaguchi et al. 2005; Zajoncová et al. 2004), electromagnetic sensing (Wu et al. 2007), and immunological methods (Svens et al. 1989). However, the most popular, robust, and accurate method of estimation of α-amylase in human serum involves spectrophotometry (Chavez et al., 1990), which is expensive, non-portable, and requires skilled personnel for operation and analysis. Unfortunately, point-of-care detection tool for α-amylase in human body fluids is yet to appear in the market.

Recent studies suggest that, the paper based diagnostic tools can lead to the development of simple point-of-care devices for monitoring of environmental parameters, quality of food products, immunoassays, and human health condition (Li et al. 2014b; Liana et al. 2012; Martinez et al. 2007). The popularity of the paper-based micro analytical devices (μ-PADS) is attributed to the advantages associated with lower cost, easy disposability, biodegradability, and portability (Ballerini et al. 2012; Cate et al. 2015; Cheng et al. 2010a; Cheng et al. 2010b; Dungchai et al. 2009; Fu et al. 2010; Li et al. 2012; Martinez

2011; Martinez et al. 2010a; Martinez et al. 2008b; Pelton 2009; Wang et al. 2012; Zhao and van der Berg 2008). Further, the compatibility of the cellulosic materials with the biomarkers makes them ideal candidate for biomedical applications (Li et al. 2012). For example, while blood group detection, for ages we know that the agglutinated red blood cells cannot pass through a porous paper matrix indicating a positive interaction between antibody and antigen while the non-agglutinated blood can disperse easily through the paper structure indicating a negative interaction (Then et al. 2015). Furthermore, the white color serves as an excellent background for the colorimetric assays employing the paper as substrate.

Herein, we report the fabrication of a paper-sensor for quantitative estimation of α-amylase in human blood serum. The schematic illustration in Figure 3.1 shows the steps to fabricate the α-amylase sensor. Initially, a Prussian blue colored starch-iodine (SI) solution was coated on the paper-surface. Following this, the aqueous α-amylase solution was dispensed on the SI coated paper, which led to hydrolysis of starch molecules and subsequent fading of the blue color. Thereafter, the paper-surface was illuminated with a light emitting diode (LED) source (Sorouraddin and Saadati 2010) and the transmitted (reflected) rays emitted through (from) the paper were collected on a photoresistor. The variations in the electrical resistance of the photoresistor were correlated with the change in color intensity and amylase concentration. The sensor showed remarkable potential to graduate into a point-of-care device for the rapid detection of α-amylase because it could faithfully reproduce amylase level in human blood serum when compared with a standard testing methodology.

3.2. Experimental Section

3.2.1. Materials

Starch $(C_6H_{10}O_5)_n$, potassium iodate (KIO_3), and iodine (I) were procured from Merck (India). Porcine α-amylase enzyme was procured from Sigma-Aldrich (India). 10X phosphate buffer, L-ascorbic acid ($C_6H_8O_6$), and potassium iodide (KI) were procured from SRL (India). Filter papers (diameter: 125 mm) were obtained from Whatmann (India). The chemicals above were of analytical grade and used without any further processing. Milli-Q grade water was used in the experiments unless stated otherwise.

3.2.2. Preparation of solutions

The solutions employed for experiments were freshly prepared. The optimized concentrations for the starch and iodine were obtained by a systematic trial and error method. For example, in the first trial, the iodine concentration was fixed to 0.2% and the starch concentration was varied between 0.05% – 4%. It may be noted here that the photoresistor employed for the experiments had light (dark) resistance in the range of 5 – 200 kΩ (0.6 – 10 MΩ). The first set of trial experiments showed that until 2% starch loading the photoresistor could faithfully convert the optical signal into the electrical resistance because the measured values were less than 200 kΩ. The concentrations of starch beyond 2% could not be detected owing to the fact that the electrical resistances were rather large (>200 kΩ). The other set of trial experiments began with fixing the starch concentration to 2% and then varying the iodine concentration between 0.05% – 0.4%. The experiments uncovered that until 0.2% of the iodine loading the photoresistor could reliably convert the optical signal into the electrical one whereas the iodine loading beyond this level could not be detected because they were out of range. The

aforementioned trial runs helped us in fixing the starch and iodine loading to 2% (w/v) and 0.2% (w/v) because these values ensured that the capacity of the photoresistor was exploited to the fullest for the detection of the amylase. Mixing the equal volumes of optimum 2% (w/v) starch and 0.2% iodine solutions led to the blue colored solution, which was dispensed on the paper surface to fabricate the sensors. As discussed earlier, the optimized concentrations of starch and iodine solutions were found to be 2% (w/v) and 0.2% (w/v) respectively. The 2% (w/v) starch solution was prepared by adding 0.2 g starch in 10 ml distilled water followed by a controlled heating to obtain a transparent solution. The Lugol's 5% iodine stock solution was prepared by dissolving 10% (w/v) potassium iodide and 5% (w/v) iodine in water. The stock solution was diluted to 0.2% (w/v).

The α-amylase solutions of concentrations ranging between 10 – 110 U/L (22 U = 1 mg) were prepared by dissolving the required amount of enzyme in 1X phosphate buffer solution of pH 7. Ascorbic acid stock solution was prepared by dissolving 5 mg L-ascorbic acid in 1 ml distilled water and then the stock solution was diluted to 2 mg/dL. Experiments were carried out to optimize the concentration and volume of potassium iodate solution to be used and they are described in detail in the supplemental information. The optimized concentration of 5 mg/ml potassium iodate solution was prepared by dissolving potassium iodate in water. The potassium iodate solution was mixed with ascorbic acid solution (2 mg/dL) in 2:1 volume ratio to allow oxidation of ascorbic acid to dehydroascorbic acid. The potassium iodate treated ascorbic acid solutions were mixed with α-amylase solutions in proportions corresponding to human blood serum to investigate the effect of ascorbic acid.

3.2.3. Methods

The schematic illustration in the Figure 3.1 shows the steps to fabricate the α-amylase sensor. Initially, the filter papers were cut into pieces of dimension, 1 cm × 1 cm. Following this, equal quantities (v/v) of starch and Lugol's iodine were mixed to obtain the dark blue colored SI solution. Thereafter, 60 µl of SI solution was dispensed on the paper, which led to a dark blue colored coating on the surface of the paper, as shown in the image (I) of Figure 3.1. The dark blue colored paper kit loaded with SI was then dried and preserved in the vacuum desiccator at room temperature. Later, 5 µl of the α-amylase solutions of different known concentrations were dispensed on the SI coated paper kit (image (I)) before keeping them in the incubator at 37 $^{\circ}$C for about 15 min.

The SI coated paper kits showed fading of the dark blue coloration with increase in the concentration of α-amylase, which was estimated by an experimental set up consisting of a LED source, a photoresistor (LDR, PMTC), and a digital multimeter (Mastech, India, range: 0 – 2 MΩ ± 1.0%). The images (II) and (III) in Figure 3.1 highlights two different types of experimental measurements of the amylase levels in the reflected and transmitted modes. Initially, the paper-surface was illuminated with the help of a LED source. Following this, the reflected rays from the paper-surface were collected on a photoresistor, as shown in the image (II). The transmitted rays emitted through the paper-surface were also collected on another photoresistor, as shown in the image (III). The electrical resistance of the photoresistor for different SI coated paper was measured with the help of a digital multimeter for both the transmitted and reflected rays. Thereafter, 5 µl α-amylase solutions of known concentrations (10 – 110 U/L) were dispensed on the SI loaded paper kits before incubating for 15 min at 37°C. Finally, the changes in the electrical resistance

of the photoresistor were noted for different α-amylase concentrations for both the transmitted and reflected rays. Measurements were repeated for five times for each amylase concentration to assure consistency in the measurements.

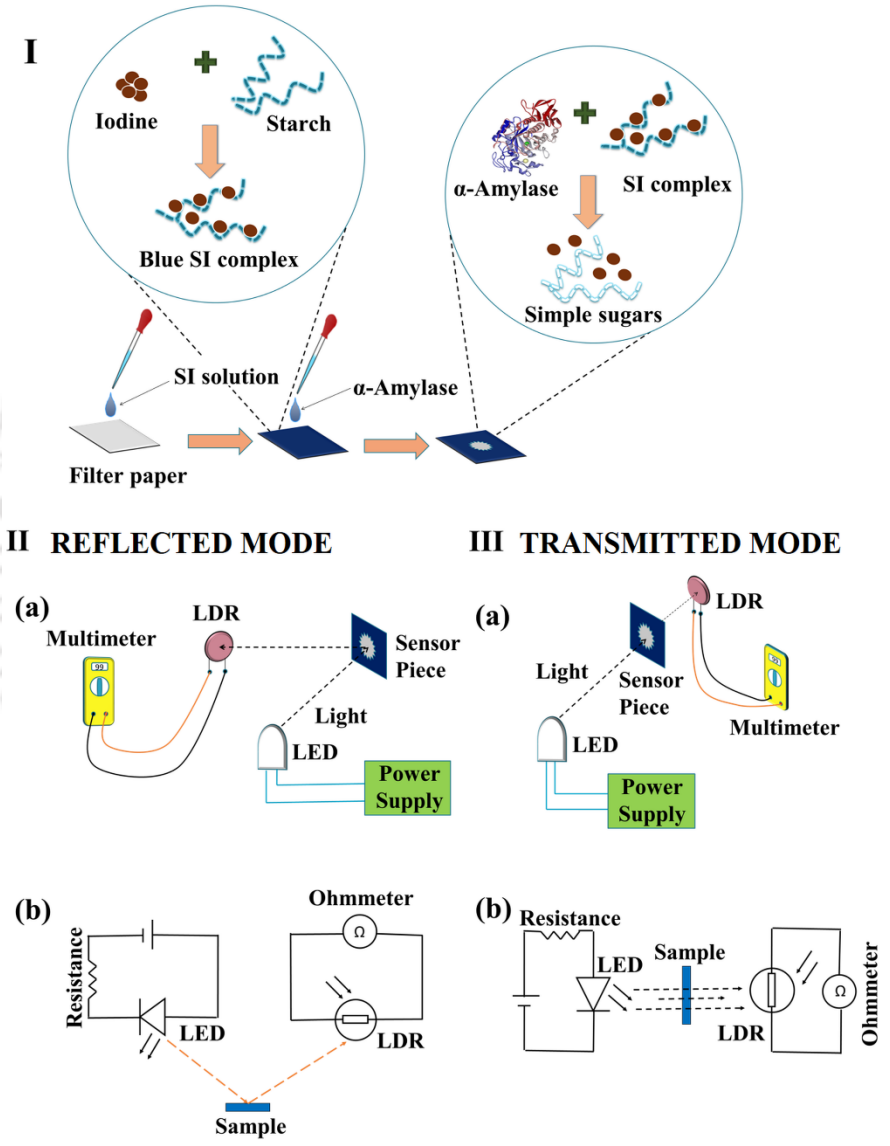

Figure 3.1: (I) Schematic illustrations of the steps to fabricate paper-sensor. (II) Reflection mode – images (a) and (b) show the experimental setup and corresponding circuit diagram for resistance measurement. (III) Transmitted mode – images (a) and (b) show the experimental setup and the corresponding circuit diagram for resistance measurement. The notation LDR (LED) represents photoresistor or photodetector (light emitting diode).

The electrical resistances measured for the virgin SI coated paper kits before the addition of the analytes were termed as R_i^T and R_i^R for the transmitted and reflected modes, respectively. The electrical resistances measured for the transmitted and reflected modes after the addition of analytes were termed as, R_f^T and R_f^R, respectively. The differences in resistances before and after the addition of the amylase were normalized by the initial resistances, R_i^T and R_i^R, to obtain the reported variables, $\Delta R_N^T = (R_i^T - R_f^T)/R_i^T$ and $\Delta R_N^R = (R_i^R - R_f^R)/R_i^R$ for the transmitted and the reflected modes.

For performing optical and materials characterization field emission scanning electron microscopy (FESEM, Supra 55, Zeiss, Oberkochen, Germany) was used to examine the surface morphology and elemental composition of the sensors. The pH of the solutions was measured with Cyber Scan pH 510 meter (Eutech Instruments). The pictures of the sensor were taken by Nikon D5100 digital camera (Nikon Corp., Japan). The FTIR analysis was performed using Thermo Scientific Nicolet iS10 FT-IR spectrometer, U.S.A. UV-vis spectroscopy was carried out using Perkin-Elmer Lambda 25 spectrophotometer, U.S.A.

3.3. Results and Discussion

3.3.1 Reaction mechanism

In the present study, we employed a selective and specific bio-reaction to detect the activity of α-amylase because the objective was to develop a sensor having equal sensitivity towards human body fluids such as the saliva, urine, or blood serum. The sensors were developed based on colorimetric effects originating from two different reactions.

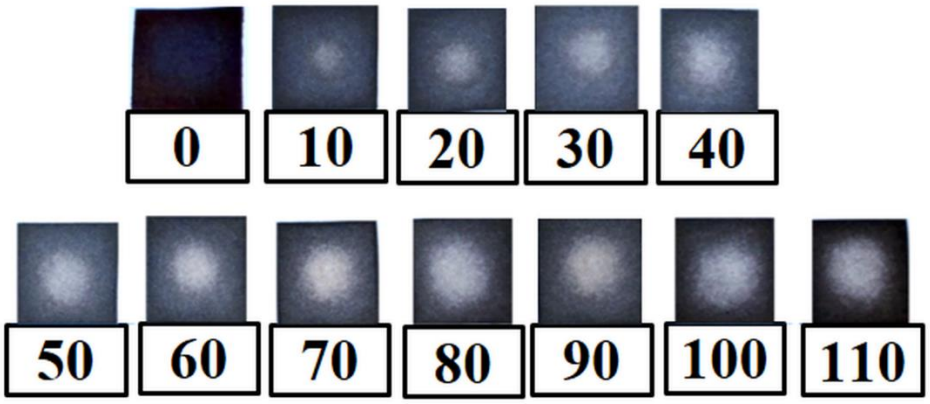

Figure 3.2: Top views of the paper-sensors in which the numbers indicate the concentration of α-amylase in units/litre (U/L) in the analyte. The first image corresponds to the SI coated paper-sensor before amylase was added while the other images were taken after the addition of different concentration of α-amylase solution.

The reaction between starch and Lugol's iodine led to the dark blue colored SI complex (Gibson et al. 1997; Metzler 2012; Minick et al. 1991; Teitelbaum et al. 1980; Wilding 1965). The first image in the Figure 3.2 shows the typical appearance of the sensors from the top when SI solutions were coated on the paper. Following this, when α-amylase analyte was dispensed on these SI coated paper-sensors, the enzyme cleaved the α-1,4 glycosidic bonds of the starch molecules to form simple sugars (Metzler 2012). The intensity of the blue colored complex reduced not only because of the breaking of the SI complex but also due to the evaporation of iodine as the simple sugars formed due to the reaction did not bind with it. The images in the Figure 3.2 depict the fading of the blue color with increase in concentration of α-amylase in the analyte. A temperature effect study on the evaporation of iodine was also carried out as the reported α-amylase detector is expected to be integrated with a point-of-care testing device under the ambient conditions. Since the temperature under ambient condition varies widely depending upon the geographical location, evaporation of iodine from the paper surface can be a serious

issue with the variations in the temperature. Thus, we performed experiments to identify the extent of evaporation of iodine from the paper surface from 20°C until 40°C. For this purpose, initially, freshly prepared 80 U/L amylase solution was dispensed on five different sets of SI coated paper-sensors and the sets were kept at temperatures of 20°C, 25°C, 30°C, 35°C, and 40°C, respectively, for 15 minutes. There after ΔR_N^T was calculated for each of the sample and plotted in the plot shown in figure 3.3 (b).

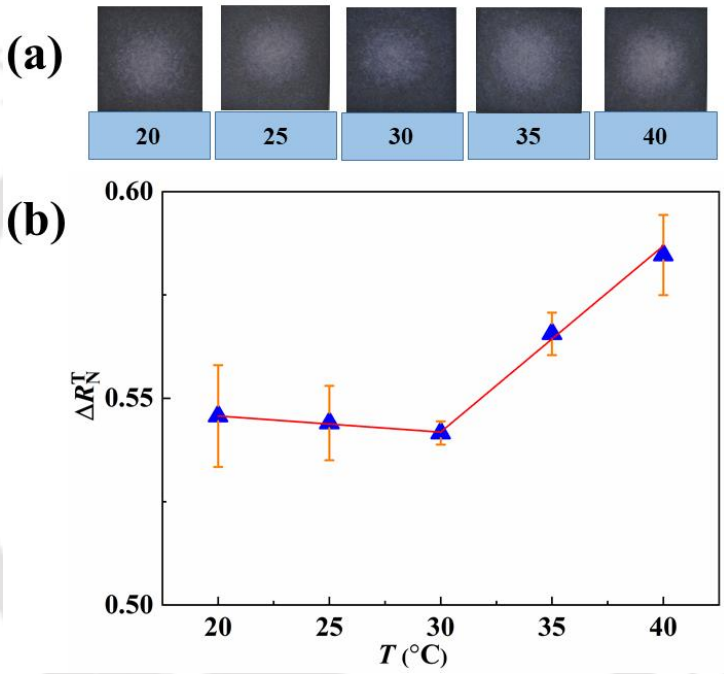

Figure 3.3: (a) Top views of the paper-sensors in which the numbers indicate temperatures in °C. (b) Variations in the normalized resistance differences (ΔR_N^T) with temperature (T) for the transmission mode. Equal amount of α amylase (80 U/L) has been dispensed on the sensors.

Image (a) in the Figure 3.3 shows the top views of these paper-sensors at different temperatures. Image (b) in the Figure 3.3 shows the variations in ΔR_N^T with T, which corroborates that the loss of iodine due to thermal evaporation was minimal. Figure 3.3 suggests that the variation in the temperature in the range of 20-40°C does not alter the

iodine loading much on the surface of the paper and had little effect on the evaporation of iodine.

3.3.2 Characterization of the sensor material and function

A detailed FTIR analysis was performed to study the reactions on the paper surface. For this, we coated a SI film on a glass substrate and another SI film on another glass substrate followed by addition of α-amylase.

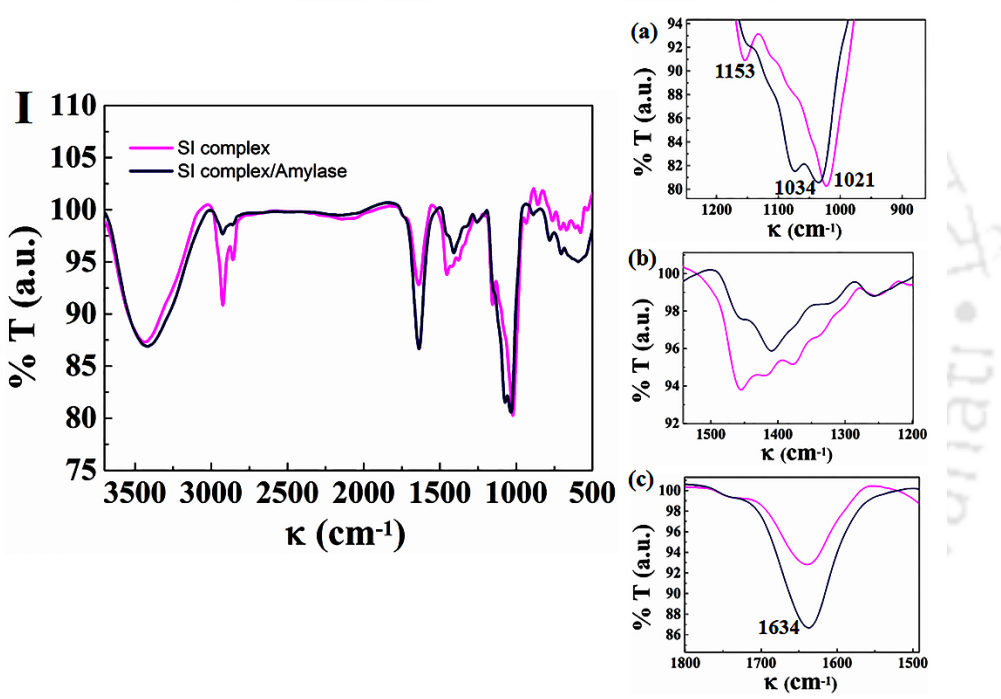

Figure 3.4: (I) The light (dark) colored curve shows the FTIR spectra (%Transmittance (T) to wavenumber (κ)) of SI complex before (after) the addition of α-amylase solution on the paper-sensor coated with SI complex. Images (a) – (c) show the magnified regions of the image (I).

The samples for the FTIR analyses were prepared by lifting equal mass from these two films, which later helped in comparing the intensities of the peaks during the analysis. Even the mass of potassium bromide added to the samples for the FTIR study was kept identical. The FTIR spectra for the SI complex before and after the addition of α-amylase

are shown by the curves with lighter and darker shades in Figure 3.4. The peaks around 1153 – 904 cm^{-1} for C-O and C-C stretching modes were observed in magnified plot (a) and image (I). The image (a) also showed the presence of the starch specific peaks at 1021 and 1153 cm^{-1}. Weakening of the peak intensities at 1034 and 1154 cm^{-1} were observed in image (a), which indicated starch hydrolysis in presence of amylase (Krieg et al. 1996). The peaks between 1474 – 1199 cm^{-1} were attributed to the bending modes of O-C-H, C-C-H, C-O-H angles, as shown in the images (I) and (b). The reduction in intensity of the peaks between 1500 – 1200 cm^{-1} in image (b) was caused due to the broken glycoside linkages after the starch hydrolysis by amylase. (Lambert 2011) The increased water peak at 1634 cm^{-1} in figure (c) indicated water penetration into the film.

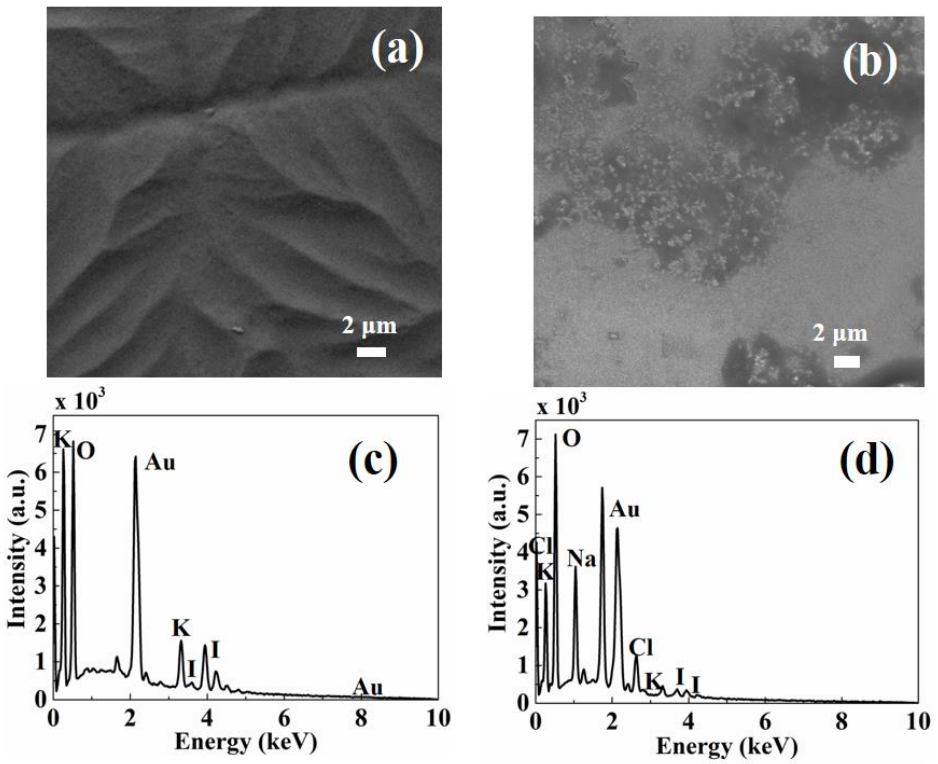

Figure 3.5: Images (a) and (b) show the FESEM micrographs of the paper-surface having the SI coating before and after the addition of α-amylase while images (c) and (d) show the corresponding EDX data.

The FESEM images and the corresponding EDX data shown in the Figure 3.5 confirmed that the color change was indeed due to the hydrolysis of the starch molecules. The images (a) and (b) show the surface morphologies of the paper coated with the SI complex before and after the amylase treatment. In image 3.5 (a) the frills of the SI film is visible where as in image 3.5 (b) the white and black portion suggest the hydrolysis of the SI film. Again, the EDX data shown in the images **(**c) and (d) suggest that there was net reduction in the iodine weight from 20.51% to 4.58 % before and after the amylase treatment on the SI coated paper, which suggested evaporation of the iodine from the paper surface after the starch hydrolysis.

3.3.3 Electrical Response of the sensor

Figure 3.6 shows variations in normalized resistance differences for transmitted (ΔR_N^T) and reflected (ΔR_N^R) modes with the variation in α-amylase concentration (C). Initially, the electrical resistances from the photoresistor were obtained for the SI loaded paper-sensors before the addition of α-amylase solutions for both the transmitted (R_i^T) and reflected (R_i^R) modes. Thereafter, the electrical resistances were measured for paper-sensors after addition of the analytes for both the transmitted (R_f^T) and reflected (R_f^R) modes. Finally, ΔR_N^T and ΔR_N^R were evaluated for each sensor. Image (a) in the Figure 3.6 shows the results obtained for the reflected mode while the images (b) and (d) show the same for the transmitted mode. Image (a) suggests that the increase in amylase loading (C) in analyte increased starch hydrolysis on the paper-surface, which led to the higher fading of the dark blue coloration. Thus, with increase in C the difference in resistance, $\left(R_f^R - R_i^R\right)$ increased. The discoloration of the paper surface increased the intensity of reflected rays to the photoresistor. Since the resistance of a photoresistor decreased with increase in the

light exposure, the normalized change in the resistance (ΔR_N^R) also increased with *C*. The images (b) in Figure 3.6 shows that the normalized change in resistance (ΔR_N^T) increased with *C* in transmitted mode. Hydrolysis of starch by α-amylase produced simple sugars and released iodine vapor from the paper surface to create more open space for light transmission. Thus, the electrical resistance of the photoresistor reduced with increase in α-amylase activity and subsequently, the normalized change in resistance (ΔR_N^T) also increased. It is important to mention that there was no effect of sunlight or ambient light as the experiment was carried out inside a dark room. Also, the sensor holder was made with black colour plastic material so as to absorb all the stray light. Further, the equation and R^2 value for figure 3.6 (a) is $y = \exp(-4.90842 + 0.02611\,x)$ and 0.98, respectively. Similarly, the equation and R^2 value for figure 3.6 (b) is $y = \exp(-0.80514 + 0.00376\,x)$ and 0.97, respectively.

Experiments were also carried out with human serum to test the efficiency of the paper sensor in estimating the amylase levels in the real samples. It may be noted here that all the tests with human serum were carried out in a nearby diagnostic center under the supervision of medical experts following standard protocols for pathological tests which includes stringent safety measures during the tests and waste disposal after the tests. Initially, the amylase levels of different serum samples were measured employing the standard protocol for the instrument, Dimension RxL Max Integrated Chemistry System, SIEMENS. Following this, we used the same samples on the paper-sensors and measured the change in resistance employing the transmitted mode. It is well known that human

serum contains ascorbic acid (vitamin C) in trace amounts (0.4 – 1.5 mg/dL) alongside amylase (Burtis et al. 2012). Importantly, presence of ascorbic acid inhibits the starch-

iodine reaction because it readily oxidizes in presence of iodine to form dehydroascorbic acid (Burgess and Davidson 2014; Sharma et al. 1990; Sigmann and Wheeler 2004). Thus, it was essential to neutralize the ascorbic acid present in the blood samples before we employed the SI coated paper-sensors. For this reason, we pre-treated the human serum with optimum volume of potassium iodate (KIO_3) solution to oxidize ascorbic acid (Sigmann and Wheeler 2004). The optimum volume of aqueous KIO_3 solution to be mixed with human serum to neutralize the effects of ascorbic acid was found to be 1:2 (volume of ascorbic acid: volume of KIO_3). We employed UV-Vis spectroscopy to determine these optimal loadings. The image (a) and (b) of **Figure 3.7** shows the peaks at around 260 nm and 280 nm for pure ascorbic acid (2 mg/dl) and KIO_3 (5 mg/ml) respectively, obtained from the UV-Vis spectroscopy (Kleszczewska and Misiuk, 1999). It may be noted here that the range of ascorbic acid in human serum is found to be ~ 0.4 – 1.5 mg/dl as mentioned earlier, we prepared a 2 mg/dl aqueous solution of ascorbic acid, which was around the maximum limit of ascorbic acid that could be present in the human serum. Following this, in order to optimize the volume of KIO_3, UV-Vis spectroscopy was performed using different volume ratios of ascorbic acid and KIO_3, as shown in the Figure 3.7.

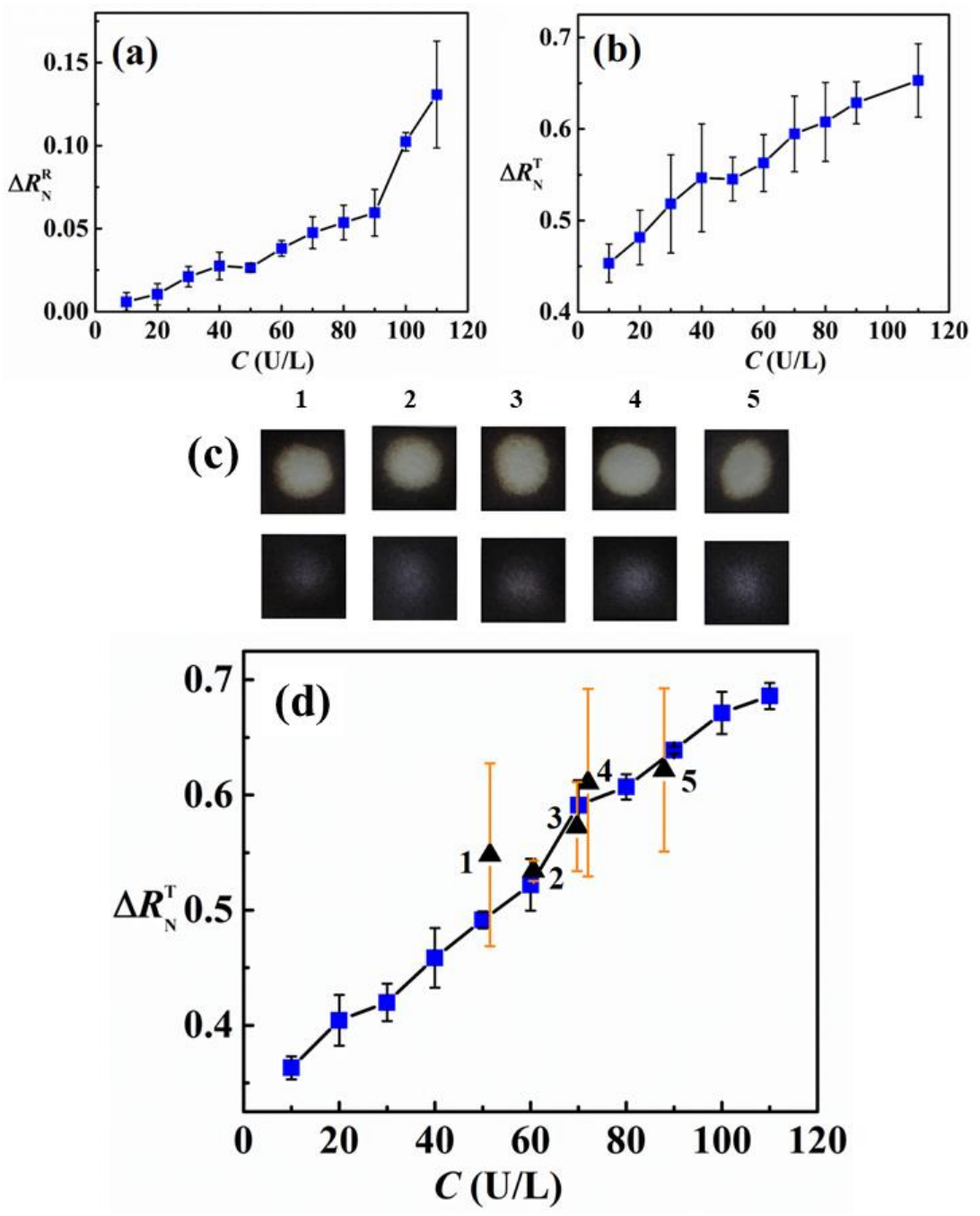

Figure 3.6: Variations in, (a) the normalized change in resistance (ΔR_N^R) with concentration of α-amylase (C) for the reflectance mode, and (b) normalized change in resistance (ΔR_N^T) with C for the transmission mode. (c) The images of the paper-sensors show the colorimetric change when blood serums of different α-amylase loading were dispensed. The first (second) row shows the results without (with) the pre-treatment of KIO_3. (d) The variation in ΔR_N^T with C in transmission mode when the initial analyte was composed of a mixture of ascorbic acid and α-amylase and then were pre-treated with KIO_3 before dispensing on the paper-sensor. The square (triangular) symbols show the plot with known (unknown) amylase concentration in the analyte (human serum).

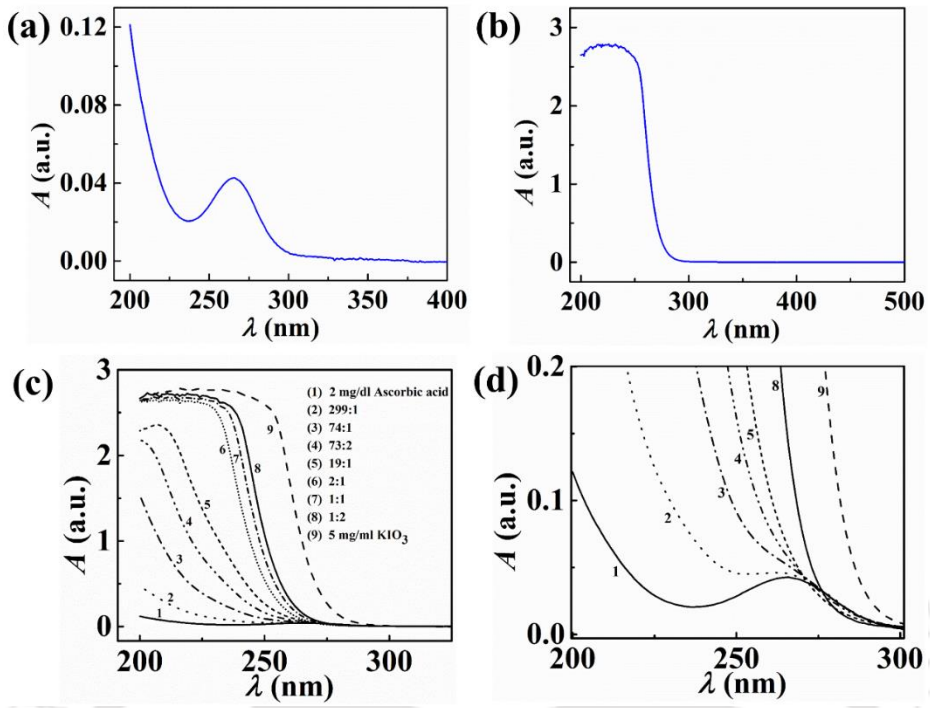

Figure 3.7: UV-Vis spectra showing the variations in % absorbance (*A*) with wavelength (*λ*). Image (a) shows the same of pure ascorbic acid (2 mg/dl) while image (b) is of pure KIO_3 (5 mg/ml). Image (c) represents mixture of ascorbic acid - KIO_3 solutions in which the curves 1 and 9 represent pure ascorbic acid (2 mg/dl) and KIO_3 (5 mg/ml) respectively. Curves 2 – 8 represent mixtures (v/v) of ascorbic acid and KIO_3 as mentioned in the line legend. Image (d) shows the magnified regions of image (c).

Curves 1 and 9 in this plot represent the plots for pure ascorbic acid and KIO_3 while the curves 2 – 8 represent the ratios 299:1 to 1:2 of the volumes of ascorbic acid to KIO_3, respectively. The plot suggests that with increase in the proportion of aqueous KIO_3 volume, the peak of ascorbic acid progressively diminished. In particular, we observed that with the volume ratios 2:1, 1:1 and 1:2 of ascorbic acid to KIO_3 there was complete quenching of the ascorbic acid peak, as shown in the images (c) and (d). Since the amount of ascorbic acid content in blood serum varies between individuals, an excess KIO_3 solution with 1:2 volume ratio of ascorbic acid to KIO_3 was employed for the experiments to neutralize the effect of ascorbic acid with the SI complex. Thereafter, we dispensed a drop (5 μl) of this KIO_3 pre-treated human serum on the paper-sensor before measuring the

change in resistance in the transmitted mode. Figure 3.6(c) shows the images of the paper-sensors when the human serum was dispensed without (1st row) and with (2nd row) pre-treatment. Clearly, presence of ascorbic acid in human serum inhibited the sensor performance because the amylase level could not be measured from the first row of Figure 3.6(c). The sensors showed larger degree of the fading of the SI coating on the surface due to the combined effects of ascorbic acid and amylase.

Table 3.1. Amylase in Serum using POCT and Commercial Devices.

No.	Amylase level in blood serum from clinically approved method (U/L)	ΔR_N^T	$\Delta R_{NE}^T \pm error$
1	28	0.422	0.438 ± 0.041
2	32	0.436	0.396 ± 0.026
3	60.6	0.536	0.534 ± 0.004
4	69	0.564	0.572 ± 0.019
5	72	0.577	0.611 ± 0.041
6	87.9	0.630	0.622 ± 0.035
7	93	0.648	0.693 ± 0.006

However, after removal of the ascorbic acid through pre-treatment of the human serum with KIO_3, the paper-sensor regained sensitivity, as can be observed in the second row of Figure 3.6(c). Figure 3.6 (d) summarizes the performance of the paper-sensor as compared to a standard method for amylase detection. The discrete triangular points on the Figure 3.6(d) and the subsequent numbers on the Table 3.1 suggest that the predictions from the paper-sensors were very similar to that obtained from the standard methods. Further, the Figure 3.6(d) shows that the amylase levels obtained from the serum were very close to the calibration curve for the transmitted mode of measurement. Concisely, the results shown in this figure and the table highlight the potential of the proposed sensor for point-of-care detection of amylase levels in the human serum.

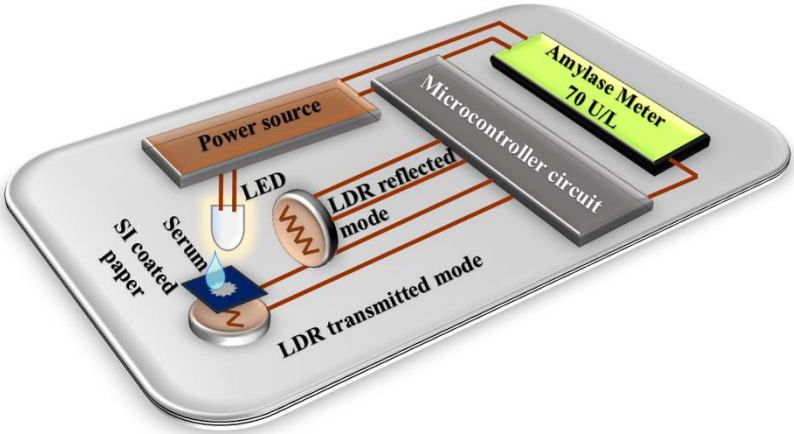

Figure 3.8: Schematic illustration of the proposed device for simple, fast, reliable, economic, and point-of-care detection of amylase level in human blood serum.

Figure 3.8 shows a typical schematic diagram of the point-of-care prototype for amylase detection. The device is envisioned to measure the change in the color intensity of the SI coated paper in both the reflected and transmitted modes. The illuminator LED and the photodetector (LDR) are placed strategically to capture both the reflected and transmitted rays from the sensor and obtain the analog data. The microcontroller circuit is expected to convert the analog data obtained from the photoresistors and translate into a digital output for the display of the amylase level.

3.4. Conclusions

We report the fabrication of a simple, rapid, reliable, and economic paper based optical α-amylase detector. The detector is calibrated over 10-110 U/L of α-amylase concentration. The operating principle of is based on the change in color intensity of starch-iodine solution with the variation in the amylase activity in the analyte. The study showed a facile way to measure the change in the color intensity on a paper with the help of a LED light

source and a photoresistor, integrated in two different arrangements, reflected and transmitted modes. The variation in the concentration of amylase was correlated with the change in the resistance of the photoresistor. In the reflected mode, the increased amylase loading in the analyte led to the fading of the dark blue color on the paper which in turn increased the intensity of the reflected rays collected on the photoresistor to reduce its resistance. In contrast, evaporation of iodine from the paper-surface led to the pore opening when larger amount of starch hydrolyzed in presence of a larger quantity of amylase in the analyte. This eventually increased the intensity of the transmitted rays to reduce the resistance of the photoresistor in the transmitted mode. The change of resistance of the photoresistor could easily be correlated to the amylase loading in the analyte for both the reflected and transmitted modes. Since we employed a very selective and specific bio-reaction to detect the activity of the α-amylase, the sensor was found to be equally responsive towards human blood serum. However, the blood serum needed a pre-treatment with potassium iodate in order to destroy the trace of ascorbic acid present in the blood serum. Comparison of the results obtained from the newly developed sensor with one of the standard procedures available for pathological detection of amylase showed a remarkable similarity. The proposed methodology is expected also to work for the other body fluids such as saliva, sebum, or urine, which is kept as a future scope of research work.

References

Attia, M.S., Zoulghena, H., Abdel-Mottaleb, M.S.A., 2014. Analyst 139(4), 793-800.

Ballerini, D., Li, X., Shen, W., 2012. Microfluid. Nanofluid. 13(5), 769-787.

Battershell, V.G., Henry, R.J., 1990. J. Cereal Sci. 12(1), 73-81.

Burgess, A.E., Davidson, J.C., 2014. J. Chem. Educ. 91(2), 300-304.

Burtis, C.A., Ashwood, E.R., Bruns, D.E., 2012. Tietz Textbook of Clinical Chemistry and Molecular Diagnostics. Elsevier Health Sciences. pp. 482

Cate, D.M., Adkins, J.A., Mettakoonpitak, J., Henry, C.S., 2015. Anal. Chem. 87(1), 19-41.

Chen, Y.-H., Kuo, Z.-K., Cheng, C.M., 2015. Trends Biotechnol. 33(1), 4-9.

Cheng, C.M., Martinez, A.W., Gong, J., Mace, C.R., Phillips, S.T., Carrilho, E., Mirica, K.A., Whitesides, G.M., 2010a. Angew. Chem., Int. Ed. 49(28), 4771-4774.

Cheng, C.M., Mazzeo, A.D., Gong, J., Martinez, A.W., Phillips, S.T., Jain, N., Whitesides, G.M., 2010b. Lab Chip 10(23), 3201-3205.

Chin, C.D., Laksanasopin, T., Cheung, Y.K., Steinmiller, D., Linder, V., Parsa, H., Wang, J., Moore, H., Rouse, R., Umviligihozo, G., Karita, E., Mwambarangwe, L., Braunstein, S.L., van de Wijgert, J., Sahabo, R., Justman, J.E., El-Sadr, W., Sia, S.K., 2011. Nat. Med. 17(8), 1015-1019.

Chin, C.D., Linder, V., Sia, S.K., 2007. Lab Chip 7(1), 41-57.

Chin, C.D., Linder, V., Sia, S.K., 2012. Lab Chip 12(12), 2118-2134.

Costa, M.N., Veigas, B., Jacob, J.M., Santos, D.S., Gomes, J., Baptista, P.V., Martins, R., Inácio, J., Fortunato, E., 2014. Nanotechnology 25(9), 094006.

Donofrio, J.M., Labus, D., 2009. Diagnostic Tests Made Incredibly Easy! Lippincott Williams & Wilkins. pp. 29-252.

Dungchai, W., Chailapakul, O., Henry, C.S., 2009. Anal. Chem. 81, 5821.

Ellerbee, A.K., Phillips, S.T., Siegel, A.C., Mirica, K.A., Martinez, A.W., Striehl, P., Jain, N., Prentiss, M., Whitesides, G.M., 2009. Anal. Chem. 81(20), 8447-8452.

Foo, A.Y., Bais, R., 1998. Clin. Chim. Acta 272(2), 137-147.

Fu, E., Lutz, B., Kauffman, P., Yager, P., 2010. Lab Chip 10(7), 918-920.

Gella, F.J., Gubern, G., Vidal, R., Canalias, F., 1997. Clin. Chim. Acta 259(1), 147-160.

Gibson, T.S., Solah, V.A., McCleary, B.V., 1997. J. Cereal Sci. 25(2), 111-119.

Haschek, W.M., Rousseaux, C.G., Wallig, M.A., 2013. Haschek and Rousseaux's Handbook of Toxicologic Pathology. Elsevier Science.

Krieg, P., Lendl, B., Vonach, R., Kellner, R., 1996. Fresenius' J. Anal. Chem. 356(8), 504-507.

Lambert, J.B., 2011. Organic Structural Spectroscopy. Pearson Prentice Hall.

Li, B., Fu, L., Zhang, W., Feng, W., Chen, L., 2014a. Electrophoresis 35(8), 1152-1159.

Li, L., Huang, X., Liu, W., Shen, W., 2014b. ACS Appl. Mater. Interfaces 6(23), 21624-21631.

Li, X., Ballerini, D.R., Shen, W., 2012. Biomicrofluidics 6(1), 011301.

Li, Z.a., Hou, L., Zhang, W., Zhu, L., 2014c. Anal. Methods 6(3), 878-885.

Liana, D.D., Raguse, B., Gooding, J.J., Chow, E., 2012. Sensors 12(9), 11505.

Mahosenaho, M., Caprio, F., Micheli, L., Sesay, A., Palleschi, G., Virtanen, V., 2010. Microchim. Acta 170(3-4), 243-249.

Mao, X., Huang, T.J., 2012. Lab Chip 12(8), 1412-1416.

Martinez, A.W., 201. Bioanalysis 3(23), 2589-2592.

Martinez, A.W., Phillips, S.T., Butte, M.J., Whitesides, G.M., 2007. Angew. Chem., Int. Ed. 46(8), 1318-1320.

Martinez, A.W., Phillips, S.T., Nie, Z., Cheng, C.-M., Carrilho, E., Wiley, B.J., Whitesides, G.M., 2010a. Lab Chip 10(19), 2499-2504.

Martinez, A.W., Phillips, S.T., Whitesides, G.M., 2008a. Proc. Natl. Acad. Sci. 105(50), 19606-19611.

Martinez, A.W., Phillips, S.T., Whitesides, G.M., Carrilho, E., 2010b. Anal. Chem. 82(1), 3-10.

Martinez, A.W., Phillips, S.T., Wiley, B.J., Gupta, M., Whitesides, G.M., 2008b. Lab Chip 8(12), 2146-2150.

Metzler, D., 2012. Biochemistry: The Chemical Reactions Of Living Cells. Elsevier Science.

Minick, M., Fotta, K., Khan, A., 1991. Biopolymers 31(1), 57-63.

Murayama, T., Tanabe, T., Ikeda, H., Ueno, A., 2006. Bioorg. Med. Chem. 14(11), 3691-3696.

Peeling, R.W., 2006. Sex. Transm. Infect. 82(6), 425-430.

Pelton, R., 2009. TrAC, Trends Anal. Chem. 28(8), 925-942.

Sakač, N., Sak-Bosnar, M., 2012. Int. J. Electrochem. Sci. 7(4), 3008-3017.

Sakač, N., Sak-Bosnar, M., Horvat, M., Madunić-Čačić, D., Szechenyi, A., Kovacs, B., 2011. Talanta 83(5), 1606-1612.

Sasaki, T., Noel, T.R., Ring, S.G., 2008. J. Agric. Food Chem. 56(3), 1091-1096.

Sharma, S.S., Sharma, S., Rai, V.K., 1990. Ann. Bot. 65(3), 281-283.

Sigmann, S.B., Wheeler, D.E., 2004. J. Chem. Educ. 81(10), 1475-1478.

Sorouraddin, M.H., Saadati, M., 2010. Determination of copper in urine and water samples using a simple led-based colorimeter. J. Anal. Chem. 65(4), 423-428.

Svens, E., Käpyaho, K., Tanner, P., Weber, T.H., 1989. Clin. Chem. 35(4), 662-664.

Takeuchi, T., Matsushima, T., Sugimura, T., 1975. Separation of human α-amylase isozymes by electro-focusing and their immunological properties. Clin. Chim. Acta 60(2), 207-213.

Teitelbaum, R.C., Ruby, S.L., Marks, T.J., 1980. J. Am. Chem. Soc. 102(10), 3322-3328.

Then, W.L., Li, M., McLiesh, H., Shen, W., Garnier, G., 2015. Vox Sang. 108(2), 186-196.

van Staden, J.F., Mulaudzi, L.V., 2000. Anal. Chim. Acta 421(1), 19-25.

Wang, S., Ge, L., Song, X., Yu, J., Ge, S., Huang, J., Zeng, F., 2012. Biosens. Bioelectron. 31(1), 212-218.

Watanabe, T., Yamamoto, A., Nagai, S., Terabe, S., 1998. Electrophoresis 19(13), 2331-2337.

Wilding, P., 1965. Clin. Chim. Acta 12(1), 97-104.

Wu, S., Zhu, Y., Cai, Q., Zeng, K., Grimes, C.A., 2007. Sens. Actuators, B 121(2), 476-481.

Yamaguchi, M., Deguchi, M., Wakasugi, J., 2005. Biomed Microdevices 7(4), 295-300.

Yetisen, A.K., Akram, M.S., Lowe, C.R., 2013. Lab Chip 13(12), 2210-2251.

Zajoncová, L., Jílek, M., Beranová, V., Peč, P., 2004. Biosens. Bioelectron. 20(2), 240-245.

Zhang, Z., Seitz, W.R., O'Connell, K., 1990. Anal. Chim. Acta 236, 251-256.

Zhao, W.A., van der Berg, A., 2008. Lab Chip 8(12), 1988-1991.

भारतीय प्रौद्योगिकी संस्थान गुवाहाटी
Indian Institute of Technology Guwahati

CHAPTER 4

Paper-Based Sensors for Point-of-Care Kidney Function Monitoring

Contents

भारतीय प्रौद्योगिकी संस्थान गुवाहाटी
Indian Institute of Technology Guwahati

ABSTRACT

The ratio of albumin to creatinine (ACR) in urine is a measure of human kidney-health. In this study, we report the development of a paper-based point-of-care (POC) kidney function test (KFT) kit, which is composed of paper-based ACR sensors, opto-electrochemical measurement unit, a display, and facility to transfer data to a smartphone. For the albumin sensor, the pieces of filter papers were coated with a mixture of alcoholic bromophenol blue and citrate buffer leading to a chrome-yellow coloration while for the creatinine sensor the papers were coated with alkaline picrate solution leading to a lemon-yellow coloration of the surface. Dispensing albumin solution of known concentration on the albumin-sensor led to the conversion of chrome-yellow coloration to bluish-green while dispensing the creatinine solution on the creatinine-sensor led to the conversion of lemon-yellow to orange coloration of the surface. For both the albumin or creatinine sensors, the intensity of the bluish-green or orange coloration varied with the concentration of the analytes in the solutions. The variations in the intensities of colors with albumin and creatinine loadings in the analytes were quantified by integrating a light emitting diode (LED) at one side of each sensor and a light dependent resistor (LDR) on the other side. The intensity of the transmitted rays from the source LED, passing through the sensors, was found to vary the electrical resistance of the LDR monotonically with the loading of the albumin or creatinine in the analyte, which helped in obtaining the calibration plots for the ACR sensors. The portable and fast proof-of-concept POC prototype was employed for the on-spot detection of the unknown ACR in the real human urine samples.

4.1. Introduction

In the modern human life, regular detection of diverse health biomarkers such as body weight (Fader et al. 2009; Meza and Carrillo 2016; Must et al. 1999), body-mass index (van der Pals et al. 2014), blood sugar or pressure, lipid profiles (Bruen et al. 2017; Flynn et al. 2017), T3-T4-TSH (Christ and Burger 2015; Dayan 2001), hemoglobin (Brown et al. 2003), sodium or potassium (Metheny 1981; Walker 2016), have become indispensable to maintain a minimum quality of health (Chen et al. 2015; Chin et al. 2007; Mao and Huang 2012; Martinez et al. 2010). In general, such personal care practices are done with the help of commercially available point-of-care testing (POCT) devices. For example, weighing machine, glucometer, blood pressure meters, or pregnancy kits, help us evaluating diverse necessary health parameters at the patients site. Regular monitoring of such markers in the form of primary health care not only help in early stage detection of many severe diseases but also necessary for the management of a chronic disease for a longer period of time.

This procedure also helps in avoiding critical health hazards, which require attention from secondary or tertiary healthcare ecosystems. Over the years, although the development of POCT devices has been very rapid (St John and Price 2014), however, there are many clinically important biomarkers for which such devices are not yet available commercially (Shaw 2016). For example, the prior-art suggest that there is an immediate need of a POCT kidney function test (KFT) kit. Kidneys are the filtration units of a human body, which cleanse the blood continuously to screen out the excretory products through urine before recycling the important nutrients and water back to the mainstream (Hall 2010; Makanjuola and Lapsley 2014).

A generic term for various disorders affecting the structure and function of the kidney is chronic kidney disease (CKD) (Good et al. 2010; Levey and Coresh ; Levey et al. 2003). Diabetic nephropathy (2003; Gross et al. 2004; Mauer et al. 1983), micro-albuminuria (Babazono et al. 2004; Borch-Johnsen et al. 1999; Viberti et al. 1982), or uremia (Madore 2003; Stenvinkel and Alvestrand 2002) are some of the severe CKDs, which can lead to kidney failure if not taken care of regularly (2003; Levey and Coresh ; Levey et al. 2003; Makanjuola and Lapsley 2014). Albuminuria is caused by the persistent increased albumin in urine, which is an early and sensitive biomarker for CKD (Levey and Coresh). During the normal operation, the filtration in kidney allow excretion of a meagre amount of protein in which albumin is perhaps the most common type (Borch-Johnsen et al. 1999). Previous studies indicate that the micro- or macro-albuminuria assays are important in nephrology for the early detection and management chronic kidney diseases (Babazono et al. 2004; Mogensen 1987).

The common test for proteinuria is the urinalysis dipstick in which the colorimetric assays help in measuring the urinary albumin (Comper and Osicka 2005; Kumar and Banerjee 2017). However, since the patients may have variable fluid intake within and/or between the test-dates, the evaluation of the parameter albumin to creatinine ratio (ACR – mg/g) provides a normalization of this process (Chae et al. 2012; Justesen et al. 2006). Creatinine is one of the standard excretory products available in urine, which is found in larger quantities (Hare 1950; Narayanan and Appleton 1980). Estimation of ACR helps in eliminating the effects of the dilution since the creatinine (measured in g/dL) and albumin (mg/dL) are measured in the same sample of urine (Justesen et al. 2006; Leaños-Miranda et al. 2007; Mattix et al. 2002). A moderately increased micro-albuminuria (ACR 30-300 mg/g) refers to albumin excretion above the normal range whereas more severe macro-

albuminuria (ACR > 300 mg/g) refers to a higher elevation of albumin associated with progressive decline in glomerular filtration rate (Levey et al. 1999; Levey and Coresh 2012). Importantly, the lower limit micro-albumin detection is sensitive and cannot be evaluated with the help of the conventional dipsticks (Bakris 1996; Comper et al. 2003) Further, the 24-hour data collection has been the "gold standard" for the final diagnosis of the early kidney diseases (Levey and Coresh 2012).

Thus, at this stage, it is of utmost importance to develop POCT devices, which are capable of tracking ACR in human urine following the gold-standards. Importantly, there are several existing methods for the quantitative estimation of albumin and/or creatinine in human urine. For example, while the dye binding (Husdan and Rapoport 1968; Tayyab and Qasim 1990), immunochemical assay (Choi et al. 2004), HPLC (Tsikas et al. 2004; Valko et al. 2003), Electrophoresis (Doumas et al. 1971; Laurell 1966; Paroni et al. 2004)or near infrared (NIR) spectroscopy (Shaw et al. 1996) have been employed so far for albumin detection, a number potentiometric (Killard and Smyth 2000; Pandey and Mishra 2004) amperometric (Jin et al. 1997; Khan and Wernet 1997), electrochemical (Kwon et al. 2011; Lad et al. 2008) and nanoparticle based (Du et al. 2016; Kwon et al. 2011) methods have been employed to detect creatinine.

However, the literature suggests that there is no such POCT device available for the quantitative determination of albumin, creatinine and ACR from human urine. In the present study, we have developed an economic, paper-based, and portable POCT device for estimating important biomarkers present in urine such as, albumin(Fanali et al. 2012; Majoor 1978; Margarson and Soni 1998; Rothschild et al. 1988), creatinine(Narayanan and Appleton 1980; Wyss and Kaddurah-Daouk 2000) and ACR (Assadi 2002; Babazono

et al. 2004; Chae et al. 2012; Justesen et al. 2006; Mattix et al. 2002; Roberts et al. 1998; Tayeh et al. 2016; Warram et al. 1996), which has shown the potential to track the health of human kidneys following the gold-standards. The schematic illustration in Figure 4.1 shows the steps to fabricate the respective paper-sensors for detection of the aforementioned biomarkers. Initially, citric acid along with an alcoholic solution of bromophenol blue was coated on a paper surface to develop the albumin sensor, as schematically shown in the image (a).

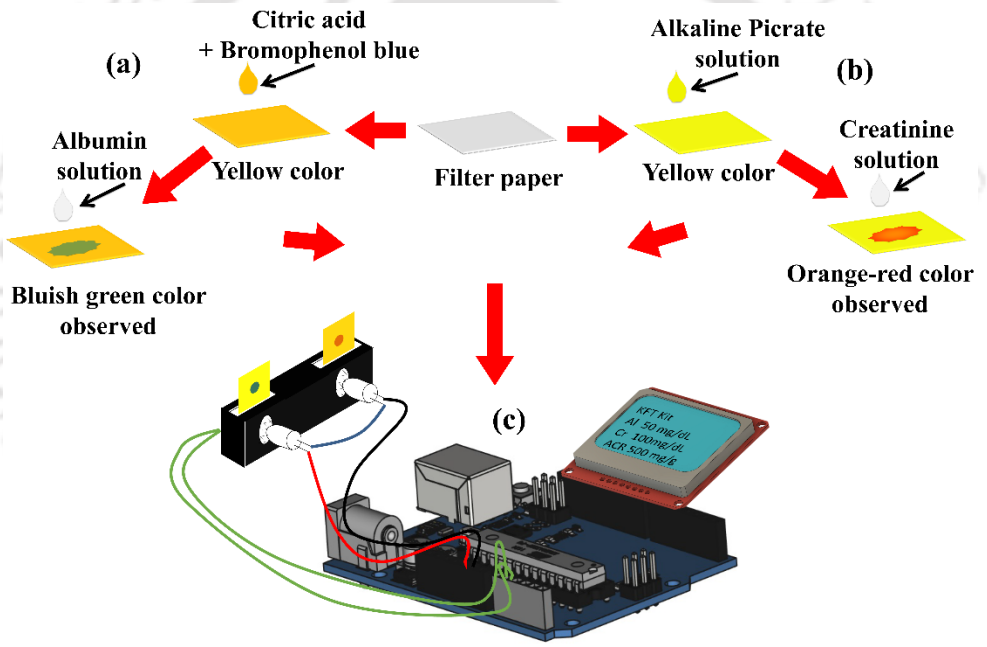

Figure 4.1: Images (a) and (b) are schematic illustrations of the steps involved in the fabrication of the paper-sensors for quantitative detection of albumin and creatinine. Images (c) illustrates the electronic setup for the measurement of the albumin, creatinine and ACR.

Further, the alkaline picrate solution was coated on another paper surface to develop the creatinine sensor, as schematically shown in the image (b). Subsequently, the aqueous albumin and creatinine solution was dispensed on the respective paper-sensors before the the change in intensity of color on the sensor surface was observed, as schematically

shown in the images (a) and (b). Thereafter, the paper-sensor was placed between a light emitting diode (LED) source and a light dependent resistor (LDR), as schematically shown in the image (c). The arrangement allowed the LED to shine light on the paper surface from one side while the transmitted light passing through the sensor was collected on a LDR. The change in color intensity on the sensor surface with the variation in the albumin or creatinine concentration in the analyte was found to have a direct correlation with variations in the electrical resistance of the LDR. The calibrations thus generated for the albumin and creatinine were employed to detect the unknown levels of albumin, creatinine and ACR in the human urine sample. The sensors were integrated with a signal processing unit (SPU) to display and wirelessly transfer the data to the mobile interfaces, which led to the proof-of-concept prototype of a fast, portable, and user-friendly KFT kit.

4.2. Experimental Section

4.2.1. Materials

Bovine serum albumin (BSA) and creatinine were procured from SRL (India), bromophenol blue, citric acid monohydrate, sodium hydroxide, were procured from Merck (India) and Ethanol was procured from Tedia (USA). Filter paper (diameter: 125 mm) were obtained from Whatmann (India). The chemicals were of analytical grade and used without any further processing. Milli-Q grade water was used in the experiments unless stated otherwise. The Arduino Uno R3 development board, Liquid crystal display (LCD), white light emitting diode (LED)resistors (220 kΩ and 1 kΩ) were procured from Rhydo Labz (India).

4.2.2. Sensor fabrication and optimization

The reagent solutions used to perform the experiments were freshly prepared. The 0.1% (w/v) bromophenol blue solution was prepared by dissolving 10 mg of bromophenol blue powder in 10 ml ethanol to obtain a yellow colored solution. The citric buffer solution was prepared by dissolving 0.5 g of citric acid monohydrate in water. The albumin solutions of varying concentrations ranging between 10 – 500 mg/dL were prepared by dissolving the required amount of bovine serum albumin in water. The 1.2% (w/v) picric acid solution was prepared by dissolving 0.12 g picric acid in water. Sodium hydroxide 1M solution was prepared by dissolving 400 mg of sodium hydroxide pellets in 10 ml water. Creatinine solutions of different concentrations ranging between 10 – 500 mg/dL were prepared by dissolving the required amount of creatinine in water. The optimization of the concentration of bromophenol blue and picric acid was done by employing a trial and error method. For example, initially, different concentrations ranging from 0.01% to 1.0% (w/v) of bromophenol blue were used to prepare the paper sensors. In such a situation, it was noted that the resistance varied from very low to nearly open circuit resistance. The initial set of experiments indicated that, when 0.1% (w/v) bromophenol blue was coated on the paper sensors, the resulting resistance could faithfully convert the entire range of the urinary albumin concentration. The concentrations of bromophenol blue beyond 0.01% (w/v) were undetectable because the electrical resistances were rather large and out of measuring range of the integrated electronic device. Similarly, the other set of trial experiments were done using picric acid concentration of 0.5% – 1.5% (w/v). The results showed that the picric acid concentration of 1.2% (w/v) could detect the range of the creatinine present in the urine samples reliably, which were also within the quantifiable limit of the integrated electronic device. Further, the picric acid concentration beyond this

level gave a very low resistance to open circuit resistance. Thus, the aforementioned concentrations of bromophenol blue and picric acid were used to fabricate the albumin and creatinine sensors. The illustration in Figure 4.1 shows the steps to fabricate the albumin and creatinine the sensors. Initially, the filter papers were cut into pieces of dimension 1 cm × 1 cm. Following this, 30 µl of citric buffer solution was dispensed on the paper surface and dried. Thereafter, 30 µl alcoholic bromophenol blue solution was dispensed on top of the previously dried sensor which led to the chrome-yellow color coating on the surface of the paper, as shown in the image (a) of Figure 4.1. Similarly, for creatinine sensor, again the filter papers were cut into pieces of dimension 1 cm × 1 cm. Equal quantities (v/v) of the picric acid solution and sodium hydroxide solution were mixed to obtain the yellow colored alkaline picrate solution. Thereafter, 60 µl of alkaline picrate solution was dispensed on the paper and dried, that led to a lemon-yellow colored coating on the surface of the paper, as shown in the image (b) of Figure 4.1. All the sensors prepared were kept in air tight container until further use.

4.2.3. Methods

About 5 µl of different concentration of albumin and creatinine were dispensed on the albumin and creatinine sensors. The albumin sensor showed the formation of bluish-green color while the creatinine sensor showed the formation of orange color. The intensity of the color for both the sensors increased with increase in the concentration of albumin and creatinine in the analyte. The variation in the color change with the concentration of the biomarker in the analyte was quantified by an experimental set up consisting of a LED, LDR, and digital multimeter (Mastech, India), as schematically illustrated in the images (c) and (d) of Figure 4.1. At first, the sensor surfaces were illuminated with the light

source LED before the transmitted rays through the sensor-surface were collected on the LDR. For different albumin and creatinine sensors, the electrical resistance from the respective LDRs were measured with the help of the multimeter. Following this, 5 µl of analyte solution, containing either albumin or creatinine, of known concentrations (10 – 500 mg/dL) were dispensed on the middle of the sensors the respective reagent loaded sensors. The color of the sensor surface changed simultaneously and the variations in the electrical resistance of the LDR were recorded for different albumin and creatinine concentrations. Measurements were repeated for five times for each analyte concentration to assure repeatability in the results. The electrical resistances for the unreacted paper sensors before the addition of the analytes were termed as (R_0^a) and (R_0^c) for albumin and creatinine, respectively, while the same after the addition of analytes were termed as (R^a) and (R^c) for albumin and creatinine, respectively.

The pictures of the sensor were taken by Nikon D5100 digital camera (Nikon Corp., Japan). The FTIR analysis was performed using Thermo Scientific Nicolet iS10 FT-IR spectrometer, U.S.A. The UV-Vis spectroscopic analysis was done using Shimadzu UV-2600 spectrophotometer, U.S.A. The NMR analysis was done using 600MHz FT NMR Ascend 600 (Bruker, U.S.A). The pH measurements were done using Oakton pH 150 Waterproof Portable pH/Temperature Meter (Cole-Parmer, U.S.A)

4.3. Results and Discussion

4.3.1 Reaction mechanism characterization

The Figures 4.2(a) and (b) show the UV-Vis spectra and the mechanism of reaction for the albumin sensor. In Figure 4.2(a), the absorption spectrum of bromophenol blue (BPB) solution at pH 2.3 is denoted by the black line. The absorption peaks were obtained at 436

nm and at 590 nm. The absorption peak at 436 nm was for the acidic species of free-state BPB and similarly, the basic species absorption peak at 590 nm corresponds to the proton dissociation of BPB. The blue line in Figure 4.2(a) indicates the mixture alcoholic BPB together with citric acid solution. The alcoholic BPB-citric acid mixture is yellow in color as the phenolic structure predominates, as observed from the peaks in the Figure 4.2(a). The pink line in Figure 4.2(a) shows the plot after addition of albumin (BSA) to the system. The plot shows absorption spectra of BPB–BSA mixtures at pH 2.3 under conditions where the BSA concentration is the sole contributor to the spectral features. With addition of BSA to alcoholic BPB/citric acid mixture solution, the BPB absorption peak at 436 nm decreased with a bathochromic shift from 436 to 440 nm, while the absorption peak at 590 nm increased with a bathochromic shift from 590 to 604 nm.

Figure 4.2(a) indicates that there are interactions between BPB and BSA. In acidic solution, BPB had negative charges, which could bind with positively charged basic amino acid (Arg, Lys, His) residues of BSA by electrostatic forces (Tal et al. 1985). On this basis, the hydrophobic benzene rings of BPB could bind with the hydrophobic cavities of BSA. Since one BPB molecule could combine with two BSA molecules (Ray et al. 1966; Wei et al. 2000), the BPB–BSA complex was stable. With an increase in BSA concentration, the yellow coloration changed to green and then to bluish green due to conversion of the phenolic form of the BPB to quinoid form (Waldmann-Meyer and Schilling 1956). Figure 4.2(b) shows the reaction between BSA and BPB, which was confirmed by the aforementioned UV-Vis spectroscopy.

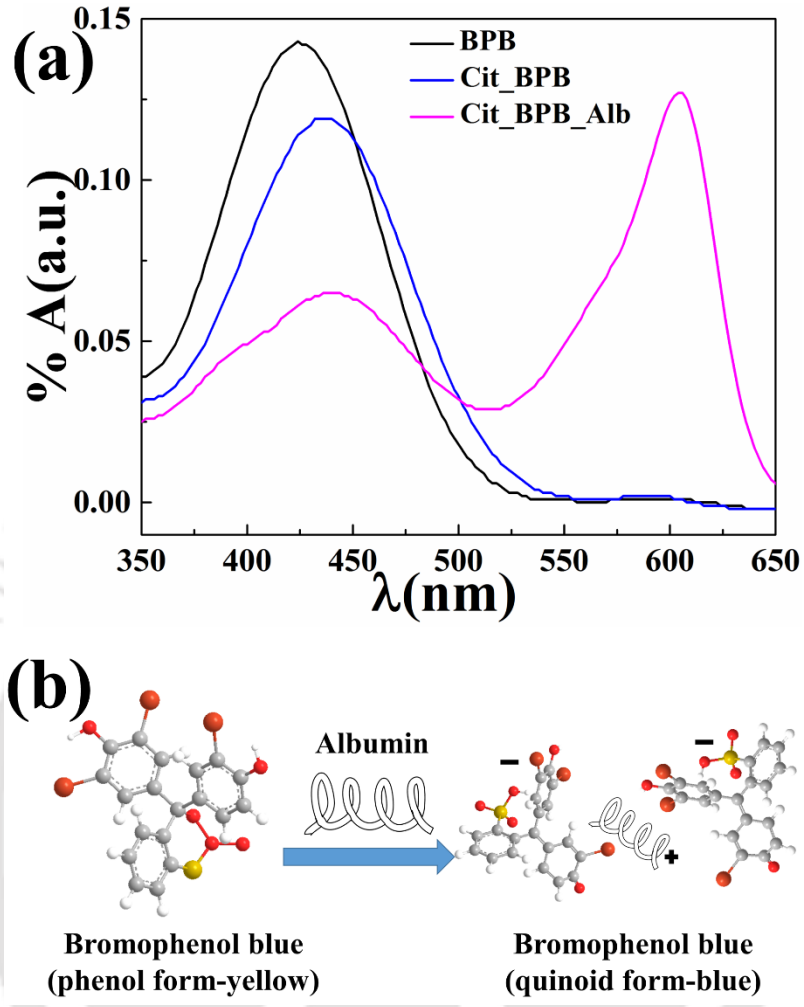

Figure 4.2: (a) shows the UV-Vis spectra for the albumin detection reaction. Image (b) illustrates the reaction mechanism of the albumin detection.

For the mechanism characterization studies, the picric acid and alkaline picrate were mixed in the DMSO-d_6 while creatinine was dissolved in D_2O. A mixed solvent containing 90% DMSO-d_6 and 10% D_2O was used for the NMR of the reaction mixture of alkaline picrate and creatinine. Plots (a) – (c) in the Figure 4.3 illustrate the ^1H NMR spectra of picric acid, creatinine, and mixture of alkaline picrate with creatinine, respectively. In Figure 4.3 (a), the singlet at 8.61 ppm is the characteristic for the picric acid. The absorptions at 2.89 and 3.89 ppm indicate the presence of methyl and the methylene groups of creatinine as seen in Figure 4.3 (b). Further, in Figure 4.3 (c), the reduction in

the absorption at 8.61 ppm with the appearance of peaks 2.93 ppm, and 2.90 ppm indicate the reaction in the mixture of alkaline picrate and creatinine. The ^{13}C NMR of picric acid is illustrated in the Figure 4.3(d). The absorption at 160.86 ppm is due to the carbon one (C1) attached to the hydroxyl group of the picric acid molecule while the peak at 142.21 ppm is due to the absorption by the equivalent carbon having an attached nitrogen group (C2, C4, and C6). The carbon attached to a non-equivalent nitro group para (C4) to carbon one shows an absorption at 125.68 ppm. The equivalent meta carbons (C3 and C5) with attached hydrogen gives an absorption peak at 125.25 ppm. The ^{13}C NMR creatinine is shown in Figure 4.3(e). The characteristic absorption peaks are found at 188.90 ppm (C=O), 169.25 ppm (C=NH), 56.36 ppm (CH_2) and 30.12 ppm (CH_3) (Pavia et al. 2014; Vasiliades 1976).

The Figure 4.3 (f) represents the ^{13}C NMR spectra of the product of the reaction between alkaline picrate and creatinine, which is known as Janovsky's complex, which is shown by the ball-stick diagram in the Figure 4.3 (g). Absorption peaks due to creatinine were observed at 30.92 ppm, 170.0 ppm, and 186.42 ppm, including a lesser absorption at 56.52 ppm. Absorption peaks at 56.52 ppm and 186.42 were due to (-CH_2-) and (C=O), groups of the creatinine molecules, which suggest that the creatinine was not enolized entirely in the solvent mixture. Absorptions at 125.90 ppm and 142.01 ppm were due to the two equivalent *meta* (C3 and C5) and *ortho* (C2 and C6) carbons of picric acid respectively. Absorption due to the *para* carbon on picric acid was observed at 125.34 ppm. An absorption peak owing to carbon 1 of picric acid was not observed. The presence of the two unchanged peaks for picric acid gave the indication that the reaction of picric acid and creatinine to form the 1/1 complex, which did not involve attack at the *meta* positions. Thus, the aromatic structure of the ring was maintained in the final product.

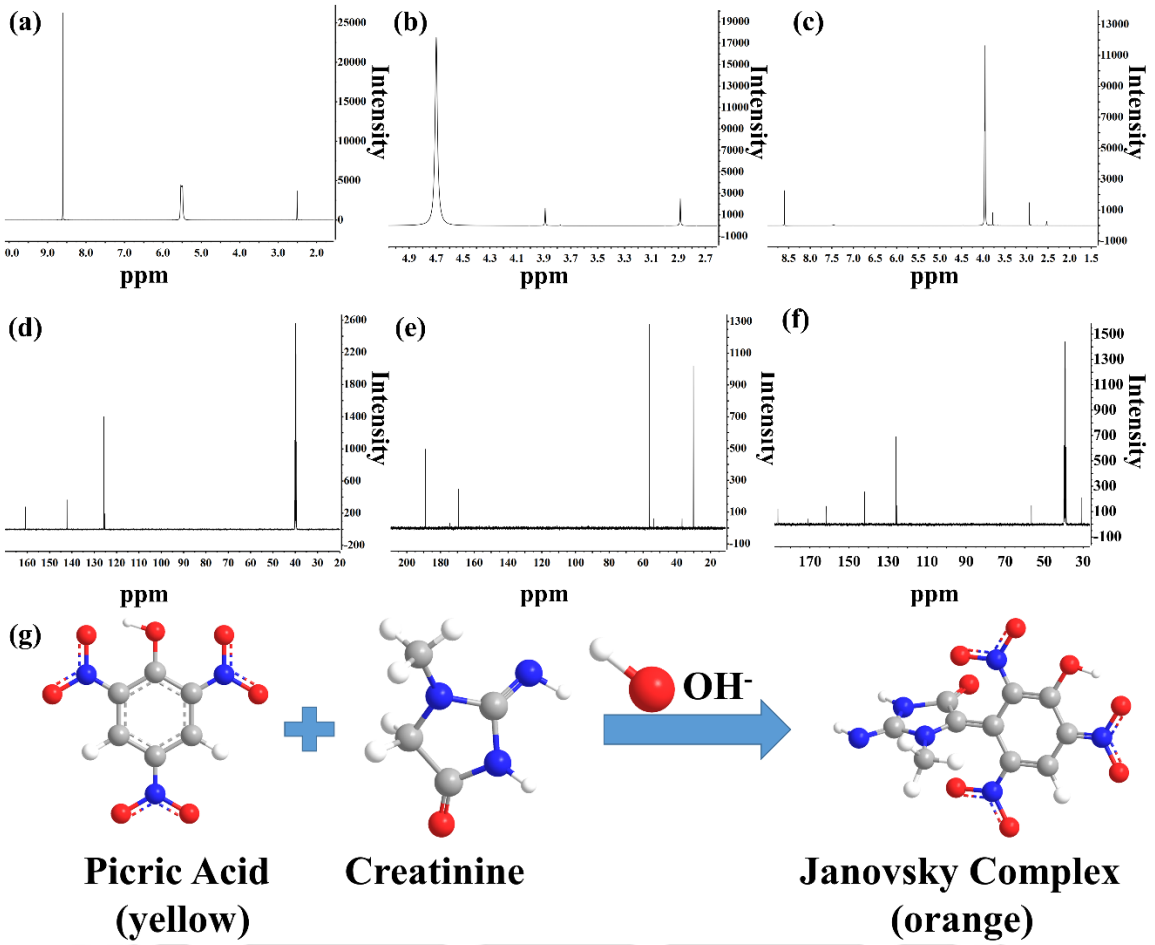

Figure 4.3: Plots (a) – (c) illustrate the ^{1}H NMR spectra of picric acid, creatinine, and mixture of alkaline picrate and creatinine, respectively. The ^{13}C NMR of picric acid, creatinine, and mixture of alkaline picrate and creatinine are illustrated in the images (d) – (f). The reaction mechanism is illustrated in image (g).

A possible site of attack could be at carbon 1 and a probable adduct formation had taken place due to the reaction between the enolized creatinine and picrate ion in the presence of sodium hydroxide (Vasiliades 1976). We have also conducted the stability study of the sensor response over time and is shown in Figure 4.4. For albumin sensor R_0 varies with t according to the equation $y = 2.3943\ x^{0.0086}$ and for the creatinine sensor R_0 varies with t according to the equation$y = 2.6142\ x^{0.0382}$. From the exponent obtained, it is seen that the variation of R_0 with t for both the sensors is negligible. The study suggests that the

responses of the albumin and creatinine sensors were reasonably stable for ~6 months as the variations in the electrical resistances were noted to be very less.

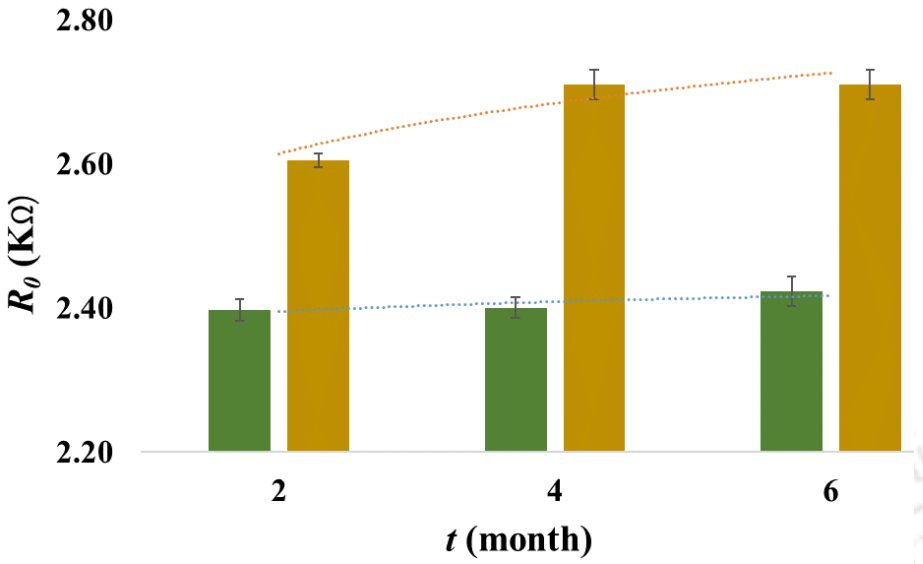

Figure 4.4: The image shows the variation in the electrical resistance of an albumin sensor (green bar, R_0^a) and a creatinine sensor (yellow bar,R_0^c) with time (t).The image shows the variation in the electrical resistance (R_0) of a sensor with time (t).

4.3.2 Electrical Response of the sensor

Figure 4.5 (a) depicts the variation in normalized resistance, R^a/R_0^a, of the albumin sensor with the variation in the albumin concentration (C_a) in the analyte. Similarly, Figure 4.5(b) shows the variation in normalized resistance, R^c/R_0^c, with the change in creatinine concentration (C_c) in the analyte. Initially, the electrical resistances from the photoresistor were obtained as, R_0^a and R_0^c, respectively, for albumin and creatinine paper-sensors before the addition of the respective analytes. Following this, the electrical resistances were measured to be, R^a and R^c, respectively, for the albumin and creatinine paper-sensors after addition of the respective analytes. Finally, the normalized resistances, R^a/R_0^a and R^c/R_0^c were evaluated for albumin and creatinine sensors respectively. Image (a) in Figure 4.5 shows the result obtained for albumin sensors, which suggests that,

with the increase in C_a intensity of coloration on the paper surface increased resulting in decrease in intensity of transmitted rays to the photoresistor. The image set (c) shows the color change of the paper-sensors when C_a was varied. Since, the resistance of a photoresistor increased with decrease in the light exposure, R^a/R_0^a also increased.

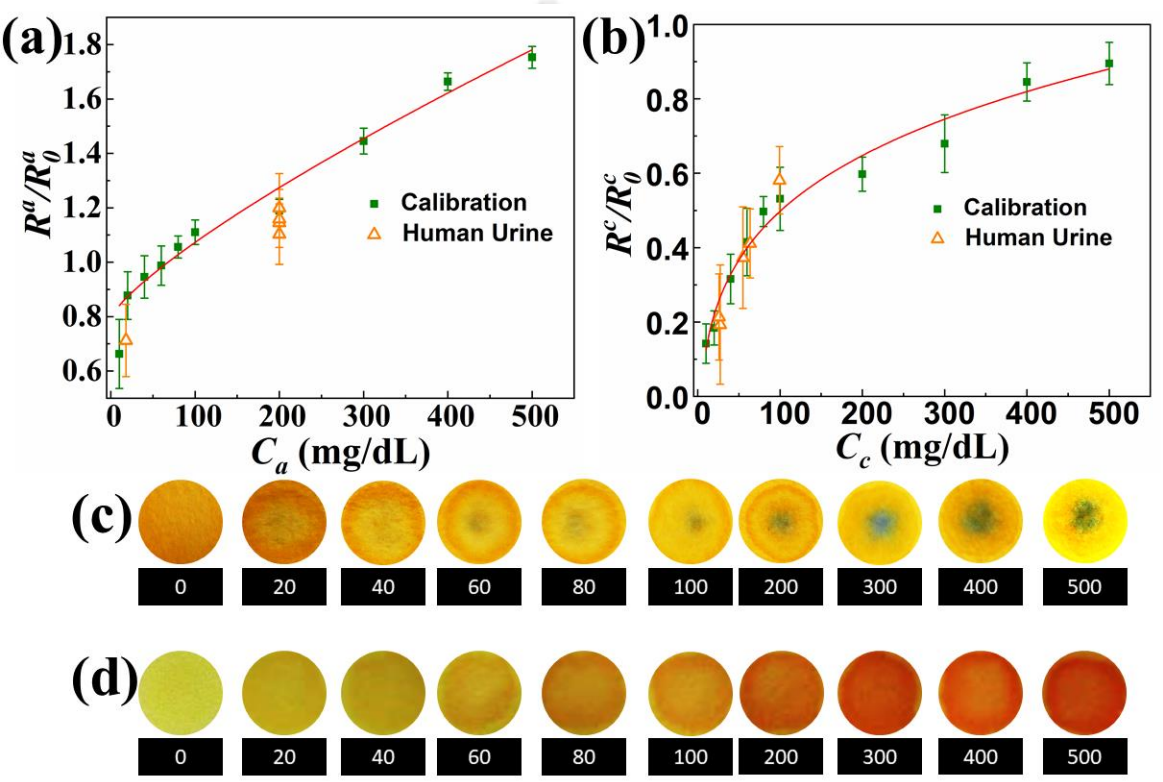

Figure 4.5: Variations in the, (a) normalized resistance (R^a/R_0^a) with concentration of albumin (C_a) and (b) normalized resistance (R^c/R_0^c) with concentration of creatinine (C_c). The points (square and triangle) represents the mean value and the error bar signifies the range in which it varies (standard deviation from the mean). The image set (c) shows the colorimetric change of the paper-sensors when solution different loadings of albumin were dispensed. The image set (d) Illustrates the colorimetric change on the surface of the paper-sensors when sample solution containing different creatinine concentrations were dispensed.

Figure 4.5(b) suggests that with the increase in C_c the parameter R^c/R_0^c also enhanced. Increase in the intensity of the color again allowed lesser amount of light to transmit through, which eventually increased the R^c/R_0^c of the photoresistor with C_c. The Figure

4.5(d) illustrates the colorimetric change of the sensor surface before and after dispensing of the sample containing different concentrations of creatinine. The equation for the plot 4.5 (a) was found out to be $y = 0.7948 + 0.00739\, x^{0.78733}$ while the R^2 value obtained was 0.98. The equation and the R^2 value for the plot 4.5 (b) was found to be $y = -0.52563 + 0.41201\, x^{0.1975}$ and 0.98 respectively. Further, the test was conducted within the normal ranges of analyte found in human urine and it is possible that the values will reach saturation but experiments have to be done to reach a definite conclusion which we keep as our future scope

In order to determine the efficiency of the paper sensors in estimating the albumin and creatinine levels experiments were also conducted with human urine samples. It may be noted here that all the tests with human urine samples were carried out in a nearby diagnostic center under the supervision of medical experts following clinically approved protocols for pathological tests and ethical guidelines. Initially, the albumin and creatinine levels of different urine samples were measured using the clinically approved auto-analyzer instrument Dimension RxL Max Integrated Chemistry System, SIEMENS. Subsequently, we used the same samples on the respective paper-sensors and measured the change in resistance for albumin and creatinine.

Table 4.1. Quantitative measurement of urine albumin and creatinine using the proposed KFT kit and the clinically approved commercial devices.

No.	Clinically approved methodology		Proposed device (KFT Kit)	
	Al (mg/dL)	Cr (mg/dL)	Al (mg/dL)	Cr (mg/dL)
1	200	99.5	145	172
2	200	27.3	204	22
3	200	63.7	100	57
4	18	25.9	12	24
5	200	55	164	50

Images (a) and (d) in Figure 4.5 summarize the performance of the paper-sensor as compared to a clinically approved method for quantitative determination of albumin, creatinine, and ACR. The discrete triangular points on the image (a) and (b) of Figure 4.5 and Table 4.1 show that the albumin and creatinine concentrations acquired from human urine samples were very close to the calibration curve obtained. The data obtained from the diagnostic center and from the proposed method is tabulated in Table 4.1**,** which suggests that the predictions from the KFT kit were very similar to that obtained from the clinically approved methods of diagnostic center. It may be noted here that there are a number of existing methodologies for quantitative measurement of albumin and creatinine, which are briefly summarized in the Table 4.2 and Table 4.3.

Table 4.2. Existing and proposed methods for the albumin detection in urine (Kumar and Banerjee 2017).

No.	Principle for albumin detection	Range
1	Dye binding	1.5 – 58.4 g/L
2	Immuno-chemical assays	1 – 200 mg/L
3	HPLC	2 – 95.9 mg/L
4	Electrophoresis	upto 7.5 mg/L
5	Near infrared (NIR) spectroscopy	0 – 5 g/dL
6	Proposed Method	20 – 500 mg/dL

It is important to note that most of the previous methods detect either albumin or creatinine.

Table 4.3. Existing methods and proposed methods for detection of urine creatinine (Pundir et al. 2013).

No.	Principle for creatinine detection	Range
1	Potentiometric	5 - 60000 µM
2	DO metric	3 – 8840 µM
3	Amperometric	0.004 – 5000 µM
4	Non-Enzymatic electrochemical	1 – 10000 µM
5	Nanoparticle based amperometric	1 – 800 µM
6	Proposed Method	20 – 500 mg/dL

The other limitations with these methods have been the cost of analysis, non-portability, requirement of experts for analysis, and availability of the facilities only in the centralized agencies. In comparison, the proposed proof-of-concept-prototype is one step portable, user-friendly, fast, specific, and low-cost POCT process to quantitatively detect albumin, creatinine, and their ratio with the help of the integrated electronic arrangement, as shown later. The device can be crucial in diagnosing kidney function at the patient's site. Figure 4.6(a), shows the image of the point-of-care prototype for kidney function monitoring POCT device, which can quantitatively measure albumin, creatinine and ACR. A pair of illuminator LEDs and the LDRs have been placed strategically around the albumin and creatinine paper sensors, which are marked as 'Cr' and 'AL' on the image', to capture the transmitted rays from the sensor and obtain the analog data. The chambers where the sensors were integrated where made dark to improve the sensitivity of the results.

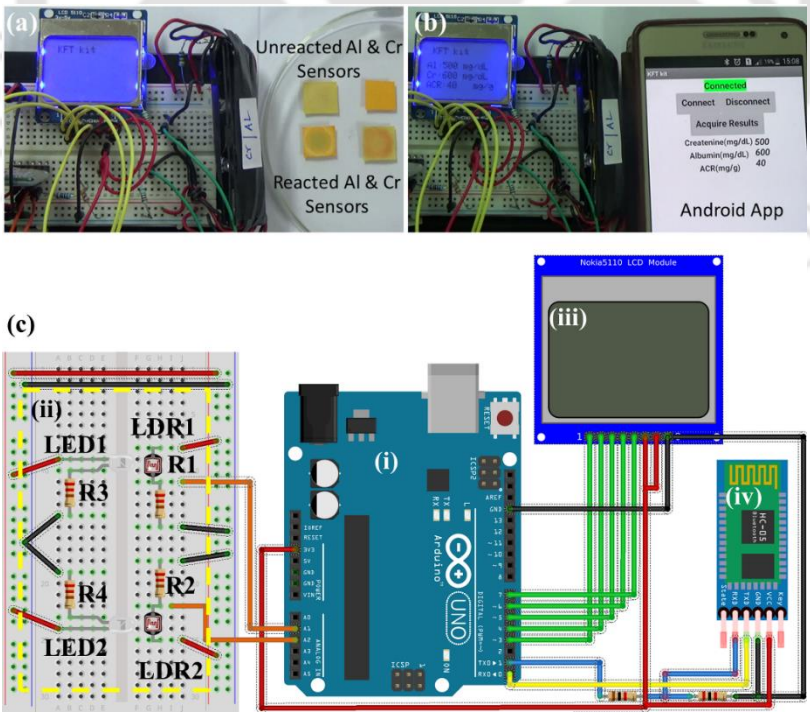

Figure 4.6. Image (a) illustrates the working prototype of the proposed device for simple, fast, reliable, economic, and point-of-care detection of albumin, creatinine, and ACR in

the human urine. Image (b) illustrates the smartphone application, which can be used for remote monitoring of kidney health. Image (c) illustrates the different part of the POCT device circuit.

The microcontroller circuit converts the analog data obtained from the photoresistors and translate into a digital output for displaying albumin, creatinine and ACR levels. An android application has also been developed for wireless data transfer through bluetooth to smartphone, which is illustrated in Figure 4.6(b). The Figure 4.6(c) shows the different components used in the development of the POCT kidney monitoring device such as, (i) the open source microcontroller board, (ii) the sensing module consisting of sensors and a pair of LED-LDR setups, (iii) the liquid crystal display (LCD) module, and (iv) the HC-05 Bluetooth module. The microcontroller board used in developing the working prototype for the albumin and creatinine sensors was Arduino UNO R3 while the LCD module was procured from commercial sources. The LEDs, LDRs, resistors, jumper wires and breadboard were also procured from the commercial sources. The albumin sensor setup consisted of LED 1, one end of which was connected to the voltage supply (3.3 V) while the other end was connected to ground (GND) via (R_3). The LED 2, for creatinine sensing, was connected in similar fashion with one end being connected to 3.3 V and the other end connected to the GND via (R_4). The corresponding LDRs, one of the terminals LDR1 (for albumin) was connected to the 3.3 V and the other end was connected to analog-pin 1 (A1) on the microcontroller board via resistor (R_1) of 220 kΩ. In a similar fashion, one of the terminals LDR2 (for creatinine) was connected to the 3.3 V and the other end was connected to analog-pin 2 (A2) on the microcontroller board via resistor (R_2) of 220 kΩ. The microcontroller had an integrated 10-bit analog to digital converter (ADC) for digitizing the analog inputs. The analog input from the sensors was given to the analog input pin A1 (albumin) and analog input pin A2 (creatinine) on the Arduino UNO R3

development board. The controlling pins of LCD module 1, 2, 3 and 5 were connected to the pins 3, 4, 5 and 7 of the development board while pin 8 of LCD module was connected to the GND and pins 6 and 7 were connected to 3.3 V. The data pin 4 of LCD was connected to the pin 6 of the microcontroller board. The Rx pin of the Bluetooth module was connected to the pin 1 of the development board via a 1 kΩ resistor and the Tx pin of the Bluetooth module was connected to pin 0 of the development board. The VCC pin was connected to 3.3 V and the GND pin of the Bluetooth module was connected to the ground. The Key and State pins were not connected.

4.4. Conclusions

We report the design and development of portable, rapid, reliable, and economic POCT device for real time monitoring of kidney function through human urine analysis. The operating principle of the device is based on the change in color intensity of a pair of reagent coated paper sensors with the variation in the concentration of albumin and creatinine in human urine. For the albumin sensor, the paper substrates were coated with a mixture of alcoholic bromophenol blue and citric buffer leading to a chrome-yellow coloration while for the creatinine sensor the papers were coated with alkaline picrate solution leading to a lemon-yellow coloration. Dispensing albumin solution of known concentration on the albumin-sensor led to the conversion of chrome-yellow coloration to bluish-green while dispensing the creatinine solution on the creatinine-sensor led to the conversion of lemon-yellow to orange coloration. Importantly, the intensity of the variation in the coloration of the sensors changed with the albumin or creatinine loading in the analytes. The study showed a simple way to measure the change in the color intensity on the paper-sensors with the help of a LED illuminator and a photoresistor. A proof-of-

concept working prototype has been developed for an immediate display of the albumin, creatinine and ACR in urine, which can be crucial in the development of a kidney function kit (KFT) to detect and monitor chronic kidney diseases (CKD).

References

American Diabetes Association,2003. Diabetes Care 27, s79-s83.

Assadi, F.K., 2002. Pediatr. Nephrol. 17(2), 107-110.

Babazono, T., Takahashi, C., Iwamoto, Y., 2004. Diabetes Care 27(7), 1838-1839.

Bakris, G.L., 1996. Curr. Opin. Nephrol. Hypertens. 5(3), 219-223.

Borch-Johnsen, K., Feldt-Rasmussen, B., Strandgaard, S., Schroll, M., Jensen, J.S., 1999. Arterioscler., Thromb., Vasc. Biol. 19(8), 1992.

Brown, W.W., Peters, R.M., Ohmit, S.E., Keane, W.F., Collins, A., Chen, S.-C., King, K., Klag, M.J., Molony, D.A., Flack, J.M., 2003. Am. J. Kidney Dis. 42(1), 22-35.

Bruen, D., Delaney, C., Florea, L., Diamond, D., 2017. Sensors 17(8), 1866.

Chae, H.W., Shin, J.-I., Kwon, A.R., Kim, H.S., Kim, D.H., 2012. J. Korean Med. Sci. 27(7), 784-787.

Chen, Y.H., Kuo, Z.K., Cheng, C.M., 2015. Trends Biotechnol. 33(1), 4-9.

Chin, C.D., Linder, V., Sia, S.K., 2007. Lab Chip 7(1), 41-57.

Choi, S., Choi, E.Y., Kim, D.J., Kim, J.H., Kim, T.S., Oh, S.W., 2004. Clin. Chim. Acta 339(1), 147-156.

Christ, E.R., Burger, A.G., 2015. Thyroid Function Tests. In: Huhtaniemi, I., Martini, L. (Eds.), Encyclopedia of Endocrine Diseases, Second Ed, Academic Press. pp. 477-485.

Comper, W.D., Jerums, G., Osicka, T.M., 2003. Diabetes Care 26(11), 3195.

Comper, W.D., Osicka, T.M., 2005. Adv. in Chronic Kidney Dis. 12(2), 170-176.

Dayan, C.M., 2001. Lancet 357(9256), 619-624.

Doumas, B.T., Ard Watson, W., Biggs, H.G., 1971. Clin. Chim. Acta 31(1), 87-96.

Du, H., Chen, R., Du, J., Fan, J., Peng, X., 2016. Ind. Eng. Chem. Res. 55(48), 12334-12340.

Fader, A.N., Arriba, L.N., Frasure, H.E., von Gruenigen, V.E., 2009. Gynecol. Oncol. 114(1), 121-127.

Fanali, G., di Masi, A., Trezza, V., Marino, M., Fasano, M., Ascenzi, P., 2012. Mol. Aspects Med. 33(3), 209-290.

Flynn, J.T., Kaelber, D.C., Baker-Smith, C.M., Blowey, D., Carroll, A.E., Daniels, S.R., De Ferranti, S.D., Dionne, J.M., Falkner, B., Flinn, S.K., 2017. Pediatrics 140(3), e20171904.

Good, D.M., et al. 2010. Mol. Cell. Proteomics 9(11), 2424-2437.

Gross, J.L., de Azevedo, M.J., Silveiro, S.P., Canani, L.H., Caramori, M.L., Zelmanovitz, T., 2004. Diabetes Care 28(1), 164-176.

Hall, J.E., 2010. Guyton and Hall Textbook of Medical Physiology. Elsevier Health Sciences.

Hare, R.S., 1950. Proc. Soc. Exp. Biol. Med. 74(1), 148-151.

Husdan, H., Rapoport, A., 1968. Clin. Chem. 14(3), 222.

Jin, W., Weng, Q., Wu, J., 1997. Anal. Chim. Acta 342(1), 67-74.

Justesen, T.I., Petersen, J.L.A., Ekbom, P., Damm, P., Mathiesen, E.R., 2006. Diabetes Care 29(4), 924-925.

Khan, G.F., Wernet, W., 1997. Anal. Chim. Acta 351(1), 151-158.

Killard, A.J., Smyth, M.R., 2000. Trends Biotechnol. 18(10), 433-437.

Kumar, D., Banerjee, D., 2017. Clin. Chim. Acta 469, 150-160.

Kwon, D.H., An, H.H., Kim, H.-S., Lee, J.H., Suh, S.H., Kim, Y.H., Yoon, C.S., 2011. Appl. Surf. Sci. 257(10), 4650-4654.

Lad, U., Khokhar, S., Kale, G.M., 2008. Anal. Chem. 80(21), 7910-7917.

Laurell, C.-B., 1966. Anal. Biochem. 15(1), 45-52.

Leaños-Miranda, A., Márquez Acosta, J., Romero-Arauz, F., Cárdenas-Mondragón, G.M., Rivera-Leaños, R., Isordia-Salas, I., Ulloa-Aguirre, A., 2007. Clin. Chem. 53(9), 1623.

Levey, A.S., Bosch, J.P., Lewis, J., et al., 1999. Ann. Intern. Med. 130(6), 461-470.

Levey, A.S., Coresh, J., 2012. Lancet 379(9811), 165-180.

Levey, A.S., Coresh, J., Balk, E., Kausz, A.T., Levin, A., Steffes, M.W., Hogg, R.J., Perrone, R.D., Lau, J., Eknoyan, G., 2003. Ann. Intern. Med. 139(2), 137-147.

Madore, F., 2003. Semin. Dial. 16(2), 148-156.

Majoor, C.L.H., 1978. Serum albumin in clinical practice: A historical review. In: Yap, S.H., Majoor, C.L.H., van Tongeren, J.H.M. (Eds.), Springer. Clinical Aspects of Albumin, pp. 97-116.

Makanjuola, D., Lapsley, M., 2014. Chapter 7 - The kidneys, renal function and kidney disease. In: Marshall, W.J., Lapsley, M., Day, A.P., Ayling, R.M. (Eds.), Clinical Biochemistry: Metabolic and Clinical Aspects (Third Edition), Churchill Livingstone. pp. 124-151.

Mao, X., Huang, T.J., 2012. Lab Chip 12(8), 1412-1416.

Margarson, M.P., Soni, N., 1998. Anaesthesia 53(8), 789-803.

Martinez, A.W., Phillips, S.T., Whitesides, G.M., Carrilho, E., 2010. Anal. Chem. 82(1), 3-10.

Mattix, H.J., Hsu, C.Y., Shaykevich, S., Curhan, G., 2002. J. Am. Soc. Nephrol. 13(4), 1034-1039.

Mauer, S.M., Steffes, M.W., Goetz, F.C., Sutherland, D.E.R., Brown, D.M., 1983. Diabetes 32, 52-55.

Metheny, N., 1981. J. Infus. Nurs. 4(1), 38-44.

Meza, M.N., Carrillo, J.A.B., 2016. Biomarkers, Obesity, and Cardiovascular Diseases. In: Wang, Mu., Witzmann, F. (Eds.), Role of Biomarkers in Medicine, Intechopen. pp. 119-147.

Mogensen, C.E., 1987. Kidney Int. 31(2), 673-689.

Must, A., Spadano, J., Coakley, E.H., Field, A.E., Colditz, G., Dietz, W.H., 1999. J. Am. Med. Assoc. 282(16), 1523-1529.

Narayanan, S., Appleton, H.D., 1980. Clin. Chem. 26(8), 1119.

Pandey, P.C., Mishra, A.P., 2004. Sens. Actuators, B 99(2), 230-235.

Paroni, R., Fermo, I., Cighetti, G., Ferrero, C.A., Carobene, A., Ceriotti, F., 2004. Electrophoresis 25(3), 463-468.

Pavia, D.L., Lampman, G.M., Kriz, G.S., Vyvyan, J.A., 2014. Introduction to Spectroscopy. Cengage Learning.

Pundir, C.S., Yadav, S., Kumar, A., 2013. TrAC, Trends Anal. Chem. 50, 42-52.

Ray, A., Reynolds, J.A., Polet, H., Steinhardt, J., 1966. Biochemistry 5(8), 2606-2616.

Roberts, W.L., Calcote, C.B., Cook, C.B., Gordon, D.L., Moore, M.L., Moore, S., Scheer, W.D., Snazelle, B.A., 1998. Clin. Chim. Acta 273(1), 21-33.

Rothschild, M.A., Oratz, M., Schreiber, S.S., 1988. Hepatology 8(2), 385-401.

Shaw, J.L.V., 2016. Pract. Lab. Med. 4, 22-29.

Shaw, R.A., Kotowich, S., Mantsch, H.H., Leroux, M., 1996. Clin. Biochem. 29(1), 11-19.

St John, A., Price, C.P., 2014. Clin Biochem Rev. 35(3), 155-167.

Stenvinkel, P., Alvestrand, A., 2002. Semin. Dial. 15(5), 329-337.

Tal, M., Silberstein, A., Nusser, E., 1985. J. Biol. Chem. 260(18), 9976-9980.

Tayeh, O., Taema, K.M., Eldesouky, M.I., Omara, A.A., 2016.. Egyptian J. Crit. Care Med. 4(2), 47-55.

Tayyab, S., Qasim, M.A., 1990. Int. J. Biol. Macromol. 12(1), 55-58.

Tsikas, D., Wolf, A., Frölich, J.C., 2004. Clin. Chem. 50(1), 201.

Valko, K., Nunhuck, S., Bevan, C., Abraham, M.H., Reynolds, D.P., 2003. J. Pharm. Sci. 92(11), 2236-2248.

van der Pals, M., Myléus, A., Norström, F., Hammarroth, S., Högberg, L., Rosén, A., Ivarsson, A., Carlsson, A., 2014. BMC Pediatr. 14(1), 165.

Vasiliades, J., 1976. Clin. Chem. 22(10), 1664-1671.

Viberti, G.C., Jarrett, R.J., Mahmud, U., Hill, R.D., Argyropoulos, A., Keen, H., 1982. Lancet 319(8287), 1430-1432.

Waldmann-Meyer, H., Schilling, K., 1956. Arch. Biochem. Biophys. 64(2), 291-301.

Walker, M.D., 2016. J. Infus. Nurs. 39(6), 382-386.

Warram, J.H., Gearin, G., Laffel, L., Krolewski, A.S., 1996. J. Am. Soc. Nephrol. 7(6), 930-937.

Wei, X., Ding, X., Liu, H., 2000. Spectrosc. Spectral Anal. 20(4), 556-559.

Wyss, M., Kaddurah-Daouk, R., 2000. Physiol. Rev. 80(3), 1107.

भारतीय प्रौद्योगिकी संस्थान गुवाहाटी
Indian Institute of Technology Guwahati

CHAPTER 5

Paper-Sensors for Point-of-Care Monitoring of Drinking Water Quality

Contents

भारतीय प्रौद्योगिकी संस्थान गुवाहाटी
Indian Institute of Technology Guwahati

ABSTRACT

Contamination of water bodies due to the disposal of natural and anthropogenic pollutants is one of the major global concerns in the recent times. Regular on-spot monitoring of water quality has become mandatory wherein diverse classes of materials such as organic, inorganic, heavy metals, or biological wastes are detected employing standard protocols. However, most of the existing laboratory techniques are either costly and/or time consuming owing to the process involving the expert driven sophisticated analysis techniques. Herein, we report the development of three paper based colorimetric sensors for the on-spot quantitative detection of the levels of fluoride (F^-), lead (Pb^{2+}), and pH in drinking water. The variations in the color-intensities of the paper sensors with the variation in the concentration of fluoride (F^-), lead (Pb^{2+}), and pH were converted into electronic signals to enable the development of a point-of-care-testing (POCT) device. For this purpose, initially, the sensors were characterized and calibrated with known concentrations of contaminates before successful validations with real samples. Thereafter, the sensors were illuminated with a light emitting diode from one side while the transmitted rays passing through the sensor was captured by a light dependent resistor (LDR) from the other side. The variation in the color intensity of the paper-sensor with the contaminant loading was found linearly varying with the resistance of the LDR. The sensor was then translated into a specific, stable and user-friendly POCT device, which enabled inexpensive on spot detection of pollutants in drinking water.

This chapter is submitted in *IEEE Sensors Journal* (2019).

5.1. Introduction

Real-time measurements of diverse hazardous environmental pollutants have become one of the major research focus in the recent years owing to their significance in the mitigation of many long-term health hazards (Andrade et al. 2018; Efstratiou et al. 2017). In this regard, of late, the portable, low-cost, and user-friendly point-of-care-testing (POCT) devices are envisioned to play a pivotal role (St John and Price 2014; Vashist 2017; Yager et al. 2008). Among the other important environmental markers, POC detections of the various pollutants in various water sources (Ejeian et al. 2018; Tuna et al. 2013; Zulkifli et al. 2018) have perhaps taken the center stage of attention owing to their far-reaching implications related to the global health. For example, soluble or insoluble inorganic (Kumar and Puri 2012), and organic contaminants (Kumar and Puri 2012), heavy metal ions (Kumar and Puri 2012), biological (BOD) (Bourgeois et al. 2003; Pasternak et al. 2017), and chemical (COD) (Bourgeois et al. 2003; Li et al. 2018a) oxygen demands, and pathogens (Reta et al. 2018), are now expected to be detected on-spot with the help of commercially available POCT devices (Kokkali and van Delft 2014). Although, in this direction a substantial progress has been made in the past few decades (Justino et al. 2017), a number of issues still remain unaddressed.

For example, there is an immediate necessity of a POCT device for the detection of fluoride (F^-) and/or lead (Pb^{2+}) contaminations in the drinking water. As per the World Health Organization (WHO) guidelines the maximum permissible limits for F^- is 1.5 ppm in the drinking water while for Pb^{2+} the same is 0.05 ppm.(Kumar and Puri 2012) Higher levels of F^- and/or Pb^{2+} in water can cause fluorosis or lead poisoning (Kumar et al. 2015).

Further, presence of excess F^- and Pb^{2+} in drinking water can also cause various other chronic ailments in associated with skin, teeth and bones (Peckham and Awofeso 2014), brain (Bondy and Campbell 2017; C Papanikolaou et al. 2005), lungs and heart (Chowdhury et al. 2018; Navas-Acien et al. 2007). On the other hand, the WHO guidelines also suggest that the pH of the water should be in range of 6.0 to 8.0 (Kumar and Puri 2012). The pH of drinking water deviating from this range can affect the mucin layer in the various parts of the digestive system which in turn can harm the immune system of a human body triggering many critical ailment (Kumar and Puri 2012). Importantly, many of the previous studies suggest that the lowering of pH than the normal range in most of the commercially available bottled mineral waters is one of the key reasons of old-age osteoporosis across the globe (Garzon and J Eisenberg 1998).

Certainly, there is an immediate need of a POCT device, which can immediately provide information about the F^-, Pb^{2+} and pH levels in the drinking water. It may be noted here that the conventional methods of determining these constituents in water involve either optical (Gangopadhyay et al. 2016; Parveen and Rohan 2011) or electrochemical (Bansod et al. 2017; Lu et al. 2018) methodologies. Yet, most of these methodologies are either costly and/or consume time and require expertise for testing and analyses (Deibler and Basu 2013). In this regard, of late, the advent of micro or nanoscale technologies have provided a glimmer of hope in the design and development of economic, specific, stable, portable, fast, and user friendly POCT devices to detect these pollutants. For example, the use of diverse nanomaterials (Li et al. 2018b; Ullah et al. 2018), nanostructures (Reta et al. 2018), and carbon allotropes (Bhattacharjee et al. 2017), have led to quantitative detection of dissolved F^-, Pb^{2+} and pH of water. However, these sensors are yet to be translated into

POCT applications owing to their higher cost of fabrication, requirement of expertise handing, and time required for detection.

In view of this background, in the present study, we have developed paper based colorimetric sensors to quantitatively detect F^-, Pb^{2+} and pH levels in the drinking water. The use of reagent coated paper sensors to develop the colorimetric sensors has been inspired by a number of recent seminal contributions (Bhattacharjee et al. 2017; Dutta et al. 2016). The use of paper as the substrate enabled the making of a sensor, which is less complicated to fabricate, of low cost, and easily disposable. The working principle of the colorimetric sensor depends on the color change due to the following specific reactions between, (a) F^- and iron (III) thiocyanate for fluoride sensing, (b) Pb^{2+} and 1,5-Diphenylthiocarbazone (dithizone) for lead sensing and (c) protonated bromothymol blue (BTB) for pH sensing, on the paper surface. While the reagents were coated on the paper surface, the network of microchannels in paper enabled immediate mixing with the analyte through capillary action, leading to a fast chemical reaction and colorimetric response.

The variations in the color on the surface of the paper sensor were detected with the help of a light emitting diode (LED) and a light dependent resistor (LDR). The paper sensors were illuminated with the LED from one side while the light transmitting through the sensors were captured by the LDR (Dutta et al. 2016). The resistance of the LDR was found to vary monotonically with the change in the concentration of dissolved F^-, Pb^{2+} and pH of the water sample. The sensors were found to be specific and detect the unknown levels of F^-, Pb^{2+} and pH of real water samples when compared and contrasted with standard methodologies. The sensors, LED, and LDR were integrated in an Arduino

platform to translate into a portable and user-friendly POCT device for on-site, low-cost, and instantaneous monitoring of water quality.

5.2. Experimental Section

5.2.1. Materials

Ammonium thiocyanate, Iron (iii) Chloride, Bromothymol blue, 1,5-Diphenylthiocarbazone (Dithizone), Sodium Fluoride, Lead (ii) Chloride, Potassium sodium tartrate, Dimethyl formamide (DMF), Carbon tetra chloride (CCl4), Sodium hydroxide, Hydrochloric acid, 125 mm filter paper (grade 1), were obtained from Merck (India). The chemicals above were of analytical grade and used without further purification. The Milli-Q grade water was used in all the experiments unless stated otherwise. The Arduino Uno R3 development board, Liquid crystal display (LCD), resistors were procured from Rhydo Labz (India).

5.2.2. Methods

The schematic representation of sensor fabrication for quantitative determination of fluoride Pb^{2+}, F^{-}, pH and their respective sensing principle is shown in Figures 5.1(a), (b), and (c). Whatmann filter paper (Grade 1) was cut into 1 cm × 1 cm size, which was used as substrate for the sensor fabrication. For the F^{-} sensor, firstly, 0.1 M of ammonium thiocyanate solution (w/v) and 0.1 M of iron (iii) chloride solution (w/v) were mixed in equal amounts to obtain a brick red colored iron (iii) thiocyanate solution (v/v). Following this 60 µl of iron (iii) thiocyanate solution was dispensed on each of the potassium sodium tartrate coated paper pieces before vacuum dried at 37°C. For Pb^{2+} sensor, initially, the paper pieces were coated with 30 µl of potassium sodium tartrate saturated solution and vacuum dried at 37°C. Following this, 60 µl of 0.05% solution of dithizone in CCl_4 was

dispensed on the paper pieces before vacuum drying at 37°C. For the pH sensor, the paper pieces were coated with 10 µl of 250 mM citric acid solution and vacuum dried at 37°C. Following this, the sensors were coated with 90 µl of 0.4% (w/v) of bromothymol blue in DMF before again drying at 37°C. All the sensors fabricated were stored in airtight condition until further use.

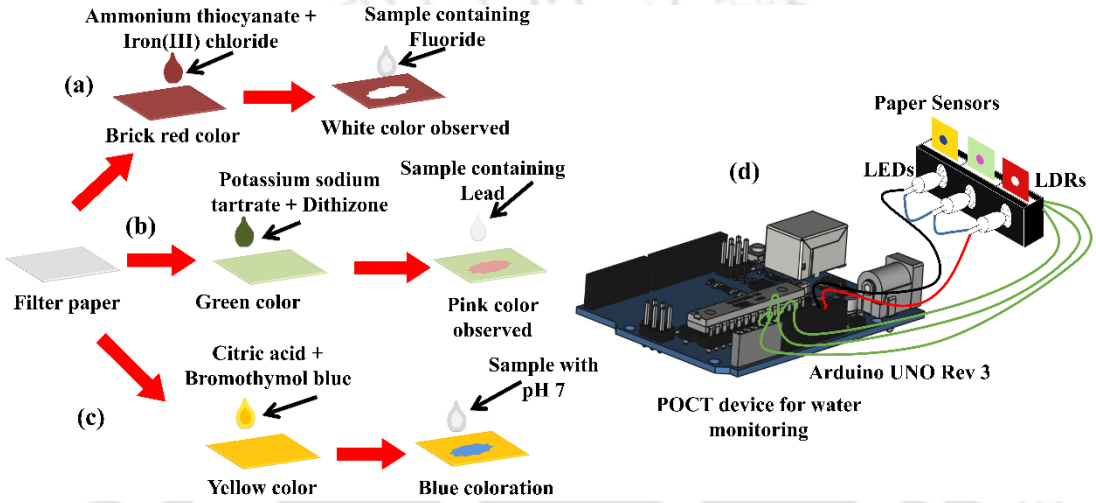

Figure 5.1: Images (a)-(c) schematically illustrate the steps of colorimetric sensor fabrication for F^-, Pb^{2+} and pH, respectively, and their color change. Image (d) shows the integration of LED and LDR with the sensor and subsequent measurement of the change in resistance using Arduino based POCT device for the display of water quality.

The pH of the solutions was measured with Cyber Scan pH 510 meter (Eutech Instruments). The pictures of the sensor were taken by Nikon D5100 digital camera (Nikon Corp., Japan). The FTIR analysis was performed using Thermo Scientific Nicolet iS10 FT-IR spectrometer, U.S.A. UV-Vis spectroscopy was carried out using Perkin-Elmer Lambda 25 spectrophotometer, U.S.A. The Raman spectroscopy was done using the Horiba LabRam HR Evolution Raman spectrophotometer, Japan.

5.3. Results and Discussion

5.3.1 Characterization of the sensor material and mechanism of detection

Figure 5.2 illustrates the UV-Vis spectroscopic results. The Figure 4.2(a) illustrates the UV-visible spectra of the interaction between iron (iii) thiocyanate and fluoride. In the plot the blue curve represents the UV-Vis spectra for the iron (iii) thiocyanate whose

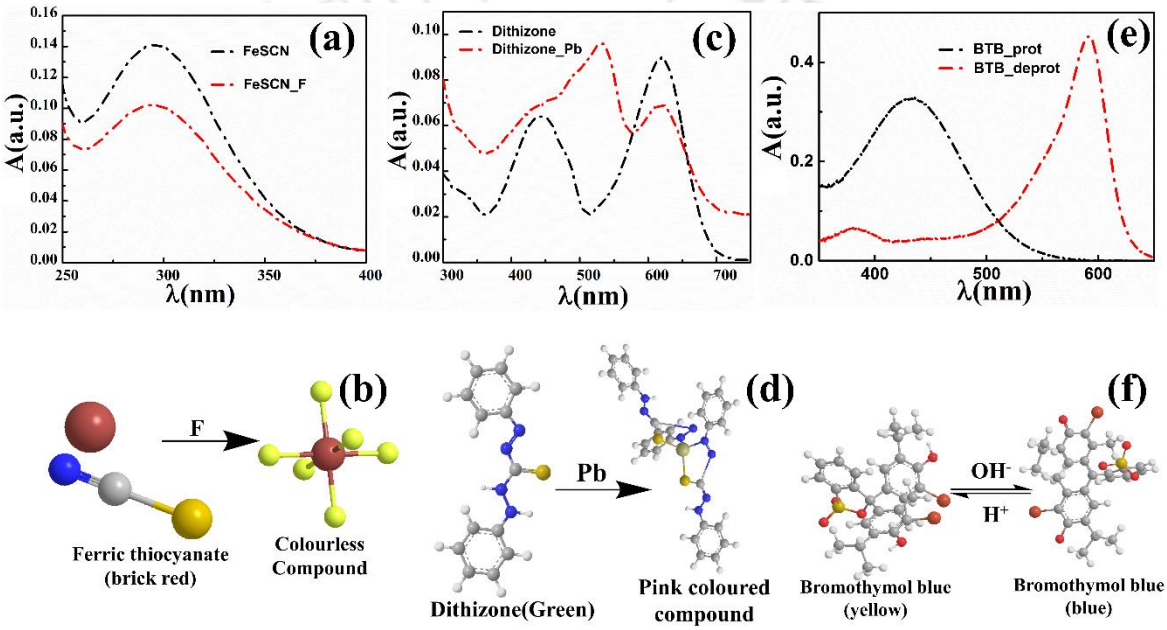

Figure 5.2: The images (a) and (b) illustrates the UV-Vis spectra and mechanism of the interaction between iron (iii) thiocyanate and fluoride. Images (c) and (d) shows the UV-Vis spectra and mechanism interaction between dithizone and lead. Images (e) and (f) illustrates the UV-Vis spectra and mechanism of interaction of bromothymol blue with different pH.

absorption peak is at 295 nm while the red curve represents the fading of the color product of the reaction whose absorption peak is at 290 nm (M.Najib and Hayder 2011). It is well known that F^- on interaction with brick red colored iron (iii) thiocyanate gives colorless iron (iii) fluoride, as shown in the figure 5.2(b). In this regard, the specific reaction can be written as,

$$Fe(SCN)_3 + 6NaF \rightarrow [FeF_6]^{3-} + 6Na^+ + 3(SCN)^-$$

Figure 5.2(c) demonstrates the UV-Vis spectra of the interaction between dithizone and Pb^{2+}. In the plot the blue curve represents the UV-Vis spectra of the dithizone whose absorption peak is at 445 nm and 620 nm, respectively, whereas the red curve represents the pinkish Pb^{2+} (ii) dithizone, for which a new absorption peak is formed at 533 nm. (Khan et al. 2006; Ruengsitagoon et al. 2010) The structural changes of the dithizone due to complexation with Pb^{2+} is as shown in Figure 5.2(d). The specific reaction can be written as,

$$PbCl_2 + 2C_{13}H_{12}N_4S \rightarrow Pb(C_{13}H_{12}N_4S)_2 + 2Cl^-$$

Figure 5.2(e) shows the UV-Vis spectra of the bromothymol blue in lower pH (blue curve) whose absorption peak is at 427 nm whereas at higher pH (red curve) its absorption peak being 600 nm (Hou et al. 2017). The bromothymol blue in its protonated form is yellow in color. The color changes to greenish blue to dark blue as the deprotonation of bromothymol blue occurs due to increase of alkaline pH which is shown in Figure 5.2(f). In this regard, the specific reaction can be written as,

$$C_{27}H_{28}Br_2O_5S \xrightarrow{OH^-} (C_{27}H_{26}Br_2O_5S)^{2-}$$

The following tables shows the performance of the proposed sensors as compared to the previously available ones.

Table 5.1: Comparison table between the existing methods and the proposed method for the Pb^{2+} detection in water (Deibler and Basu 2013; Ding et al. 2010; Huang et al. 2003; Saito et al. 2006).

No.	Principle for Pb^{2+} detection	Range
1	UV-Vis Spectrometry	10.36 ppb
2	Fluorimetry	10.36 ppb
3	Voltammetry	0.5 to 100 ppb
4	Graphite Furnace Atomic Absorption Spectrometry (GFAAS)	0.7 ppb
5	Inductively Coupled Plasma Atomic Emission Spectroscopy (ICP-AES)	42 ppb
6	Inductively Coupled Plasma Mass Spectrometry (ICP-MS)	0.6 ppb
7	Reversed-Phase High-Performance Liquid Chromatography (RP-HPLC)	0.01-120 ppb
8	Proposed Method	1×10^4- 1×10^5 ppb

Table 5.2: Comparison table between the existing methods and the proposed method for the F^- detection in water.

No.	Principle for F^- detection	Range
1	UV-Vis Spectrometry	65 ppb
2	Fluorimetry	1-100 ppb
3	Ion Selective Electrode (ISE)	1-100 ppm
4	Proposed Method	1-10 ppm

Table 5.3: Comparison table between the existing methods and the proposed method for the pH detection in water.

No.	Principle for pH detection	Range
1	Ion Selective Electrode (ISE)	1.00-14.00
2	pH strips	1-14
3	Proposed Method	6.0-8.0

The methods tabulated in Table 5.1, Table 5.2 and Table 5.3 are all efficient tools for Pb^{2+}, F^- and pH detection, but they are time-consuming, expensive and require sophisticated equipment with expertise work force. In both pure and contaminated waters, there are many ions present. Those ions should not interfere while detecting a particular ion concentration from the mixture of ions. There was negligible influence of anions, e.g., SO_4^-, Cl^-, $Cr_2O_7^-$, NO_3^-, I^-, Br^-, IO_3^-, and a mixture of all these ions on the fluoride sensor. Similar study was performed for Pb^{+2} sensors. Interference by cations such as, Mg^{+2}, K^+, Na^+, Al^{+3}, Mn^{+2}, Ca^{+2}, Pb^{+2}, was found to be negligible on the lead sensor. However, many other chemicals whose possibilities of interference needs to be tested. This we have kept as our future direction and scope of work. The development of simple, inexpensive, reliable and rapid methods for measuring Pb^{2+}, F^- and pH with sensitivity and selectivity is highly desirable. However there are certain limitations which restrict the application of the sensors over larger range such as, sensor size and shape need to be constant, amount of reagent as well as analyte dispensed on the sensor surface should be done in a controlled way, the packaging and storage of the sensor should be done in proper manner, the output

signals of the electronic component used should be stabilized by the development of PCB, sophisticated sensors are to be used to increase the accuracy and range of measurement. The proposed method measures Pb^{2+} ranging from 10-100 ppm, F^- ranging from 1-10 ppm and pH ranging from 6.0-8.0 which is much lower that the sophisticated method tabulated but it qualifies the qualities of being simple, inexpensive, sensitive, selective method for rapid detection of Pb^{2+}, F^- and pH.

5.3.2 Response of the sensor

The initial resistance, R_i^0 of the F^- sensor was recorded from the LDR when light was irradiated on the sensor from an LED light source before the water sample was dispensed. Thereafter, final resistance R_i the F^- sensor was measured after dispensing of various concentration of F^- sample in water ranging from 1.0 – 10 ppm. It was observed that when the sample containing F^- was dispensed on the sensor surface discoloration occurred due to the reaction resulting in increased transmission of light to the LDR, which in turn resulted in a decrease of R_i. The Figure 5.3(a) demonstrates the variation in the normalized resistance R_i^0/R_i with the concentration of fluoride in water sample, C_F The R_i^0/R_i was found to linearly and monotonically decrease with C_F in the water sample. The images in the Figure 5.3(d) illustrate the visual increase in the discoloration of the sensor surface due to increase in the C_F in the water sample dispensed on the sensor surface. A higher discoloration led to the transmittance of higher amount of LED light through the paper surface, which led to a higher reduction in the electrical resistance of the LDR when the C_F was higher in the water sample. The Figure 5.3(b) demonstrates the variation in the normalized resistance R_i^0/R_i with C_{Pb} in water. The R_i^0/R_i was found to increase with C_{Pb} in the water sample. The images in the Figure 5.3(e) illustrate the visual increase in

the pink color intensity of the sensor surface due to increase in C_{Pb} in the water sample dispensed on the sensor surface. A higher pink coloration led to the transmittance of lower amount of LED light through the paper surface, which led to an increase in the electrical resistance of the LDR when C_{Pb} was higher in the water sample. The calibration for the pH sensor was performed after dispensing of various samples of water having pH in the range of 6.0 – 8.0. Once the sample was dispensed on the sensor surface, a greenish blue coloration occurred due to the reaction, which resulted in the decreased transmission of light through the paper surface to the LDR. Figure 5.3(c) demonstrates the variation in R_i^0/R_i with pH of water samples. The images in the Figure 5.3(f) illustrate the visual increase in the greenish blue coloration on the sensor surface due to increase in pH of the water sample dispensed on the sensor surface. The deformation of the paper sensor affects the accuracy of the readings. This is why we have discarded the deformed paper sensors.

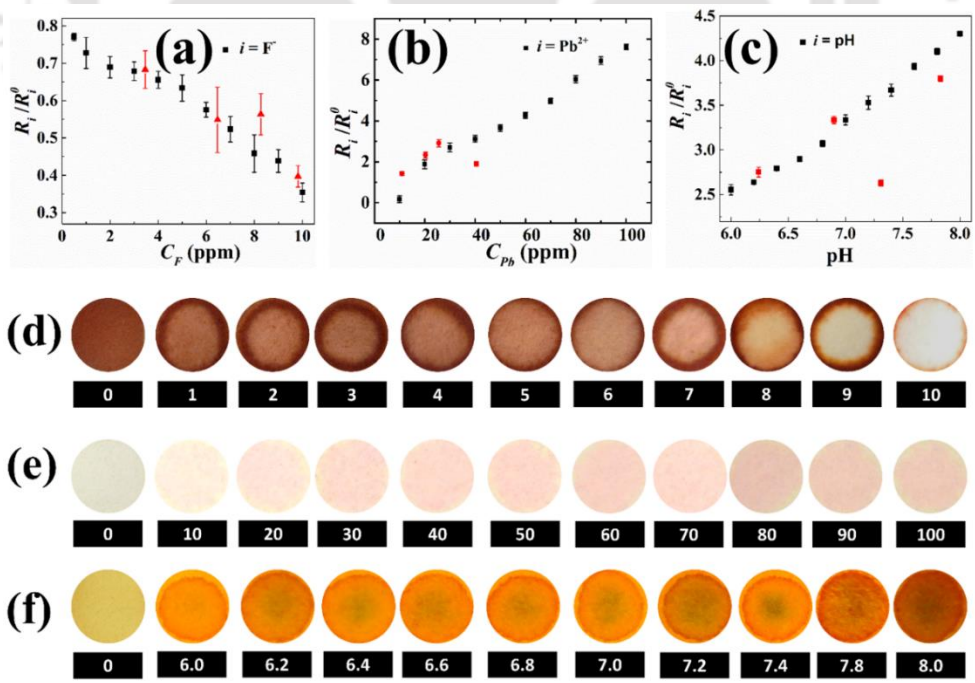

Figure 5.3: Plots (a) – (c) show the variation in the normalized resistance change (R_i^0/R_i) with the fluoride concentration (C_F) in water, lead concentration (C_{Pb}) in water and pH of

water, respectively. The squares (black) denotes the calibration points and the triangles (red) denotes the unknown samples. Images (d)-(f) illustrate the color change of the F^-, Pb^{2+} and pH sensors, respectively, due to the change in concentrations as written at the bottom. The numbers below the images (d)-(e) denotes concentration in ppm, and pH in image (f).

The sensor holder in such a fashion that the light only passes through the centre of the sensor. Thus, the colouration of the periphery of the drops was not considered.

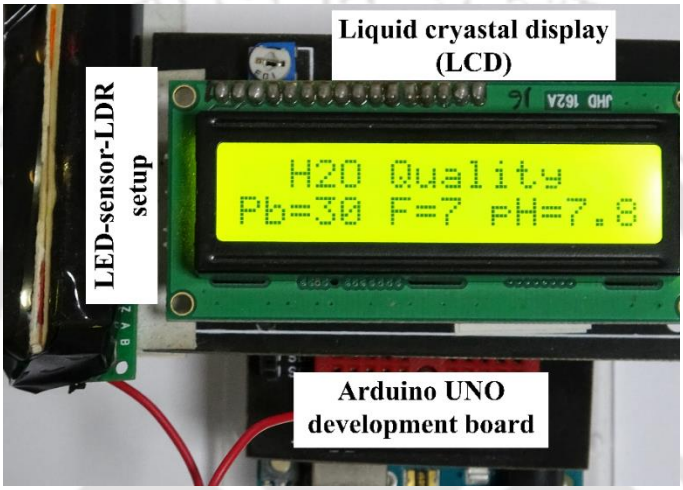

Figure 5.4: Image shows a POCT device for monitoring of F^-, Pb^{2+} and pH of water.

Figure 5.4 show a typical POCT device for the water quality monitoring. We tested a range of water samples with unknown levels of F^-, Pb^{2+} and pH, which are plotted as solid red triangular, circular and square symbols on the plots (a) – (c) in the Figure 5.3 respectively. The plots suggest that the POCT device could detect the levels of these pollutants with reasonable accuracy when compared with standard methodologies.

Table 5.4. Comparison of the contaminates in water using POCT and Commercial Devices.

No.	Standard methodology			Proposed methodology		
	Fluoride (ppm)	Lead (ppm)	pH	Fluoride (ppm)	Lead (ppm)	pH
1	8.27	20.32	6.90	6.21 ± 0.055	25.42 ± 0.14	7.0 ± 0.042
2	9.82	10.97	7.31	9.47 ± 0.0289	17.21 ± 0.097	6.1 ± 0.035
3	3.46	25.64	7.83	2.51 ± 0.050	35.17 ± 0.181	7.5 ± 0.030

The Table 5.4 suggest that the predictions by the POCT device was rather close with some deviations as compared to the standard approved methodology. The deviations obtained in the proposed POCT methodology as compared to the costly approved method can be rectified by the optimization and improvement of the proposed water quality sensor. The analysis for fluoride F^- was performed using UV-Vis Spectroscopy Lambda 25 (Perkin Elmer, U.S.A). The analysis for Pb^{2+} was done using Atomic absorption spectroscopy 240FS AA (Agilent technologies, U.S.A). The pH analysis was performed with pH meter Eutech pH 150 (Thermo Scientific, U.S.A).

Table 5.5. Comparison of cost and expertise in water quality monitoring using POCT and Commercial Devices.

	Proposed Method	Standard Method
Cost	Approx. INR 90	Approx. INR 500
Expertise required	User him or herself	Laboratory technician

The Table 5.5 shows a comparision of cost and expertise required for the water quality monitoring using the proposed and the commercially available devices and can be concluded that the proposed sensors are fairly economical.

5.4. Conclusions

In summary, we report the development of three paper sensors for the on-spot detection of F^-, Pb^{2+} and pH in the drinking water. The colorimetric sensors show monotonic variation in the color with the loading of F^-, Pb^{2+} and pH in the water sample, which were detected with the help of an electronic arrangement. The sensors were illuminated with LED before the transmitted rays through them was captured in an LDR. The variation in the resistance of LDR was found to monotonically vary with the F^-, Pb^{2+} and pH loading in the water sample. The LED-sensor-LDR combination was integrated with and Arduino circuit to develop an economic, specific, stable, portable, fast, and user friendly POCT device, which enabled spot detection of pollutants in drinking water. The novel aspect being that

the device is portable and measures multiple parameters of drinking water. The paper sensors can be used independently as a colourimetric sensor without the electronic device. The test results are obtained instantaneously and the fabrication process is also simple.

References

Andrade, L., O'Dwyer, J., O'Neill, E., Hynds, P., 2018. Environ. Pollut. 236, 540-549.

Bansod, B., Kumar, T., Thakur, R., Rana, S., Singh, I., 2017. Biosens. Bioelectron. 94, 443-455.

Bhattacharjee, M., Nemade, H.B., Bandyopadhyay, D., 2017. Biosens. Bioelectron. 94, 544-551.

Bondy, S.C., Campbell, A., 2017. Int. J. Environ. Res. Public Health 15(1), 2.

Bourgeois, W., Romain, A.-C., Nicolas, J., Stuetz, R.M., 2003. J. Environ. Monit. 5(6), 852-860.

C Papanikolaou, N., Hatzidaki, E., Belivanis, S., Tzanakakis, G., Tsatsakis, A., 2005. Med Sci Monit. 11(10),RA329-36.

Chowdhury, R., Ramond, A., O'Keeffe, L.M., Shahzad, S., Kunutsor, S.K., Muka, T., Gregson, J., Willeit, P., Warnakula, S., Khan, H., Chowdhury, S., Gobin, R., Franco, O.H., Di Angelantonio, E., 2018. Br. Med. J. 362, k3310.

Deibler, K., Basu, P., 2013. Eur. J. Inorg. Chem. 2013(7), 1086-1096.

Ding, N., Cao, Q., Zhao, H., Yang, Y., Zeng, L., He, Y., Xiang, K., Wang, G., 2010. Sensors 10(12), 11144.

Dutta, S., Mandal, N., Bandyopadhyay, D., 2016. Biosens. Bioelectron. 78, 447-453.

Efstratiou, A., Ongerth, J.E., Karanis, P., 2017. Water Res. 114, 14-22.

Ejeian, F., Etedali, P., Mansouri-Tehrani, H.-A., Soozanipour, A., Low, Z.-X., Asadnia, M., Taheri-Kafrani, A., Razmjou, A., 2018. Biosens. Bioelectron. 118, 66-79.

Gangopadhyay, D., Sharma, P., Nandi, R., Das, M., Ghosh, S., Singh, R.K., 2016. RSC Adv. 6(113), 112562-112567.

Garzon, P., J Eisenberg, M., 1998. Am. J. Med. 105(2),125-130.

Hou, H., Zhao, Y., Li, C., Wang, M., Xu, X., Jin, Y., 2017. Sci. Rep. 7(1), 1759.

Huang, Z., Yang, G., Hu, Q., Yin, J., 2003. Anal. Sci. 19(2), 255-258.

Justino, C.I.L., Duarte, A.C., Rocha-Santos, T.A.P., 2017. Sensors 17(12), 2918.

Khan, H., Ahmed, M.J., Bhanger, M.I., 2006. Spectroscopy 20(5-6), 285-297.

Kokkali, V., van Delft, W., 2014. TrAC, Trends Anal. Chem. 61, 133-155.

Kumar, M., Garg, S., Pareek, A.K., Yadav, S.M., 2015. Interdiscip Toxicol. 8(2) 55–64.

Kumar, M., Puri, A., 2012. Indian J. Occup. Environ. Med. 16(1), 40-44.

Li, J., Luo, G., He, L., Xu, J., Lyu, J., 2018a. Crit. Rev. Anal. Chem. 48(1), 47-65.

Li, Y., Chen, Y., Yu, H., Tian, L., Wang, Z., 2018b TrAC, Trends Anal. Chem. 98, 190-200.

Lu, Y., Liang, X., Niyungeko, C., Zhou, J., Xu, J., Tian, G., 2018. Talanta 178, 324-338.

M.Najib, F., Hayder, I., 2011. Iraqi Natl. J. Chem. 42, 135-155.

Navas-Acien, A., Guallar, E., Silbergeld, E.K., Rothenberg, S.J., 2007. Environ. Health Perspect. 115(3), 472-482.

Parveen, N., Rohan, Y., 2011. Spectrophotometric Determination of Some Environmental Samples. J. Environ. Res. Dev. 6(1), 57-62.

Pasternak, G., Greenman, J., Ieropoulos, I., 2017. Sens. Actuators, B 244, 815-822.

Peckham, S., Awofeso, N., 2014. Water fluoridation: a critical review of the physiological effects of ingested fluoride as a public health intervention. Sci. World J. 2014, 293019-293019.

Reta, N., Saint, C.P., Michelmore, A., Prieto-Simon, B., Voelcker, N.H., 2018. ACS Appl. Mater. Interfaces 10(7), 6055-6072.

Ruengsitagoon, W., Chisvert, A., Liawruangrath, S., 2010. Talanta 81(1), 709-713.

Saito, S., Danzaka, N., Hoshi, S., 2006. J. Chromatogr. A 1104(1), 140-144.

St John, A., Price, C.P., 2014. Clin Biochem Rev. 35(3), 155-167.

Tuna, G., Arkoc, O., Gulez, K., 2013. Int. J Distrib. Sens. N. 9(6), 249598.

Ullah, N., Mansha, M., Khan, I., Qurashi, A., 2018. TrAC, Trends Anal. Chem. 100, 155-166.

Vashist, S.K., 2017.. Biosensors 7(4), 62.

Yager, P., Domingo, G.J., Gerdes, J., 2008. Annu. Rev. Biomed. Eng. 10(1), 107-144.

Zulkifli, S.N., Rahim, H.A., Lau, W.-J., 2018. Sens. Actuators, B 255, 2657-2689.

CHAPTER 6

Summary and Future Scope

Contents

भारतीय प्रौद्योगिकी संस्थान गुवाहाटी
Indian Institute of Technology Guwahati

6.1. Summary

In summary, the thesis describes different ways of sensing and its applications in the fields of diagnostics and quantitative measurement. Using various principles of materials' engineering, enzymatic reaction engineering, and colourimetric detection the devices were developed. Different macro, micro and nanomaterials were used to develop the sensors under the paper based microfluidic platforms. Apart from fabrication, optimization, and experimentation, multiple devices have also been developed for point-of-care diagnostic application for those devices.

The second chapter of the thesis discusses the development of an electrochemical biosensor and a proof-of-concept prototype for the detection of α-amylase in human serum. The biosensor is composed of an electrically conducting polymer poly-aniline emeraldine salt (PANI-ES) thin film, which is sparsely populated with starch-coated gold nanoparticles (SAuNPs) on the surface. The PANI-ES film acts as a base material for the electrical signal transport apart from acting as an immobilization matrix for the SAuNPs. It is well known that α-amylase selectively catalyzes the hydrolysis of starch into simple sugars. Thus, dispensing the solutions of α-amylase of different concentrations on the sensor depletes dissimilar amounts of the starch molecules coated the gold nanoparticles (AuNPs), which leads to the variation in the electrical resistance of the sensor. The change in the electrical resistance vary almost linearly with the concentration of α-amylase in phosphate buffer, which helps in the development of the calibration curve. The pathway to SAuNP formation on the PANI-ES substrate, the time-dependent starch digestion with α-amylase, and the variation in the subsequent electrical response have also been characterized to uncover the details of the sensing mechanism. Involvement of chloride

ions and AuNPs on the PANI-ES film offers a fast response time with a superior stability during the signal processing. A calibrated proof-of-concept prototype has also been developed for the fast (~60 s) detection of α-amylase level in human serum, which promises to be superior to the available clinically approved methodologies. The reported prototype has shown the potential evolve into a portable, easy-to-use, fast, reliable, economic, and biocompatible POCT diagnostic tool for the immediate detection of pancreatitis, cancer, stress, and depression.

The third chapter discusses the fabrication of a paper-sensor for quantitative estimation of α-amylase in human blood serum based on the principle of starch degradation by α-amylase. The Prussian blue-colored starch–iodine (SI) coated on the paper-surface was faded by the aqueous α-amylase solution when dispensed on the SI coated paper sensor surface. Thereafter, the paper-surface was illuminated with a light emitting diode (LED) source and the transmitted (reflected) rays emitted through (from) the paper was collected on a photoresistor. The variations in the electrical resistance of the photoresistor were correlated with the change in color intensity and amylase concentration. The sensor being economical, easily disposable, environment-friendly is a potential candidate for a point-of-care device for the rapid detection of α-amylase because it could faithfully reproduce amylase level in human blood serum when compared with a standard testing methodology.

The fourth chapter discusses the development of an economic, paper-based, and portable POCT device for estimating important biomarkers present in urine such as, albumin, creatinine and ACR, which has shown the potential to track the health of human kidneys following the gold-standards. alcoholic solution of bromophenol blue was coated on a paper surface to develop the albumin sensor, as schematically shown in the image (a). Further, the alkaline picrate solution was coated on another paper surface to develop the

creatinine sensor, as schematically shown in the image (b). Subsequently, the aqueous albumin and creatinine solution was dispensed on the respective paper-sensors before the change in intensity of color on the sensor surface was observed, as schematically shown in the images (a) and (b). Thereafter, the paper-sensor was placed between a light emitting diode (LED) source and a light dependent resistor (LDR), as schematically shown in the images (c) and (d). The arrangement allowed the LED to shine light on the paper surface from one side while the transmitted light passing through the sensor was collected on a LDR. The change in color intensity on the sensor surface with the variation in the albumin or creatinine concentration in the analyte was found to have a direct correlation with variations in the electrical resistance of the LDR. The calibrations thus generated for the albumin and creatinine were employed to detect the unknown levels of albumin, creatinine, and ACR in the human urine sample. The sensors were integrated with a signal processing unit (SPU) to display and wireless transfer the data to the mobile interfaces, which led to the proof-of-concept prototype of a fast, portable, and user-friendly KFT kit.

The fifth chapter discusses the development of a paper based colorimetric sensors to quantitatively detect F^-, Pb^{2+} and pH levels in the drinking water. The use of reagent coated paper sensors to develop the colorimetric sensors has been inspired by a number of recent seminal contributions. The use of paper as the substrate enabled the making of a sensor, which is less complicated to fabricate, of low cost, and easily disposable. The working principle of the colorimetric sensor depends on the color change due to the following specific reactions between, (a) F^- and iron (III) thiocyanate for fluoride sensing, (b) Pb^{2+} and 1,5-Diphenylthiocarbazone (dithizone) for lead sensing and (c) protonated bromothymol blue (BTB) for pH sensing, on the paper surface. While the reagents were coated on the paper surface, the network of microchannels in paper enabled immediate

mixing with the analyte through capillary action, leading to a fast chemical reaction and colorimetric response. The variations in the color on the surface of the paper sensor were detected with the help of a light emitting diode (LED) and a light dependent resistor (LDR). The paper sensors were illuminated with the LED from one side while the light transmitting through the sensors were captured by the LDR. The resistance of the LDR was found to vary monotonically with the change in the concentration of dissolved F^-, Pb^{2+} and pH of the water sample. The sensors were found to be specific and detect the unknown levels of F^-, Pb^{2+} and pH of real water samples when compared and contrasted with standard methodologies. The sensors, LED, and LDR were integrated in an Arduino platform to translate into a portable and user-friendly POCT device for on-site, low-cost, and instantaneous monitoring of water quality.

Briefly, this thesis has covered both the domain of scientific findings and its potential commercial application. The scientific findings can be listed in the following ways.

- The thesis shows that paper can be a very useful substrate for sensor fabrication as the white background of the paper make it a good candidate for colorimetric sensor-based point-of-care applications. Further paper substrate led to improvements in the sensor performance and that was not possible with other substrates. The interface between the paper and active material is very uniform compared to other substrate such as glass. Moreover, it is economical, user-friendly, abundantly available and can be easily disposed of without harming the environment.

- It was also demonstrated that conducting polyaniline is a potential candidate for fabricating innovative electronic sensors which are economical and biodegradable. There are sensors to detect α-amylase by two different principles. The electronic

method of quantitative detection of α-amylase employed material engineering to develop novel single step processes for fabrication of the sensors using conducting polymer polyaniline (PANI) as the substrate making it a rather faster detection process than most of the methods available.

- The colourimetric detection of α-amylase shows a novel way of fabrication and optimization of the sensors which resulted not only in the decrease of the material used for the fabrication but also decreased the amount of biological sample to be used for testing purpose.

- The thesis also shows a novel pathway of fabricating colorimetric paper sensors for monitoring of the kidney function for a drop of urine of a person, which can have its potential application as a healthcare device.

- Besides these, the thesis also demonstrated colorimetric sensor for the detection of F^-, Pb^{2+} and pH present in a water sample for the instant status of the water quality.

Along with the scientific findings elaborated above, the thesis also proposed a few commercial healthcare methods and prototypes for diagnosing, pancreatitis, kidney function related issues.

6.2. Future Scope

The work in the present thesis can be extended in the following ways,

i. The conductive polymer polyaniline based electronic sensors can also be targeted for other biosensing application apart from the α-amylase sensor as discussed.

ii. The AuNPs on the conducting polyaniline thin film surface can be bio-functionalized for sensing other molecules apart from α-amylase.

iii. Detailed simulation study of the polyaniline based sensor.

iv. The colourimetric sensors for monitoring for human body can be diversified for detecting many other parameters found in the biological fluids on a single paper sensor strip using paper microfluidics.

v. The colourimetric sensors for monitoring water quality can be expanded for detecting many other pollutants, heavy metals, insecticides found in water in a single paper strip using paper microfluidics.

vi. Different geometries of paper along with wax printing can be used to further miniaturize the design of the sensor.

Appendix - I

Publications, Patents, Conferences and Awards

A1.1 International Publications

1. **N. Mandal**, M. Bhattacharjee, A. Chattopadhyay, and D. Bandyopadhyay, "Point-of-care-testing of α-amylase activity in human blood serum", Biosensors and Bioelectronics, 2019. 124-125: p. 75-81. (DOI: 10.1016/j.bios.2018.09.097)
2. S. Dutta, **N. Mandal**, D. Bandyopadhyay, "Paper-based α-amylase detector for point-of-care diagnostics", Biosensors and Bioelectronics, 2016. 78: p. 447 – 453. (DOI: 10.1016/j.bios.2015.11.075)
3. S. Middya, M. Bhattacharjee, **N. Mandal** and D. Bandyopadhyay, RGO-Paper Sensor for Point-of-Care Detection of Lipase in Blood Serum, IEEE Sensors Letters, 2, 2000404, 2018.
4. **N. Mandal,** S. Mitra and D. Bandyopadhyay, "Paper-Sensors for Point-of-Care Monitoring of Drinking Water Quality", IEEE Sensors Journal, 2019. (DOI: 10.1109/JSEN.2019.2919269)
5. N. Roy, S. Mitra, N.M. Das, **N. Mandal,** D. Bandyopadhyay, H.B. Nemade and T.K. Mandal, "Paper Based Enzymatic Chemiresistor for POC Detection of Ethanol in Human breath", IEEE Sensors Journal, 2019. (DOI: 10.1109/JSEN.2019.2952940)

A1.2 International Patents

1. Dipankar Bandyopadhyay, **Nilanjan Mandal**, Satarupa Dutta. A transmittance based system/kit for point-of-care quantification of biomarkers sample and use thereof. International Patent Application No: PCT/IN2017/050023 dated 16-01-2017.

A1.3 National Patents

1. Dipankar Bandyopadhyay, **Nilanjan Mandal**, Satarupa Dutta. A transmittance based system/kit for point-of-care quantification of biomarkers sample and use thereof. Indian Patent Application No: 201631018620 dated 31-05-16.

2. **Nilanjan Mandal**, Dipankar Bandyopadhyay. Electrochemical sensor and micro-electro-mechanical-system (MEMS) for the real-time point-of-care-testing (POCT) of the clinically important biomarkers in the biological fluids. Indian Patent Application No: 201731032122 A dated 11-09-2017.
3. Ankit Chowdhury, **Nilanjan Mandal**, Mitradip Bhattacharjee, Sahil Jagnani, Pankaj Upadhyay, Dipankar Bandyopadhyay. Portable and modular POCT device for rapid multiple diagnostic. Indian Patent Application No: 201931007736 A dated 29-03-2019.

A1.4 Conferences

1. Mitradip Bhattacharjee, Seim Timung, **Nilanjan Mandal**, Harshal Nemade and Dipankar Bandyopadhyay, "Self Adhesive Nature of PDMS Thin Film", Reflux -2015, IIT Guwahati, India, March 28-29, 2015.
2. Mitradip Bhattacharjee, **Nilanjan Mandal**, Satarupa Datta, Saptak Rarotra, Harshal Nemade, Tapas Kumar Mandal and Dipankar Bandyopadhyay, "Controlled Drug Release: Attachment of Drugs on Magnetic Nanoparticles", International Conference on Translational Nanomedicine (T-NANO 2014), Ahmedabad, India, December 15-17, 2014.
3. Satarupa Dutta, **Nilanjan Mandal**, Mitradip Bhattacharjee, Harshal Nemade, Arun Chattopadhyay, and Dipankar Bandyopadhyay, "Paper Based Optical Alpha Amylase Sensor", International Conference on Translational Nanomedicine (T-NANO 2014), Ahmedabad, India, December 15-17, 2014.
4. Mitradip Bhattacharjee, **Nilanjan Mandal**, Harshal Nemade and Dipankar Bandyopadhyay, "Simulation of a Voltage Controlled Resistor Mimicking the Geometry of a MOSFET Device having Graphite Channel", In proceedings of the COMSOL conference, Bangalore, India, November 13-14, 2014.

A1.5 Awards

1. BIRAC-SRISTI GYTI Appreciation Award of Rupees 1-lac for developing the “Paper based Amylase detector for Point-of-Care Diagnostic”. The sanction letter no. is SRISTI PMU-2017/005.